NASA TECHNICAL REPORT

NASA TR R-346

NASA TR R-346

THE CONTROL AND USE OF LIBRATION-POINT SATELLITES

by Robert W. Farquhar

Goddard Space Flight Center

Greenbelt, Md. 20771

NATIONAL AERONAUTICS AND SPACE ADMINISTRATION • WASHINGTON, D. C. • SEPTEMBER 1970

1. Report No. NASA TR R-346	2. Government Accession No.	3. Recipient's Catalog No.
4. Title and Subtitle The Control and Use of Libration-Point Satellites		5. Report Date September 1970 6. Performing Organization Code
7. Author(s) Robert W. Farquhar		8. Performing Organization Report No.
9. Performing Organization Name and Address Goddard Space Flight Center Greenbelt, Maryland 20771		10. Work Unit No. 11. Contract or Grant No. 13. Type of Report and Period Covered Technical Report
12. Sponsoring Agency Name and Address National Aeronautics and Space Administration Washington, D. C. 20546		14. Sponsoring Agency Code

15. Supplementary Notes

The information presented herein was submitted as a thesis in partial fulfillment of the requirements for the degree of Doctor of Philosophy in the Astronautical Sciences, Stanford University, Stanford, California, July 1968.

16. Abstract

This study is primarily concerned with satellite station keeping in the vicinity of the unstable collinear libration points, L_1 and L_2. Simple linear feedback control laws are formulated, and stability conditions are determined for both constant and periodic coefficient systems. It was found that stability could be achieved with a single-axis control that used only range and range-rate measurements. The station-keeping cost with this control is given as a function of the measurement noise. If Earth-based measurements are available, this cost is very low. Other control analyses of this study include solar sail control at the Earth-Moon collinear points and a limit-cycle analysis for an on-off control system.

Several possible libration-point missions are proposed. It is suggested that libration points could be utilized for lunar far-side communications, lunar and interplanetary transportation systems, deep space optical communications, and monitoring solar-induced phenomena in and beyond the Earth's magnetosphere.

17. Key Words Suggested by Author	18. Distribution Statement
Libration-point satellites Station keeping	Unclassified–Unlimited

19. Security Classif. (of this report)	20. Security Classif. (of this page)	21. No. of Pages	22. Price*
Unclassified	Unclassified	125	$3.00

*For sale by the Clearinghouse for Federal Scientific and Technical Information
Springfield, Virginia 22151

CONTENTS

NOTATION AND UNITS vi

I. INTRODUCTION 1

A. Problem Statement 1

B. Previous Contributions 2

C. Contributions of This Research 3

II. PRELIMINARY DEVELOPMENTS 5

A. The Restricted Three-Body Problem 5

1. Equations of Motion 5

2. Jacobian Constant and the Surfaces of Zero Relative Velocity 7

3. Libration Points 9

B. Equations of Motion in the Vicinity of Libration Points 11

1. Collinear Points 11

2. Equilateral-Triangle Points 14

3. Isosceles-Triangle Points 17

4. Stability of the Linearized Equations of Motion in the Elliptic Case 20

C. Numerical Data for Some of the Collinear Points in the Solar System 21

1. Mass-Ratio Dependent Quantities 21

2. Conversion Factors for Normalized Units 23

3. Comparison of L_2 Distance and Extent of Planetary Shadow 26

III. PERTURBATIONS AND NOMINAL PATH CONTROL 29

A. Additional Accelerations Acting on a Libration-Point Satellite 29

1. Gravitational Perturbations 29

2. Solar Radiation Pressure 29

3. Thrust Control 30

B. Control About Nominal Path 30

1. Basic Strategy 30

2. Periodic Orbits 31

3. Higher Order Corrections for a Periodic Orbit 31

4. Linearized Equations of Motion Relative to a Nominal Path 36

C. Examples of Gravitational Perturbations 37
1. Solar Perturbation Near the Earth-Moon Collinear Points 37
2. Effect of the Moon at the Sun-Earth Collinear Points 42
3. Jupiter's Effect at the Sun-Earth Isosceles-Triangle Points 44
4. Solar Effect at the Earth-Moon Equilateral-Triangle Points 45

IV. LINEAR FEEDBACK CONTROL 47

A. Collinear Points 47
1. Routh Stability Conditions 48
2. Root Loci and Closed-Loop Response 49
3. Floquet Stability Investigations 53

B. Equilateral-Triangle Points 57
1. Routh Stability Conditions 57
2. Root Loci and Closed-Loop Response 59

V. STATION KEEPING 63

A. Average Control-Acceleration Requirements 63
1. Cost Estimates for Noise Inputs 63
2. Cost for Sinusoidal Control Acceleration With Noise 67
3. Cost for a Constant Displacement 68

B. Solar Sail Control at the Earth-Moon Collinear Points 68
1. Basic Concepts 69
2. Sail Variations With Radial-Axis Control 71
3. Examples 71

VI. ON-OFF CONTROL SYSTEM 73

A. Limit Cycles: Exact Analysis 73
1. Application of Harmonic Method 73
2. Closed-Form Solution 76

B. Stability of Limit Cycles 78
1. Tsypkin's Method 79
2. Results for Special Case ($\theta_2 - \theta_1 = \pi$) 80
3. Procedure for General Case ($\theta_2 - \theta_1 \neq \pi$) 81

C. Solar Sail Control at the Sun-Earth L_1 Point 83

D. Limit Cycles: Approximate Analysis 83
1. Accuracy of Single-Axis Approximation 83
2. Phase-Plane Method 84
3. Sample Calculation at the Earth-Moon L_2 Point 86

VII. STABLE CABLE 89

A. Stabilization Procedure 89
1. One-Dimensional Analysis 90
2. Three-Dimensional Analysis 92

B. Other Considerations 98
1. Cable Extension Limitations 98
2. Structural Comments 101

VIII. APPLICATIONS 103

A. Supporting Role for Lunar and Planetary Missions 103
1. Utilization of the Earth-Moon Collinear Points in Future Lunar Operations 103
2. An Interplanetary Transportation System With Terminals at the Sun-Planet Collinear Points 111
3. Deep Space Communications Using a Relay Satellite at an Earth-Moon Equilateral-Triangle Point 112

B. Scientific Usefulness 113
1. A Multiple-Satellite System for Monitoring Solar-Induced Phenomena in and Beyond the Earth's Magnetosphere 113
2. Low-Frequency Radio Astronomy from the Earth-Moon L_2 Point 114

CONCLUSIONS AND RECOMMENDATIONS 115

ACKNOWLEDGMENTS 115

References 116

APPENDIX A. DERIVATION OF EQUATION 5.18 121

APPENDIX B. ECCENTRICITY CORRECTION FOR THE Z-AXIS OSCILLATION AT THE EARTH-MOON L_2 POINT 125

NOTATION AND UNITS

Notation

A brief list of symbols is given here. Unlisted symbols are defined in the chapter where they appear.

A_x, A_y, A_z — oscillation amplitude along coordinate axis

B_L — defined by Equation 2.44

C_L — defined by Equation 2.45

D_L — defined by Equation 2.46

$\mathbf{F}_c$, (F_{cx}, F_{cy}, F_{cz}) — control acceleration

K — acceleration magnitude

$\mathbf{P}(t)$, (P_x, P_y, P_z) — perturbing acceleration

e — orbital eccentricity

m — (1) mass

(2) in Section C.1 of Chapter III, the ratio of the mean motions of the Earth and the Moon ($m = 0.07480133$)

(3) in Chapter VI, the fraction of the total time that the control is on (See page 76.)

s — Laplace transform variable

t — time

γ_L — distance ratio (See Figure 2.3 and page 10.)

μ — normalized mass parameter (See pages 5 and 6.)

ν — see Equation 2.34

(1) for eccentricity contribution, see Equation 2.6

(2) for Sun's effect in the Earth-Moon system, see Equation 3.32

ρ — see Equation 2.33

(1) for eccentricity contribution, see Equation 2.5

(2) for Sun's effect in the Earth-Moon system, see Equation 3.31

ω — frequency

$\odot$ Sun

$\oplus$ Earth

$\rightthreetimes$ Moon

Note: A numerical subscript is added to the symbols B_L, C_L, D_L, and γ_L for a particular libration point; e.g., B_{L1} refers to L_1.

Units

Unless other units are specified, the normalized units of the restricted three-body problem will prevail. These normalized units are defined on pages 5 and 6. Conversion factors for the normalized units are given in Tables 2.7, 2.8, 2.9, and 2.10. (See explanation on page 23 and following pages.)

Accelerations are frequently expressed in Earth gravity units ($g \equiv 9.81$ m/sec^2). Note that 1 fps/yr $\cong$ $1 \times 10^{-9} g$.

THE CONTROL AND USE OF LIBRATION-POINT SATELLITES*

by
Robert W. Farquhar
Goddard Space Flight Center

CHAPTER I

INTRODUCTION

A. Problem Statement

The five equilibrium solutions of the restricted three-body problem have intrigued mathematicians for many years. More recently these solutions have aroused the interest of engineers as well. The locations of these "libration points" relative to a rotating two-body system are essentially constant; three of them are located along the line joining the two primary bodies, while the other two form equilateral triangles with the two bodies. A satellite placed at one of these points with the proper velocity will be in equilibrium because the gravitational and centripetal accelerations acting on the satellite will cancel each other out. However, the three collinear points are unstable, and the equilateral-triangle points are only quasi-stable. Therefore, some form of translation control will usually be required to maintain the satellite's position in the vicinity of a libration point. This "station-keeping" problem is complicated by perturbative accelerations and additional control functions that are dictated by mission constraints. The primary objective of this research is to develop general analytical relationships for these control requirements.

A secondary objective is to examine critically, and in some cases to modify, existing proposals for libration-point satellite missions. This aim will be supplemented by new suggestions for possible applications of libration-point satellites. These mission analyses are needed to define various control problems and to provide motivation for the present research.

Attitude control, analysis of transfer trajectories, propulsion systems, and measurement techniques are beyond the scope of this study and are only discussed in a cursory manner.

*The information presented herein was submitted as a thesis in partial fulfillment of the requirements for the degree of Doctor of Philosophy in the Astronautical Sciences, Stanford University, Stanford, California, July 1968.

B. Previous Contributions

Since their discovery by Lagrange in 1772, the libration points of the restricted three-body problem have been a favorite topic for researchers in celestial mechanics. Although this subject has been treated extensively, with significant contributions by Hill, Darwin, Brown, Moulton, Strömgren, and others, new papers are being published at an increasing rate. With the exception of a few perturbation studies, most of this work has little direct bearing on the main problems of the present study. However, some useful results can be gleaned from the theoretical literature. An exhaustive list of references can be found in the recent treatise by Szebehely (Reference 1). A less extensive list, but one that is primarily concerned with libration points, is included in the survey paper by Steg and De Vries (Reference 2).

In sharp contrast to the vast literature concerning the classical problem, only six references that treat the problem of *control* of a libration-point satellite could be found. For an unstable collinear libration point of the Earth-Moon system, a pioneering paper by Colombo (Reference 3) has shown that

(1) To the first order, this point is an exact solution of a restricted four-body problem (Sun, Earth, Moon, and satellite).

(2) It is possible to use a simple linear feedback control for position stabilization.

(3) It is possible to obtain the acceleration needed for position and attitude stabilization of a libration-point satellite by simply varying the magnitude and direction of a solar sail.

It should be noted that the analysis and the design of the feedback control mentioned by Colombo are not treated in his paper.

An interesting paper by Dusek (Reference 4) has shown that artificial libration points can be generated by constant low-thrust forces. Dusek also proved that, by varying these forces as a function of the satellite's position, the motion in the vicinity of a point is bounded. A special class of these artificial libration points, the "isosceles-triangle points," will be considered in the present study.

Dual-axis feedback controls have been treated by Fleming (Reference 5) and by Paul and Shapiro (Reference 6). Fleming used an original method to design linear and nonlinear controls for a satellite in the vicinity of an equilateral-triangle point. Paul and Shapiro determined general Routh stability conditions for all five of the classical libration points. However, the analysis of Paul and Shapiro was limited to three rather restricted controls.

For a satellite in the vicinity of a collinear libration point, this present author (Reference 7) has shown that a single-axis linear control using only range and range-rate measurements will guarantee asymptotic stability. The station-keeping cost for this control was given as a function of the measurement noise. Some special controls that are needed for an application were also presented.

In a recent paper, Kononenko (Reference 8) used Pontryagin's maximum principle to determine the optimal trajectory between a libration point and some initial point in the vicinity of the libration point. It was assumed that the satellite was equipped with an engine of limited power.

Applications for libration-point satellites have been suggested in a number of papers (References 7 and 9 to 18). A discussion of some of these proposals will be presented in Chapter VIII.

C. Contributions of This Research

This study is a basic introduction to the libration-point satellite control problem. Most results are presented in a general analytical form and can readily be adapted to a particular application. Because the most interesting libration-point satellite applications make use of the collinear points, the major portion of this research deals with these points. Some preliminary results of this study have already been published by the present author (References 7 and 16), but more details are given here.

The following paragraphs present in summary form the principal results of this research.

In Chapter II, general equations of motion in the vicinity of a libration point (classical and artificial) are formulated, and numerical data for many of the collinear libration points of the Solar System are presented to facilitate the application of general results to specific cases.

Chapter III develops the concept of nominal path control. Also, analytical estimates for corrections to a small quasi-periodic orbit around a collinear point are given; effects of nonlinearity, eccentricity, and perturbations are considered; and examples of gravitational perturbations, including a new "equilibrium solution" of the restricted four-body problem (Sun, Earth, Moon, and satellite), are presented.

Simple linear feedback controls for collinear and equilateral-triangle points are analyzed, and Floquet stability investigations for certain cases are presented in Chapter IV.

In Chapter V, analytical estimates of station-keeping costs at collinear points are presented, costs are given as functions of the measurement noise, and a solar sail control technique at the Earth-Moon collinear points is discussed.

A limit-cycle analysis for an on-off control system at a collinear point is presented in Chapter VI. A closed-form solution is obtained for an important special case, and the stability of the limit cycle is also examined. An approximate design technique for the general case is presented as well.

In Chapter VII, a method is presented for stabilizing the position of the mass center of a cable-connected satellite at an unstable collinear libration point by simply changing the length of the cable with an internal device.

In Chapter VIII, a novel method for maintaining a continuous communication link between the Earth and the far side of the Moon is presented, and other new applications for libration-point satellites are also proposed.

CHAPTER II

PRELIMINARY DEVELOPMENTS

In this chapter, the equations of motion in the vicinity of libration points are formulated. The libration-point concept is traced to its origin in the restricted three-body problem, and various assumptions, approximations, and modifications are discussed. Relevant numerical data for many of the collinear points are listed in the final section.

A. The Restricted Three-Body Problem

1. Equations of Motion

Consider the motion of an infinitesimal body in the gravitational field of two finite bodies (e.g., Earth and Moon) revolving around their common barycenter in elliptical orbits. It is assumed that the infinitesimal body does not influence the motion of the two larger bodies, hence the terminology, *restricted* three-body problem. The geometry for this problem is shown in Figure 2.1. Here, the two finite bodies are located at P_1 and P_2, while the infinitesimal body is at P_3. An inertial reference system (ξ_0, η_0, ζ_0) is shown with its origin at the barycenter of the two finite bodies, and its ζ_0-axis normal to their orbital plane. A rotating coordinate system (ξ, η, ζ), with its ξ-axis passing through P_1 and P_2, is also introduced. From the figure, it is obvious that

$$\xi_0 = \xi \cos \theta - \eta \sin \theta,$$

$$\eta_0 = \xi \sin \theta + \eta \cos \theta, \tag{2.1}$$

and

$$\zeta_0 = \zeta.$$

Differentiation of Equation 2.1 with respect to time gives

$$\dot{\xi}_0 = (\dot{\xi} - \dot{\theta}\eta) \cos \theta - (\dot{\eta} + \dot{\theta}\xi) \sin \theta,$$

$$\dot{\eta}_0 = (\dot{\xi} - \dot{\theta}\eta) \sin \theta + (\dot{\eta} + \dot{\theta}\xi) \cos \theta, \tag{2.2}$$

and

$$\dot{\zeta}_0 = \dot{\zeta}.$$

To facilitate analytical manipulations, the following quantities are defined to be unity:

(1) The mean distance between P_1 and P_2.

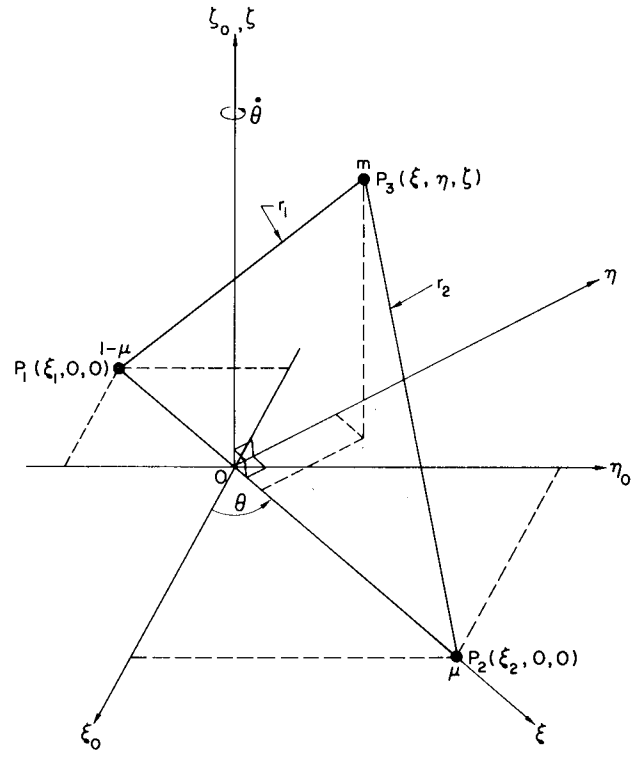

Figure 2.1–Geometry for the restricted three-body problem.

(2) The mean angular rate of the finite bodies about the barycenter.

(3) The sum of the masses of the two finite bodies. The larger mass at P_1 is taken as $1 - \mu$, while the smaller mass at P_2 is μ. Therefore, because the mass ratio is $M_R = (1 - \mu)/\mu$, then $\mu = 1/(1 + M_R)$.

Unless other units are specified, this normalization will be used throughout this research.

Because the motion of the two finite bodies can be obtained from the solution of the two-body problem, it is possible to write the distance $|\overrightarrow{P_1P_2}|$ and the angular rate $\dot{\theta}$ as power series in the eccentricity. These series are (Reference 19)

$$|\overrightarrow{P_1P_2}| = (\xi_2 - \xi_1) \equiv R = 1 + \rho \tag{2.3}$$

and

$$\dot{\theta} = 1 + \nu, \tag{2.4}$$

where

$$\rho = -e \cos (t + \phi) + \frac{e^2}{2}[1 - \cos 2(t + \phi)] + O(e^3) \tag{2.5}$$

and

$$\nu = 2e \cos (t + \phi) + \frac{5}{2}e^2 \cos 2(t + \phi) + O(e^3). \tag{2.6}$$

The phase angle ϕ is just the true anomaly at $t = 0$. It should be noted that these series converge rapidly when e is small, but are divergent when $e > 0.6627\ldots$.

Using Equation 2.2, the kinetic energy of the infinitesimal body can be written as

$$T = \frac{m}{2}\left[\dot{\xi}_0^2 + \dot{\eta}_0^2 + \dot{\zeta}_0^2\right] = \frac{m}{2}\left[(\dot{\xi} - \dot{\theta}\eta)^2 + (\dot{\eta} + \dot{\theta}\xi)^2 + \dot{\zeta}^2\right] \tag{2.7}$$

The potential energy is

$$U = -m\left[\frac{(1 - \mu)}{r_1} + \frac{\mu}{r_2}\right], \tag{2.8}$$

where

$$r_1^2 = \left(\xi - \xi_1\right)^2 + \eta^2 + \zeta^2 \tag{2.9}$$

and

$$r_2^2 = \left(\xi - \xi_2\right)^2 + \eta^2 + \zeta^2. \tag{2.10}$$

Forming the Lagrangian $L = T - U$, the equations of motion are obtained by Lagrange's method. This gives

$$\ddot{\xi} - 2\dot{\theta}\dot{\eta} = \ddot{\theta}\eta + \dot{\theta}^2\xi - \frac{(1-\mu)}{r_1^3}(\xi - \xi_1) - \frac{\mu}{r_2^3}(\xi - \xi_2),$$

$$\ddot{\eta} + 2\dot{\theta}\dot{\xi} = -\ddot{\theta}\xi + \dot{\theta}^2\eta - \left[\frac{(1-\mu)}{r_1^3} + \frac{\mu}{r_2^3}\right]\eta, \tag{2.11}$$

and

$$\ddot{\zeta} = -\left[\frac{(1-\mu)}{r_1^3} + \frac{\mu}{r_2^3}\right]\zeta.$$

For circular orbits ($e = 0$) of the two finite bodies, Equation 2.11 becomes

$$\ddot{\xi} - 2\dot{\eta} = \xi - \frac{(1-\mu)}{r_1^3}(\xi - \xi_1) - \frac{\mu}{r_2^3}(\xi - \xi_2),$$

$$\ddot{\eta} + 2\dot{\xi} = \eta - \left[\frac{(1-\mu)}{r_1^3} + \frac{\mu}{r_2^3}\right]\eta, \tag{2.12}$$

and

$$\ddot{\zeta} = -\left[\frac{(1-\mu)}{r_1^3} + \frac{\mu}{r_2^3}\right]\zeta.$$

2. Jacobian Constant and the Surfaces of Zero Relative Velocity

It is the purpose of this section to elucidate an important conservation principle of the restricted three-body problem. Denoting generalized coordinates and velocities by q's and $\dot{q}$'s, respectively, the kinetic energy of a system can be written as

$$T = T(q, \dot{q}, t) = T_2 + T_1 + T_0, \tag{2.13}$$

where

$$T_2 \equiv \sum_{i,\, j=1}^{n} \alpha_{ij}(q, t)\dot{q}_i\dot{q}_j, \tag{2.14}$$

$$T_1 \equiv \sum_{i=1}^{n} \beta_i(q, t)\dot{q}_i, \tag{2.15}$$

and

$$T_0 \equiv T_0(q, t). \tag{2.16}$$

Taking the potential energy as

$$U = U(q, t) \tag{2.17}$$

and using the definitions

$$L \equiv T - U \quad \text{(Lagrangian)}, \tag{2.18}$$

$$E \equiv T + U \quad \text{(total energy)}, \tag{2.19}$$

and

$$H \equiv \sum_{i=1}^{n} \dot{q}_i \frac{\partial L}{\partial \dot{q}_i} - L \quad \text{(Hamiltonian)}, \tag{2.20}$$

it follows that

$$H = T_2 - T_0 + U = E - T_1 - 2T_0. \tag{2.21}$$

It is important to note that, in general, the Hamiltonian is *not* equal to the total energy. Although this result is classical, it is often forgotten because "conventional" dynamical systems usually have a kinetic energy of the form $T = T_2$.

For the restricted three-body problem, it can be seen from Equation 2.7 that the kinetic energy in the inertial coordinates is $T = T_2(\dot{q})$, and therefore $H = E$. If, instead, the rotating coordinates are employed, the kinetic energy for a unit mass is $T = T_2 + T_1 + T_0$, where

$$T_2 = \frac{1}{2}(\dot{\xi}^2 + \dot{\eta}^2 + \dot{\zeta}^2), \tag{2.22}$$

$$T_1 = \dot{\theta}(\xi\dot{\eta} - \eta\dot{\xi}), \tag{2.23}$$

and

$$T_0 = \frac{1}{2}\dot{\theta}^2(\xi^2 + \eta^2). \tag{2.24}$$

Therefore, in the rotating coordinate system, $H \neq E$.

If the two finite bodies are in circular orbits, $\dot{\theta} = 1$, and an interesting relation can be found. For this special case, the potential energy in the rotating coordinates is $U = U(q)$ and $\dot{H} = 0$. Although the Hamiltonian is a constant of the motion, total energy is not conserved* because $H \neq E$. This Hamiltonian is related to the "Jacobian constant" C ($H = -\frac{1}{2}C$), which is usually found in the form

$$V^2 = 2W - C, \tag{2.25}$$

where

$$V^2 = \dot{\xi}^2 + \dot{\eta}^2 + \dot{\zeta}^2$$

and

$$W \equiv T_0 - U = \frac{1}{2}(\xi^2 + \eta^2) + \frac{(1-\mu)}{r_1} + \frac{\mu}{r_2}. \tag{2.26}$$

By determining the Jacobian constant from the initial conditions of the infinitesimal body, bounds can be placed on the region of its subsequent motion. Because V^2 is always positive, Equation 2.25 shows that motion is possible only so long as $2W > C$. Taking $V = 0$ (zero relative velocity) and making use of Equations

*This can also be seen by using inertial coordinates, where $U = U(q, t)$. It then follows that $\dot{H} \neq 0$, and because $H = E$, total energy is not conserved.

2.25 and 2.26, surfaces of zero relative velocity corresponding to different values of C can be constructed in the configuration space.*

The curves of zero relative velocity formed by the intersection of these surfaces with the orbital plane of the two finite bodies are depicted in Figure 2.2 for the Earth-Moon system ($\mu = 0.0121507$). Here the Jacobian constants are $C_0 = 3.2880$, $C_1 = 3.1883$, $C_2 = 3.1724$, $C_3 = 3.0121$, $C_4 = 2.9980$, and $C_5 = 2.9880$. As noted earlier, the possible regions of motion for an infinitesimal body with given initial conditions can be determined from its Jacobian constant. For example, if the body is initially located near the surface of the Earth and its Jacobian constant is greater than C_0, it can never leave the region bounded by the C_0 curve around the Earth. On the other hand, if its Jacobian constant is C_4, motion can take place everywhere except for the region enclosed by the C_4 curve. Figure 2.2 is a contour map of the modified potential field of the Earth and Moon in the rotating coordinates. The regions surrounding the Earth and Moon in this modified potential field can be viewed as valleys and the point at L_4 as a mountain peak. Notice that saddle surfaces exist at L_1, L_2, and L_3.

Returning to the more realistic case in which the two finite bodies are in elliptical orbits, it can be seen that even for rotating coordinates, $U = U(q, t)$ and $\dot{H} \neq 0$. This means that the Jacobian constant does not exist in the elliptical case, and the usefulness of Figure 2.2 may be severely limited. However, it is the opinion of this author that Figure 2.2 is still useful for intuitive reasoning when the eccentricity is small and time intervals are relatively short. For a discussion of this problem, see References 20 to 22.

3. Libration Points

It is well known that there are five equilibrium solutions of Equation 2.11. These equilibrium points are located in the orbital plane of the two finite bodies, and their general configuration is shown in Figure 2.3. Two of the points, L_4 and L_5, form an equilateral triangle with the finite bodies, while the remaining three, L_1, L_2, and L_3, are collinear. A common name for these points and the one that will be used here is "libration points."

The existence of these libration points is reasonable from a purely physical standpoint because they are points where the gravitational and centripetal accelerations are balanced in the rotating coordinate system. In the circular restricted three-body problem, these points will always be stationary. However, in the elliptical case, the distances from the finite bodies will vary periodically while the equilateral-triangle and collinear configurations are maintained. A thorough discussion of the equilibrium solutions for both the circular and elliptical cases can be found in Reference 1.

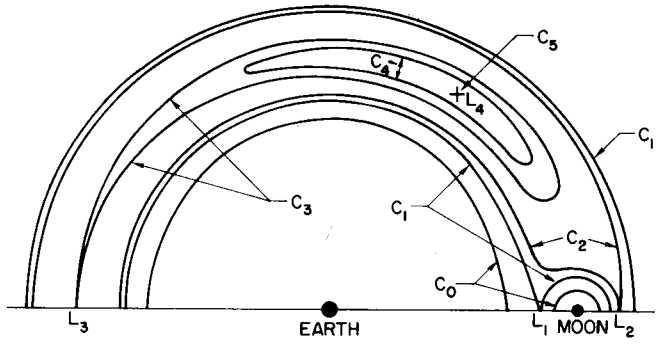

Figure 2.2–Curves of zero relative velocity for the Earth-Moon system.

From Figure 2.3, it can be seen that the collinear libration points are located at distances $\gamma_L R$ from the finite bodies.† The constant γ_L is

*Details of this construction as well as many fine examples for various values of μ can be found in Reference 1.
†An additional subscript is added for a particular point; e.g., γ_{L1} refers to L_1.

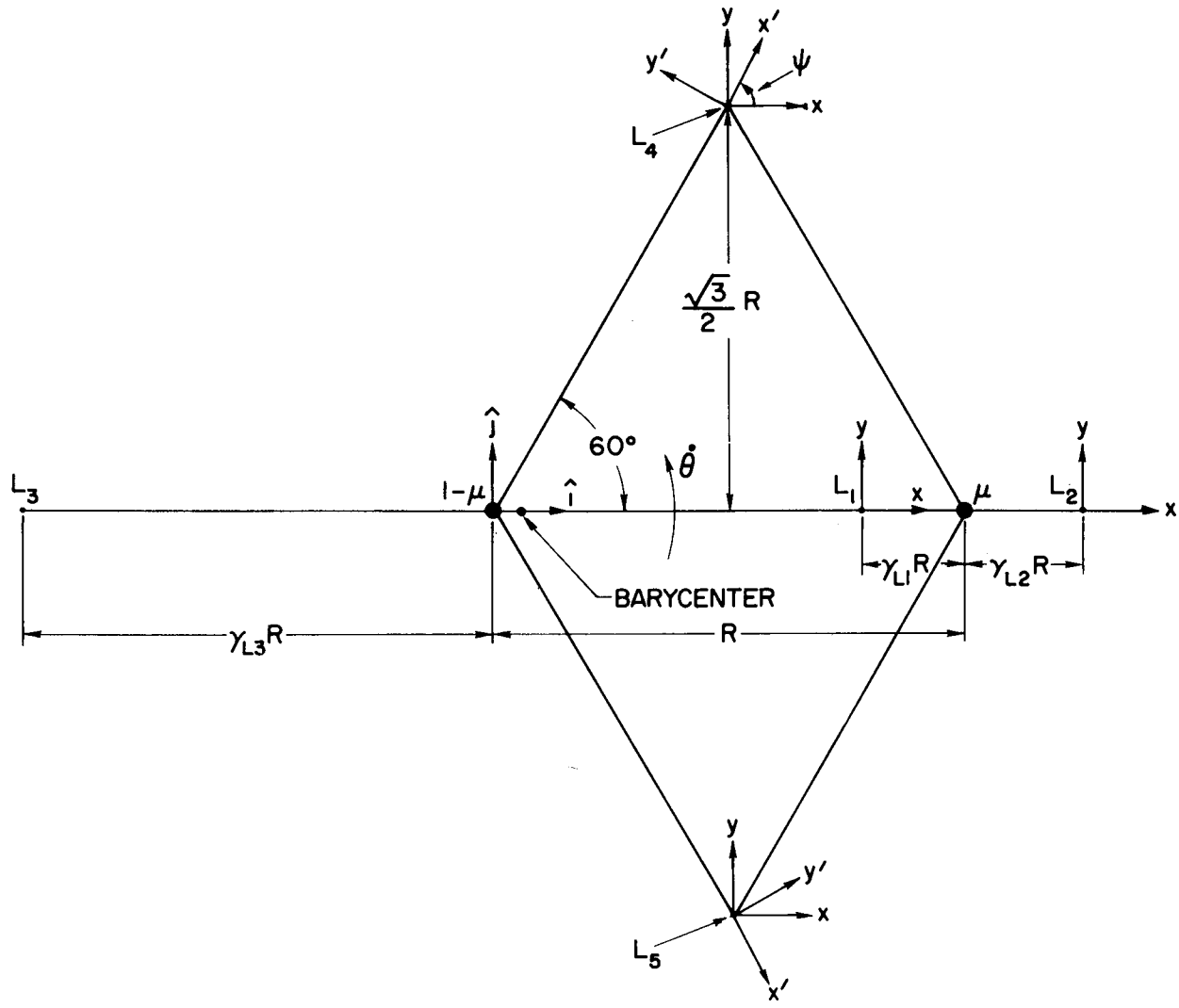

Figure 2.3–Libration-point geometry.

obtained by finding the *real root* of a certain quintic equation. The quintic equations for the three collinear points are (Reference 1)

$$\gamma_{L1}^5 - (3-\mu)\gamma_{L1}^4 + (3-2\mu)\gamma_{L1}^3 - \mu\gamma_{L1}^2 + 2\mu\gamma_{L1} - \mu = 0, \tag{2.27}$$

$$\gamma_{L2}^5 + (3-\mu)\gamma_{L2}^4 + (3-2\mu)\gamma_{L2}^3 - \mu\gamma_{L2}^2 - 2\mu\gamma_{L2} - \mu = 0, \tag{2.28}$$

and

$$\gamma_{L3}^5 + (2+\mu)\gamma_{L3}^4 + (1+2\mu)\gamma_{L3}^3 - (1-\mu)\gamma_{L3}^2 - 2(1-\mu)\gamma_{L3} - (1-\mu) = 0. \tag{2.29}$$

Series solutions for γ_L are also available, but are not recommended for numerical computations at L_1 and L_2 where the convergence is poor. However, abbreviated versions of the series at L_1 and L_2 are sometimes useful for analytic approximations. The series for L_1 and L_2 are (Reference 1)

$$\gamma_{L1} = \left(\frac{\mu}{3}\right)^{1/3}\left[1 - \frac{1}{3}\left(\frac{\mu}{3}\right)^{1/3} - \frac{1}{9}\left(\frac{\mu}{3}\right)^{2/3} + \ldots\right] \tag{2.30}$$

and

$$\gamma_{L2} = \left(\frac{\mu}{3}\right)^{1/3}\left[1 + \frac{1}{3}\left(\frac{\mu}{3}\right)^{1/3} - \frac{1}{9}\left(\frac{\mu}{3}\right)^{2/3} + \ldots\right]. \tag{2.31}$$

The series solution for L_3 converges very rapidly, and because the real root of Equation 2.29 is near +1, it is preferred for numerical computations. This series is given by (Reference 1)

$$\gamma_{L3} = 1 + \epsilon\left(1 + \frac{23}{84}\epsilon^2 + \frac{23}{84}\epsilon^3 + \frac{761}{2352}\epsilon^4 + \frac{3163}{7056}\epsilon^5 + \frac{30\,703}{49\,392}\epsilon^6\right) + O(\epsilon^8), \tag{2.32}$$

where $\epsilon \equiv 7\mu/12$.

B. Equations of Motion in the Vicinity of Libration Points

In this section, the equations of motion in the vicinity of libration points are obtained in a general form that is readily adaptable to the perturbation analyses of Chapter III. Although the derivation could proceed directly from Equation 2.11, a more basic approach is followed here. All of the classical libration points with the exception of L_3, which is not too interesting from the standpoint of possible applications, are treated. In addition, an artificial libration point that forms an isosceles triangle with the two finite bodies is examined.

1. Collinear Points

In Figure 2.3, the distance R and the angular rate $\dot{\theta}$ are defined as

$$R = 1 + \rho(t) \tag{2.33}$$

and

$$\dot{\theta} = 1 + \nu(t), \tag{2.34}$$

where the quantities $\rho(t)$ and $\nu(t)$ are functions of time that arise from the orbital eccentricity of the finite bodies and perturbations from bodies external to the primary two-body system. The unit vectors **i** and **j** are fixed in the rotating reference frame, which means that

$$\frac{d\mathbf{i}}{dt} = (1 + \nu)\mathbf{j}$$

and

$$\frac{d\mathbf{j}}{dt} = -(1 + \nu)\mathbf{i}. \tag{2.35}$$

A right-handed triad is formed by taking the cross product $\mathbf{k} = \mathbf{i} \times \mathbf{j}$.

From Figure 2.3, it is evident that, for a satellite (infinitesimal mass) in the vicinity of either L_1 or L_2, the position vector relative to the larger body $(1 - \mu)$ is*

$$\mathbf{r} = \left[(1 \pm \gamma_L)(1 + \rho) + x\right]\mathbf{i} + y\mathbf{j} + z\mathbf{k}. \tag{2.36}$$

*Whenever double signs appear in this section, the upper sign will hold at L_2, and the lower sign at L_1.

(The position vector relative to the libration point is $\mathbf{r}_L = x\mathbf{i} + y\mathbf{j} + z\mathbf{k}$.) Differentiation of Equation 2.36 yields the velocity vector (relative to the larger mass)

$$\dot{\mathbf{r}} = \left[(1 \pm \gamma_L)\dot{\rho} + \dot{x} - (1 + \nu)y\right]\mathbf{i} + \left\{(1 + \nu)\left[(1 \pm \gamma_L)(1 + \rho) + x\right] + \dot{y}\right\}\mathbf{j} + \dot{z}\mathbf{k}. \tag{2.37}$$

The position vector for the smaller finite body is

$$\mathbf{R} = (1 + \rho)\mathbf{i}. \tag{2.38}$$

For a satellite of unit mass, the kinetic energy is $T = \frac{1}{2}\dot{\mathbf{r}} \cdot \dot{\mathbf{r}}$, and the effective potential energy (for motion relative to the larger mass) is given by

$$\begin{aligned} U &= -\frac{(1 - \mu)}{|\mathbf{r}|} - \mu\left[\frac{1}{|\mathbf{r} - \mathbf{R}|} - \frac{\mathbf{R} \cdot \mathbf{r}}{|\mathbf{R}|^3}\right] \\ &= -\frac{(1 - \mu)}{r_1} - \mu\left\{\frac{1}{r_2} - \frac{\left[(1 \pm \gamma_L)(1 + \rho) + x\right]}{(1 + \rho)^2}\right\}, \end{aligned} \tag{2.39}$$

where

$$r_1^2 = \left[(1 \pm \gamma_L)(1 + \rho) + x\right]^2 + y^2 + z^2 \tag{2.40}$$

and

$$r_2^2 = \left[\gamma_L(1 + \rho) \pm x\right]^2 + y^2 + z^2. \tag{2.41}$$

Forming the Lagrangian $L = T - U$, standard manipulations lead to the equations of motion

$$\begin{aligned} \ddot{x} - 2(1 + \nu)\dot{y} + (1 \pm \gamma_L)\ddot{\rho} - \dot{\nu}y &= (1 + \nu)^2\left[(1 \pm \gamma_L)(1 + \rho) + x\right] \\ &\quad - \frac{(1 - \mu)}{r_1^3}\left[(1 \pm \gamma_L)(1 + \rho) + x\right] \\ &\quad \mp \frac{\mu}{r_2^3}\left[\gamma_L(1 + \rho) \pm x\right] - \frac{\mu}{(1 + \rho)^2}, \\ \ddot{y} + 2(1 + \nu)\left[(1 \pm \gamma_L)\dot{\rho} + \dot{x}\right] + \dot{\nu}\left[(1 \pm \gamma_L)(1 + \rho) + x\right] &= (1 + \nu)^2 y - \left[\frac{(1 - \mu)}{r_1^3} + \frac{\mu}{r_2^3}\right]y, \end{aligned} \tag{2.42}$$

and

$$\ddot{z} = -\left[\frac{(1 - \mu)}{r_1^3} + \frac{\mu}{r_2^3}\right]z.$$

Expanding Equation 2.42 in a power series* including third-order terms, a moderate amount of algebra leads to

*The complete series converges in a region that is common to the interiors of two spheres. One sphere is centered at $1 - \mu$ and has a radius of $\sqrt{2}(1 \pm \gamma_L)(1 + \rho)$; the other is centered at μ and has a radius of $\sqrt{2}\gamma_L(1 + \rho)$.

$$\ddot{x} - 2(1+\nu)\dot{y} = \left[(1+\nu)^2 + 2(1+\rho)^{-3}B_L\right]x + \dot{\nu}y$$
$$\mp \frac{3}{2}C_L(1+\rho)^{-4}\left[2x^2 - (y^2+z^2)\right]$$
$$+ 2D_L(1+\rho)^{-5}\left[2x^2 - 3(y^2+z^2)\right]x$$
$$- (1 \pm \gamma_L)\left\{\ddot{\rho} - (1+\rho)^{-2}\left[(1+\nu)^2(1+\rho)^3 - 1\right]\right\}, \tag{2.43a}$$

$$\ddot{y} + 2(1+\nu)\dot{x} = -\dot{\nu}x + \left[(1+\nu)^2 - (1+\rho)^{-3}B_L\right]y \pm 3C_L(1+\rho)^{-4}xy$$
$$- \frac{3}{2}D_L(1+\rho)^{-5}\left[4x^2 - (y^2+z^2)\right]y$$
$$- (1 \pm \gamma_L)\left[2(1+\nu)\dot{\rho} + (1+\rho)\dot{\nu}\right], \tag{2.43b}$$

and

$$\ddot{z} = -(1+\rho)^{-3}B_L z \pm 3C_L(1+\rho)^{-4}xz$$
$$- \frac{3}{2}D_L(1+\rho)^{-5}\left[4x^2 - (y^2+z^2)\right]z, \tag{2.43c}$$

where

$$B_L \equiv \left[\frac{(1-\mu)}{(1 \pm \gamma_L)^3} + \frac{\mu}{\gamma_L^3}\right], \tag{2.44}$$

$$C_L \equiv \left[\frac{\mu}{\gamma_L^4} \pm \frac{(1-\mu)}{(1 \pm \gamma_L)^4}\right], \tag{2.45}$$

and

$$D_L \equiv \left[\frac{(1-\mu)}{(1 \pm \gamma_L)^5} + \frac{\mu}{\gamma_L^5}\right]. \tag{2.46}$$

In Reference 23, it is shown that $B_L > 1$ for all values of μ. For $\mu \ll 1$, Equations 2.30 and 2.31 show that $\mu \cong 3\gamma_L^3$. In this instance, the coefficients defined in Equations 2.44 to 2.46 are $B_L \cong 4$, $C_L \cong 3/\gamma_L$, and $D_L \cong 3/\gamma_L^2$.

The accuracy of the derivation can be checked by verifying that the L_1 and L_2 points are equilibrium solutions in the elliptical case. For this to be true, the expressions for ρ and ν given in Equations 2.5 and 2.6 must vanish when they are substituted into the final terms of Equations 2.43a and 2.43b. Restricting this verification to the linear terms, it is only necessary to have

$$3\rho - \ddot{\rho} + 2\nu = 0$$

and (2.47)

$$2\dot{\rho} + \dot{\nu} = 0.$$

It can be seen by inspection that the linear eccentricity terms of Equations 2.5 and 2.6 satisfy Equation 2.47.

A linearized version of Equation 2.43 is sufficient for many applications. If the quantities ρ and ν are also neglected, Equation 2.43 reduces to

$$\ddot{x} - 2\dot{y} - (2B_L + 1)x = 0, \tag{2.48a}$$

$$\ddot{y} + 2\dot{x} + (B_L - 1)y = 0, \tag{2.48b}$$

and

$$\ddot{z} + B_L z = 0. \tag{2.48c}$$

It is readily seen that the motion perpendicular to the xy-plane is simple harmonic with frequency $\sqrt{B_L}$. The motion in the xy-plane is coupled, and the characteristic equation is given by

$$s^4 - (B_L - 2)s^2 - (2B_L + 1)(B_L - 1) = 0. \tag{2.49}$$

This equation possesses two real roots, equal in magnitude, but opposite in sign. The two remaining roots are pure imaginaries. Because a positive real root exists, the collinear points are unstable.

2. Equilateral-Triangle Points

The geometry for satellite motion in the vicinity of the equilateral-triangle points is shown in Figure 2.3. Equations 2.33, 2.34, 2.35, and 2.38 are still valid for this section, and the position and velocity vectors relative to the larger body are*

$$\mathbf{r} = \left[\frac{1}{2}(1 + \rho) + x\right]\mathbf{i} + \left[\pm\frac{\sqrt{3}}{2}(1 + \rho) + y\right]\mathbf{j} + z\mathbf{k} \tag{2.50}$$

and

$$\dot{\mathbf{r}} = \left\{\frac{1}{2}\dot{\rho} + \dot{x} - (1 + \nu)\left[\pm\frac{\sqrt{3}}{2}(1 + \rho) + y\right]\right\}\mathbf{i} + \left\{\pm\frac{\sqrt{3}}{2}\dot{\rho} + \dot{y} + (1 + \nu)\left[\frac{1}{2}(1 + \rho) + x\right]\right\}\mathbf{j} + \dot{z}\mathbf{k}. \tag{2.51}$$

(The position vector relative to the libration point is $\mathbf{r}_L = x\mathbf{i} + y\mathbf{j} + z\mathbf{k}$.) The kinetic energy $T = \frac{1}{2}\dot{\mathbf{r}} \cdot \dot{\mathbf{r}}$ and effective potential energy

$$U = -\frac{(1 - \mu)}{r_1} - \mu\left\{\frac{1}{r_2} - \frac{\left[\frac{1}{2}(1 + \rho) + x\right]}{(1 + \rho)^2}\right\} \tag{2.52}$$

where

$$r_1^2 = \left[\frac{1}{2}(1 + \rho) + x\right]^2 + \left[\pm\frac{\sqrt{3}}{2}(1 + \rho) + y\right]^2 + z^2 \tag{2.53}$$

and

$$r_2^2 = \left[-\frac{1}{2}(1 + \rho) + x\right]^2 + \left[\pm\frac{\sqrt{3}}{2}(1 + \rho) + y\right]^2 + z^2, \tag{2.54}$$

are used to form the Lagrangian $L = T - U$, which leads to the equations of motion

*Whenever double signs appear in this section, the upper sign will hold at L_4, and the lower sign at L_5.

$$\ddot{x} - 2(1+\nu)\dot{y} = -\frac{1}{2}\ddot{\rho} \pm \sqrt{3}(1+\nu)\dot{\rho} \pm \frac{\sqrt{3}}{2}(1+\rho)\dot{\nu} + \frac{1}{2}(1+\rho)(1+\nu)^2$$
$$+ (1+\nu)^2 x + \dot{\nu} y - \frac{(1-\mu)}{r_1^3}\left[\frac{1}{2}(1+\rho) + x\right]$$
$$- \frac{\mu}{r_2^3}\left[-\frac{1}{2}(1+\rho) + x\right] - \frac{\mu}{(1+\rho)^2},$$

$$\ddot{y} + 2(1+\nu)\dot{x} = \mp \frac{\sqrt{3}}{2}\ddot{\rho} - (1+\nu)\dot{\rho} - \frac{1}{2}(1+\rho)\dot{\nu} \pm \frac{\sqrt{3}}{2}(1+\rho)(1+\nu)^2 \qquad (2.55)$$
$$- \dot{\nu} x + (1+\nu)^2 y - \left[\frac{(1-\mu)}{r_1^3} + \frac{\mu}{r_2^3}\right]\left[\pm \frac{\sqrt{3}}{2}(1+\rho) + y\right],$$

and

$$\ddot{z} = -\left[\frac{(1-\mu)}{r_1^3} + \frac{\mu}{r_2^3}\right] z.$$

A power series expansion* of Equation 2.55 including terms up to the third order is given by

$$\ddot{x} - 2(1+\nu)\dot{y} = \left[(1+\nu)^2 - \frac{1}{4}(1+\rho)^{-3}\right] x + \left[\dot{\nu} \pm \frac{3\sqrt{3}}{4}(1-2\mu)(1+\rho)^{-3}\right] y$$
$$+ (1+\rho)^{-4}\left[\frac{21}{16}(1-2\mu)x^2 \mp \frac{3\sqrt{3}}{8}xy - \frac{33}{16}(1-2\mu)y^2 + \frac{3}{4}(1-2\mu)z^2\right]$$
$$- (1+\rho)^{-5}\left[\frac{37}{32}x^3 \pm \frac{75}{32}\sqrt{3}(1-2\mu)x^2 y - \frac{123}{32}xy^2 \mp \frac{45}{32}\sqrt{3}(1-2\mu)y^3\right.$$
$$\left. + \frac{3}{8}xz^2 \pm \frac{15\sqrt{3}}{8}yz^2\right] - \frac{1}{2}\ddot{\rho} \pm \sqrt{3}(1+\nu)\dot{\rho} \pm \frac{\sqrt{3}}{2}(1+\rho)\dot{\nu}$$
$$- \frac{1}{2}(1+\rho)^{-2}\left[1 - (1+\rho)^3(1+\nu)^2\right], \qquad (2.56a)$$

$$\ddot{y} + 2(1+\nu)\dot{x} = \left[\pm \frac{3\sqrt{3}}{4}(1-2\mu)(1+\rho)^{-3} - \dot{\nu}\right] x + \left[(1+\nu)^2 + \frac{5}{4}(1+\rho)^{-3}\right] y$$
$$- (1+\rho)^{-4}\left[\pm \frac{3}{16}\sqrt{3}x^2 + \frac{33}{8}(1-2\mu)xy \pm \frac{9}{16}\sqrt{3}y^2 \mp \frac{3\sqrt{3}}{4}z^2\right]$$
$$- (1+\rho)^{-5}\left[\pm \frac{25}{32}\sqrt{3}(1-2\mu)x^3 - \frac{123}{32}x^2 y \mp \frac{135}{32}\sqrt{3}(1-2\mu)xy^2\right.$$
$$\left. - \frac{3}{32}y^3 \mp \frac{15}{8}\sqrt{3}(1-2\mu)xz^2 - \frac{33}{8}yz^2\right] \mp \frac{\sqrt{3}}{2}\ddot{\rho} - (1+\nu)\dot{\rho}$$
$$- \frac{1}{2}(1+\rho)\dot{\nu} \mp \frac{\sqrt{3}}{2}(1+\rho)^{-2}\left[1 - (1+\rho)^3(1+\nu)^2\right], \qquad (2.56b)$$

*The complete series converges in a region that is common to the interiors of two spheres of radii $\sqrt{2}(1+\rho)$. These spheres are centered at $1-\mu$ and μ.

and

$$\ddot{z} = -(1+\rho)^{-3}z + \frac{3}{2}(1+\rho)^{-4}\left[(1-2\mu)x \pm \sqrt{3}\,y\right]z$$

$$-(1+\rho)^{-5}\left[\frac{3}{8}x^2 \pm \frac{15}{4}\sqrt{3}(1-2\mu)xy + \frac{33}{8}y^2 - \frac{3}{2}z^2\right]z. \tag{2.56c}$$

Some confidence can be put in the accuracy of this result because the eccentricity check of the previous section again leads to the conditions given in Equation 2.47.

If $\rho = \nu = 0$ and only linear terms are retained, Equation 2.56 is reduced to

$$\ddot{x} - 2\dot{y} - \frac{3}{4}x \mp \frac{3\sqrt{3}}{4}(1-2\mu)y = 0, \tag{2.57a}$$

$$\ddot{y} + 2\dot{x} \mp \frac{3\sqrt{3}}{4}(1-2\mu)x - \frac{9}{4}y = 0, \tag{2.57b}$$

and

$$\ddot{z} + z = 0. \tag{2.57c}$$

The coupling of x and y in Equations 2.57a and 2.57b can be eliminated by a coordinate rotation. This simplification will be useful when feedback controls are considered in a later chapter. The angle for this rotation is conveniently determined by expanding the modified potential function to second order (this is sufficient for linearized equations of motion) and then eliminating the xy-term that causes the coupling. The modified potential function to second order is written as

$$W \equiv T_0 - U = \frac{1}{2}\left[\left(\frac{1}{2} + x\right)^2 + \left(\pm\frac{\sqrt{3}}{2} + y\right)^2\right] - U$$

$$\cong \frac{1}{2}(3-\mu) + \frac{3}{8}\left[x^2 \pm 2\sqrt{3}(1-2\mu)xy + 3y^2\right] - \frac{1}{2}z^2. \tag{2.58}$$

It is readily verified that the xy-term of Equation 2.58 can be removed by utilizing the coordinate transformation (see Figure 2.3)*

$$x = x' \cos\psi - y' \sin\psi,$$

$$y = x' \sin\psi + y' \cos\psi, \tag{2.59}$$

and

$$z = z',$$

where

$$\tan 2\psi = \mp\sqrt{3}(1-2\mu). \tag{2.60}$$

With this transformation, Equations 2.58 and 2.57 become

$$2W = (3-\mu) + \alpha x'^2 + \beta y'^2 - z'^2 \tag{2.61}$$

*The barycenter lies on the x'-axis.

and

$$\ddot{x}' - 2\dot{y}' - \alpha x' = 0, \tag{2.62a}$$

$$\ddot{y}' + 2\dot{x}' - \beta y' = 0, \tag{2.62b}$$

and

$$\ddot{z}' + z' = 0, \tag{2.62c}$$

where

$$\alpha = \frac{3}{2}\left[1 + \sqrt{1 - 3\mu(1 - \mu)}\right] \tag{2.63}$$

and

$$\beta = \frac{3}{2}\left[1 - \sqrt{1 - 3\mu(1 - \mu)}\right]. \tag{2.64}$$

It can be seen at once that Equation 2.62c is simple harmonic with unit frequency. It is also worth noting that for $\mu \ll 1$, $\alpha \cong 3 - 9\mu/4$ and $\beta \cong 9\mu/4$.

The stability of the linearized equations of motion can be examined by writing the characteristic equation for the gyroscopically coupled portion of Equation 2.62

$$s^4 + s^2 + \alpha\beta = 0 \tag{2.65a}$$

or in terms of the mass parameter μ

$$s^4 + s^2 + \frac{27}{4}\mu(1 - \mu) = 0. \tag{2.65b}$$

The roots of this equation are pure imaginaries if $\mu < 0.03852\ldots$, and the system is neutrally stable. For $\mu > 0.03852\ldots$, the roots are complex with one pair possessing positive real parts, and the system is unstable.

3. Isosceles-Triangle Points

If a satellite moving in the mutual gravitational field of two finite bodies is equipped with a continuous thrust device, it is possible to artificially generate new equilibrium positions. This generalized libration-point concept was introduced by Dusek (Reference 4), who developed general conditions for the existence of these points and examined the stability of a variable thrust satellite in their vicinity. In this section, the equations of motion of a satellite at the generalized points that form an isosceles triangle with the two finite bodies are derived. This case was not explicitly treated by Dusek.

The geometry for a general isosceles-triangle point is given in Figure 2.4. Proceeding in the same manner as in the two previous sections, the position and velocity vectors are

$$\mathbf{r} = \left[(1 + \rho)\cos\theta + x\right]\mathbf{i} + \left[(1 + \rho)\sin\theta + y\right]\mathbf{j} + z\mathbf{k} \tag{2.66}$$

and

$$\dot{\mathbf{r}} = \left\{\dot{\rho}\cos\theta + \dot{x} - (1 + \nu)\left[(1 + \rho)\sin\theta + y\right]\right\}\mathbf{i} + \left\{\dot{\rho}\sin\theta + \dot{y} + (1 + \nu)\left[(1 + \rho)\cos\theta + x\right]\right\}\mathbf{j} + \dot{z}\mathbf{k}. \tag{2.67}$$

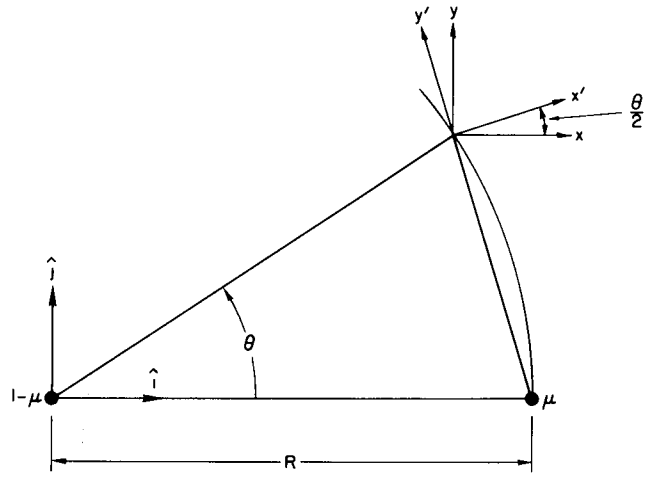

Figure 2.4–Isosceles-triangle point.

The potential energy is

$$U = -\frac{(1-\mu)}{r_1} - \mu\left\{\frac{1}{r_2} - \frac{\left[(1+\rho)\cos\theta + x\right]}{(1+\rho)^2}\right\}, \tag{2.68}$$

where

$$r_1^2 = \left[(1+\rho)\cos\theta + x\right]^2 + \left[(1+\rho)\sin\theta + y\right]^2 + z^2 \tag{2.69}$$

and

$$r_2^2 = \left[(1+\rho)(\cos\theta - 1) + x\right]^2 + \left[(1+\rho)\sin\theta + y\right]^2 + z^2. \tag{2.70}$$

This time, the equations of motion are augmented with a planar thrust acceleration (F_{cx}, F_{cy}) and are given by

$$\begin{aligned}\ddot{x} - 2(1+\nu)\dot{y} = &-\ddot{\rho}\cos\theta + 2(1+\nu)\dot{\rho}\sin\theta + (1+\rho)\dot{\nu}\sin\theta + (1+\rho)(1+\nu)^2\cos\theta \\ &+ (1+\nu)^2 x + \dot{\nu}y - \frac{(1-\mu)}{r_1^3}\left[(1+\rho)\cos\theta + x\right] \\ &- \frac{\mu}{r_2^3}\left[(1+\rho)(\cos\theta - 1) + x\right] - \frac{\mu}{(1+\rho)^2} + F_{cx},\end{aligned}$$

$$\begin{aligned}\ddot{y} + 2(1+\nu)\dot{x} = &-\ddot{\rho}\sin\theta - 2(1+\nu)\dot{\rho}\cos\theta - (1+\rho)\dot{\nu}\cos\theta + (1+\rho)(1+\nu)^2\sin\theta \\ &- \dot{\nu}x + (1+\nu)^2 y - \left[\frac{(1-\mu)}{r_1^3} + \frac{\mu}{r_2^3}\right]\left[(1+\rho)\sin\theta + y\right] + F_{cy},\end{aligned} \tag{2.71}$$

and

$$\ddot{z} = -\left[\frac{(1-\mu)}{r_1^3} + \frac{\mu}{r_2^3}\right]z,$$

with

$$\mathbf{F}_c \equiv F_{cx}\mathbf{i} + F_{cy}\mathbf{j}. \tag{2.72}$$

From Equation 2.71, it can be verified that the isosceles-triangle point is an equilibrium solution if*

$$\mathbf{F}_c = F_c\left[-\sin\frac{\theta}{2}\mathbf{i} + \cos\frac{\theta}{2}\mathbf{j}\right], \tag{2.73}$$

where

*Equations 2.73 and 2.74 are true so long as ρ and ν are functions of the eccentricity only. In this case, $\ddot{\rho} - (1+\rho)^{-2}[(1+\nu)^2(1+\rho)^3 - 1] = 0$ and $2(1+\nu)\dot{\rho} + (1+\rho)\dot{\nu} = 0$. If ρ and ν also depend on gravitational perturbations from other bodies, these relations no longer hold, and Equations 2.73 and 2.74 will be more complicated.

$$F_c = \frac{\mu}{2(1+\rho)^2(1-\cos\theta)}\left\{1-\left[2(1-\cos\theta)\right]^{3/2}\right\}. \tag{2.74}$$

In Figure 2.4, it can be seen that this thrust vector is radial with respect to μ. Therefore, a simple coordinate rotation to the (x', y', z') system will uncouple the thrust acceleration terms in Equation 2.71. Inspection of Figure 2.4 shows that this coordinate rotation is

$$x = x'\cos\frac{\theta}{2} - y'\sin\frac{\theta}{2}$$

and (2.75)

$$y = x'\sin\frac{\theta}{2} + y'\cos\frac{\theta}{2}.$$

Taking $\rho = \nu = 0$, and using Equations 2.72 to 2.75, Equation 2.71 is expanded in a power series* in the (x', y', z') coordinates. Retaining only linear terms, Equation 2.71 becomes

$$\ddot{x}' - 2\dot{y}' - h_1(\mu,\theta)x' - \frac{3}{2}\left[(1-\mu)\sin\theta\right]y' = 0, \tag{2.76a}$$

$$\ddot{y}' + 2\dot{x}' - \frac{3}{2}\left[(1-\mu)\sin\theta\right]x' - h_2(\mu,\theta)y' = 0, \tag{2.76b}$$

and

$$\ddot{z}' + h_3(\mu,\theta)z' = 0, \tag{2.76c}$$

where

$$h_1(\mu,\theta) \equiv \frac{3}{2}(1+\cos\theta) - \frac{\mu}{2}\left\{1+3\cos\theta+2\left[2(1-\cos\theta)\right]^{-3/2}\right\}, \tag{2.77}$$

$$h_2(\mu,\theta) \equiv \frac{3}{2}(1-\cos\theta) - \frac{\mu}{2}\left\{1-3\cos\theta-4\left[2(1-\cos\theta)\right]^{-3/2}\right\}, \tag{2.78}$$

and

$$h_3(\mu,\theta) \equiv 1 + \mu\left\{\left[2(1-\cos\theta)\right]^{-3/2} - 1\right\}. \tag{2.79}$$

The coefficients depending on μ and θ in Equation 2.76 are shown as functions of θ in Figures 2.5 and 2.6. Figure 2.5 is drawn for the Earth-Moon system ($\mu = 0.0121507$), and Figure 2.6 gives the coefficients for the Sun-Earth system ($\mu = 3.0404 \times 10^{-6}$). The thrust accelerations in Earth gravity units ($g \equiv 9.81$ m/sec^2) for these two systems are given in Figures 2.7 and 2.8.

Because the out-of-plane motion is once again simple harmonic, the characteristic equation for the coupled portion of Equation 2.76 is used to determine linear stability. This characteristic equation can be written in the form

$$s^4 + \left[4 - (h_1 + h_2)\right]s^2 + h_1h_2 - \frac{9}{4}(1-\mu)^2\sin^2\theta = 0. \tag{2.80}$$

*The region of convergence for this series is again a region that is common to the interiors of two spheres centered at $1-\mu$ and μ. The sphere at $1-\mu$ has a radius of $\sqrt{2}$, and the sphere at μ has a radius of $2\sqrt{1-\cos\theta}$.

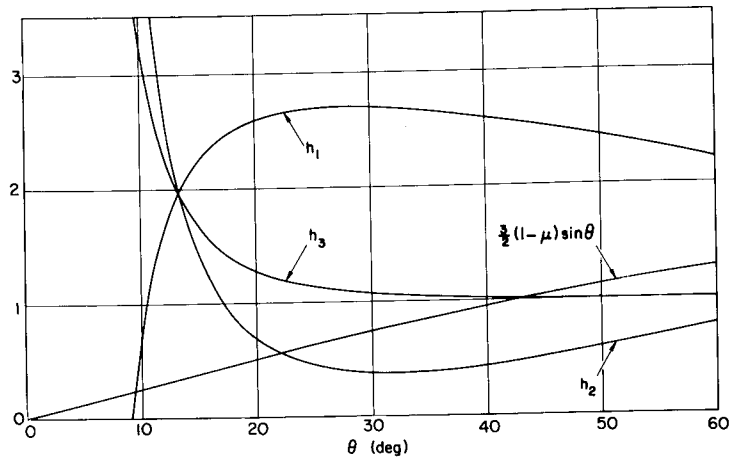

Figure 2.5–Coefficients for an isosceles-triangle point in the Earth-Moon system.

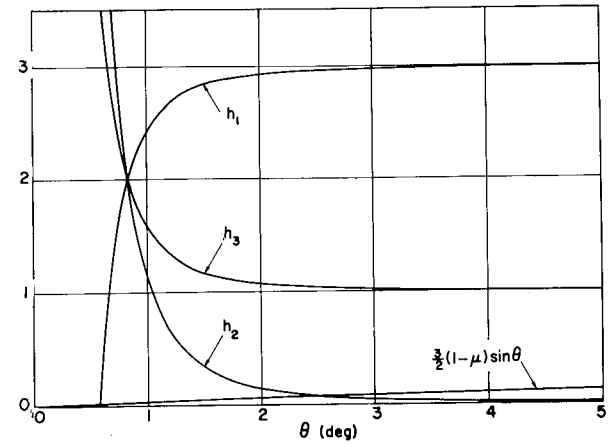

Figure 2.6–Coefficients for an isosceles-triangle point in the Sun-Earth system.

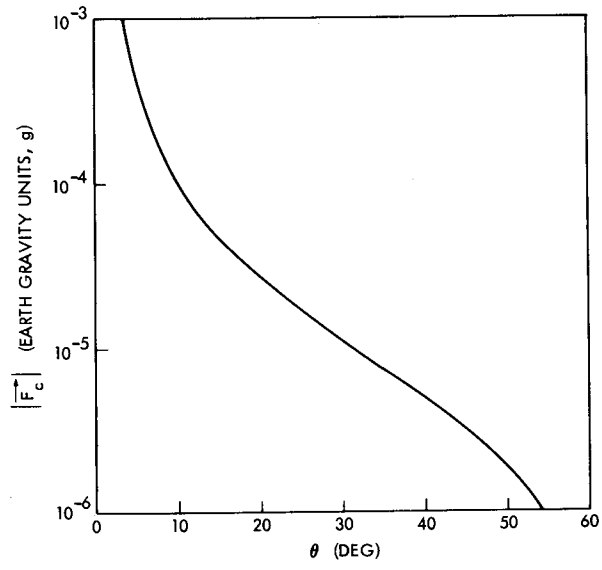

Figure 2.7–Thrust acceleration for an isosceles-triangle point in the Earth-Moon system.

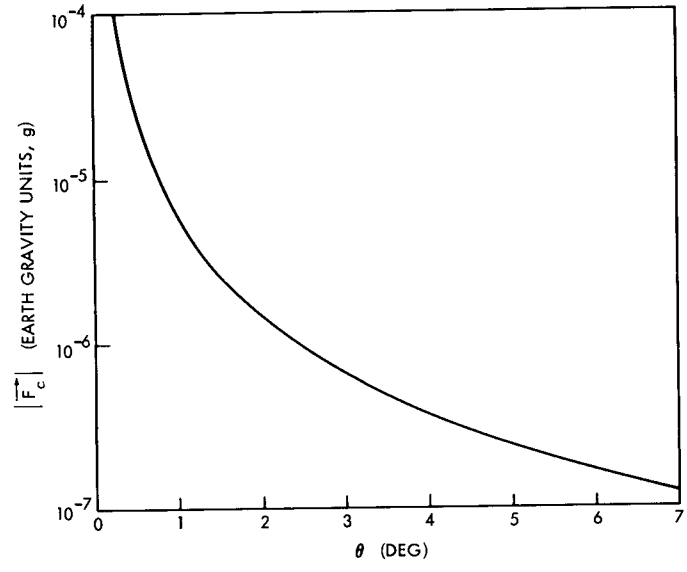

Figure 2.8–Thrust acceleration for an isosceles-triangle point in the Sun-Earth system.

For a fixed value of μ, all of the roots of Equation 2.80 are pure imaginaries when $\theta > \theta_c$, and the system is neutrally stable. When $\theta < \theta_c$, the motion is unstable. The approximate values of θ_c for the Earth-Moon and Sun-Earth systems are 38.9° and 2.45°, respectively.

4. Stability of the Linearized Equations of Motion in the Elliptic Case

In the three previous sections, the linear stability investigation was limited to the special case, $\rho = \nu = 0$. For a more realistic situation, where the two finite bodies describe elliptic orbits, the linearized equations of motion possess periodic coefficients, and the stability test is more involved. A brief summary

of some results for this problem is given below. The results of Bennett (References 24 and 25) are quoted here for he has investigated all five of the classical libration points. It should be noted that the stability results for the equilateral-triangle points were originally found by Colombo et al. (Reference 26) for the Earth-Moon system, and later by Danby (Reference 27) for the general case.

In his first paper, Bennett (Reference 24) used Floquet theory to examine the stability of the five classical libration points. For the collinear points, he found that the degree of instability increased with larger eccentricity. His results for the equilateral-triangle points are shown in Figure 2.9.

Bennett's second paper (Reference 25) gives an analytical method for finding a characteristic root λ as a power series in the eccentricity; i.e., $\lambda = \lambda_0 + \lambda_1 e + \lambda_2 e^2 + \ldots$, where λ_0 is the root for the circular problem. This paper proves that $\lambda_1 = 0$, which shows that the first correction to a characteristic root is proportional to the square of the eccentricity. For most of the systems considered in the present research, the correction will be very small and will usually be neglected.

C. Numerical Data for Some of the Collinear Points in the Solar System

In this section, numerical data for the L_1 and L_2 points of several Sun-planet and planet-satellite configurations are presented. These data will be needed to apply general results to certain Solar System points. It is important to note that although the derived parameters are given with several significant figures for consistency, their accuracy is really limited by the errors in the adopted constants.

1. Mass-Ratio Dependent Quantities

The derived constants in Tables 2.1 to 2.6 depend on only one physical parameter, the mass ratio of the two finite bodies. The values for the mass ratios listed in column 1 of Tables 2.1 and 2.2 were obtained from Reference 28* with the exception of the following:

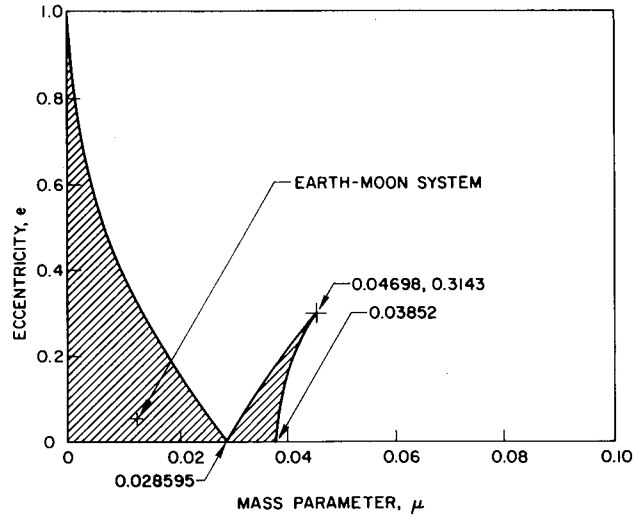

Figure 2.9–Stability chart for the equilateral-triangle points (Reference 24). Stable region is crosshatched.

(1) Mercury: This constant is so poorly known that three values are used here to bracket its probable range. Recent estimates can be found in References 29 to 31.

(2) Venus: Mariner 2 data (Reference 32).

(3) Earth: NASA Ad Hoc Standards Committee (Reference 33).

(4) Earth + Moon: Derived from adopted values for $M_\odot/M_\oplus$ and $M_\oplus/M_\leftmoon$.

(5) Mars: Mariner 4 data (Reference 34).

(6) Moon: Mariner 2 data (Reference 32).

Columns 3 and 4 of Tables 2.1 and 2.2 were obtained directly from Equations 2.27 and 2.28, respectively.

*Original sources are given in this reference.

Table 2.1–Mass parameters and distance ratios for Sun-planet systems.

Planet	1	2	3	4
	Mass ratio $(M_\odot/M_p)$	μ	γ_{L1}	γ_{L2}
Mercury – 1	5.5×10^6	1.8182×10^{-7}	3.9229×10^{-3}	3.9331×10^{-3}
Mercury – 2	6.0×10^6	1.6667×10^{-7}	3.8109×10^{-3}	3.8206×10^{-3}
Mercury – 3	6.5×10^6	1.5385×10^{-7}	3.7106×10^{-3}	3.7198×10^{-3}
Venus	4.0859×10^5	2.4474×10^{-6}	9.3148×10^{-3}	9.3730×10^{-3}
Earth	3.32951×10^5	3.0034×10^{-6}	9.9704×10^{-3}	1.0037×10^{-2}
Earth + Moon	3.28906×10^5	3.0404×10^{-6}	1.0011×10^{-2}	1.0078×10^{-2}
Mars	3.098×10^6	3.2279×10^{-7}	4.7487×10^{-3}	4.7640×10^{-3}
Jupiter	1.04736×10^3	9.5387×10^{-4}	6.6680×10^{-2}	6.9784×10^{-2}
Saturn	3.4997×10^3	2.8566×10^{-4}	4.4962×10^{-2}	4.6351×10^{-2}
Uranus	2.29×10^4	4.3666×10^{-5}	2.4216×10^{-2}	2.4613×10^{-2}
Neptune	1.889×10^4	5.2935×10^{-5}	2.5806×10^{-2}	2.6258×10^{-2}

Table 2.2–Mass parameters and distance ratios for planet-satellite systems.

Satellite	1	2	3	4
	Mass ratio (M_{sat}/M_p)	μ	γ_{L1}	γ_{L2}
Moon	81.30*	1.21507×10^{-2}	0.150935	0.167833
Io	3.81×10^{-5}	3.8099×10^{-5}	.023148	.023511
Europa	2.48×10^{-5}	2.4799×10^{-5}	.020083	.020355
Ganymede	8.17×10^{-5}	8.1693×10^{-5}	.029781	.030385
Callisto	5.09×10^{-5}	5.0897×10^{-5}	.025474	.025914
Mimas	6.68×10^{-8}	6.6800×10^{-8}	.0028107	.0028160
Enceladus	1.51×10^{-7}	1.5100×10^{-7}	.0036877	.0036967
Rhea	4×10^{-6}	4.0000×10^{-6}	.010966	.011047
Titan	2.48×10^{-4}	2.4794×10^{-4}	.042920	.044184
Triton	1.28×10^{-3}	1.2784×10^{-3}	.073339	.077111

*$M_\oplus/M_\mathbb{D}$.

In Tables 2.3 and 2.4, columns 1 and 2 were computed from Equation 2.44, and columns 3 and 4 were found by using Equation 2.45. The coefficient D_L defined in Equation 2.46 was not included in this table because B_L and C_L are sufficient for most applications. However, some representative values for D_L are

(1) Earth + Moon: $D_{L1} = 30\,240$ $D_{L2} = 29\,243$.
(2) Moon: $D_{L1} = 157.355$ $D_{L2} = 91.7003$.

Table 2.3–Constants for equations of motion for Sun-planet systems (see Equation 2.43).

Planet	1	2	3	4
	B_{L1}	B_{L2}	C_{L1}	C_{L2}
Mercury – 1	4.0237	3.9766	766.74	760.75
Mercury – 2	4.0230	3.9772	789.23	783.22
Mercury – 3	4.0224	3.9778	810.48	804.48
Venus	4.0568	3.9446	324.07	318.07
Earth	4.0608	3.9408	302.89	296.89
Earth + Moon	4.0611	3.9405	301.67	295.67
Mars	4.0287	3.9716	633.75	627.75
Jupiter	4.4462	3.6228	46.933	40.984
Saturn	4.2905	3.7412	68.699	62.721
Uranus	4.1512	3.8580	125.88	119.89
Neptune	4.1616	3.8489	118.24	112.25

Table 2.4–Constants for equations of motion for planet-satellite systems (see Equation 2.43).

Satellite	1	2	3	4
	B_{L1}	B_{L2}	C_{L1}	C_{L2}
Moon	5.14760	3.19042	21.5117	15.8451
Io	4.1443	3.8642	131.59	125.60
Europa	4.1246	3.8818	151.38	145.38
Ganymede	4.1877	3.8263	102.72	96.734
Callisto	4.1594	3.8508	119.76	113.77
Mimas	4.0169	3.9832	1069.4	1063.4
Enceladus	4.0223	3.9780	815.53	809.52
Rhea	4.0670	3.9349	275.57	269.57
Titan	4.2764	3.7525	71.876	65.896
Triton	4.4960	3.5873	42.835	36.898

The roots of the characteristic equation at L_1 and L_2, Equation 2.49, are listed in Tables 2.5 and 2.6. It should be recalled that the two pairs of roots for each point are equal in magnitude, but opposite in sign.

2. Conversion Factors for Normalized Units

Because virtually all general results will be presented in the normalized units that were introduced in Section A.1 of this chapter, a set of conversion factors will be needed to apply these results to specific

Table 2.5–Roots of characteristic equation for Sun-planet systems (see Equation 2.49).

Planet	1	2	3	4
	Roots for L_1		Roots for L_2	
	Real	Imaginary	Real	Imaginary
Mercury – 1	2.5178	2.0774	2.4989	2.0659
Mercury – 2	2.5175	2.0772	2.4991	2.0660
Mercury – 3	2.5173	2.0771	2.4994	2.0662
Venus	2.5309	2.0854	2.4860	2.0580
Earth	2.5326	2.0864	2.4844	2.0571
Earth + Moon	2.5327	2.0865	2.4843	2.0570
Mars	2.5198	2.0786	2.4969	2.0647
Jupiter	2.6811	2.1777	2.3521	1.9772
Saturn	2.6222	2.1413	2.4022	2.0073
Uranus	2.5682	2.1082	2.4507	2.0366
Neptune	2.5723	2.1107	2.4469	2.0343

Table 2.6–Roots of characteristic equation for planet-satellite systems (see Equation 2.49).

Satellite	1	2	3	4
	Roots for L_1		Roots for L_2	
	Real	Imaginary	Real	Imaginary
Moon	2.93206	2.33439	2.15867	1.86265
Io	2.5655	2.1065	2.4532	2.0381
Europa	2.5577	2.1018	2.4604	2.0425
Ganymede	2.5824	2.1169	2.4376	2.0287
Callisto	2.5714	2.1102	2.4477	2.0348
Mimas	2.5151	2.0757	2.5015	2.0675
Enceladus	2.5172	2.0770	2.4994	2.0662
Rhea	2.5350	2.0879	2.4820	2.0556
Titan	2.6167	2.1380	2.4069	2.0102
Triton	2.6997	2.1892	2.3368	1.9681

systems. The conversion factors for length and angular rate are listed in columns 1 and 3 of Tables 2.7 and 2.8. Manipulation of these two constants leads to the conversion factors for time, velocity, and acceleration given in Tables 2.9 and 2.10. To convert a normalized quantity to ordinary units, multiply by the appropriate factor. For example, if the normalized acceleration of an artificial satellite in the Earth-Moon system is given as $F = 1.186 \times 10^{-4}$, use of Table 2.10 gives

$$F = (1.186 \times 10^{-4}) \times (2.77611 \times 10^{-4} g) = 3.292 \times 10^{-8} g.$$

Table 2.7–Orbital constants for Sun-planet systems.

Planet	1a	1b	2	3
	Semimajor axis a		Eccentricity e	Mean motion n (rad/sec)
	(AU)*	(km)		
Mercury	0.387099	5.7910×10^7	0.20563	8.2668×10^{-7}
Venus	.723332	1.0821×10^8	.00679	3.2364×10^{-7}
Earth + Moon	1.000000	1.4960×10^8	.01673	1.9910×10^{-7}
Mars	1.523691	2.2794×10^8	.09337	1.0586×10^{-7}
Jupiter	5.203705	7.7847×10^8	.04863	1.6780×10^{-8}
Saturn	9.580337	1.4332×10^9	.05099	6.7152×10^{-9}
Uranus	19.14103	2.8635×10^9	.04579	2.3775×10^{-9}
Neptune	30.19825	4.5176×10^9	.00456	1.1998×10^{-9}

*AU = 1.49599×10^8 km, Mariner 2 data (Reference 32).

Table 2.8–Orbital constants for planet-satellite systems.

Satellite	1	2	3
	Mean distance from planet a (km)	Eccentricity e	Mean motion n (rad/sec)
Moon	3.84405×10^5	0.05490	2.66170×10^{-6}
Io	4.216×10^5	.0000	4.1106×10^{-5}
Europa	6.708×10^5	.0003	2.0478×10^{-5}
Ganymede	1.070×10^6	.0015	1.0164×10^{-5}
Callisto	1.882×10^6	.0075	4.3575×10^{-6}
Mimas	1.854×10^5	.0201	7.7165×10^{-5}
Enceladus	2.379×10^5	.00444	5.3073×10^{-5}
Rhea	5.267×10^5	.00098	1.6098×10^{-5}
Titan	1.221×10^6	.02890	4.5607×10^{-6}
Triton	3.534×10^5	.000	1.2374×10^{-5}

Multiplication of the distance ratios in Tables 2.1 and 2.2 by the appropriate length factor furnishes the values in columns 1 and 2 of Tables 2.11 and 2.12, which give the mean distances between the center of the smaller finite body and the collinear points. Comparison of columns 2 and 3 for the planet-satellite systems shows that the L_1 and L_2 points are sometimes located very close to the satellite's surface. The variation of the libration-point distance because of the orbital eccentricity is given for a few systems in columns 1 to 4 of Table 2.13.

Table 2.9–Conversion factors for normalized units for Sun-planet systems.

Planet	1	2	3	4
	Time (days)	Velocity (m/sec)	Acceleration	
			(m/sec^2)	(g)
Mercury	14.001	4.7872×10^4	3.9575×10^{-2}	4.0342×10^{-3}
Venus	35.762	3.5021×10^4	1.1334×10^{-2}	1.1554×10^{-3}
Earth + Moon	58.132	2.9785×10^4	5.9301×10^{-3}	6.0450×10^{-4}
Mars	109.34	2.4130×10^4	2.5543×10^{-3}	2.6038×10^{-4}
Jupiter	689.73	1.3063×10^4	2.1920×10^{-4}	2.2345×10^{-5}
Saturn	1723.6	9.6243×10^3	6.4629×10^{-5}	6.5881×10^{-6}
Uranus	4868.1	6.8081×10^3	1.6187×10^{-5}	1.6500×10^{-7}
Neptune	9646.7	5.4202×10^3	6.5031×10^{-6}	6.6291×10^{-8}

Table 2.10–Conversion factors for normalized units for planet-satellite systems.

Satellite	1	2	3	4
	Time (days)	Velocity (m/sec)	Acceleration	
			(m/sec^2)	(g)
Moon	4.34838	1.02317×10^3	2.72336×10^{-3}	2.77611×10^{-4}
Io	.28157	1.7330×10^4	7.1237×10^{-1}	7.2617×10^{-2}
Europa	.56519	1.3737×10^4	2.8131×10^{-1}	2.8675×10^{-2}
Ganymede	1.1387	1.0876×10^4	1.1055×10^{-1}	1.1269×10^{-2}
Callisto	2.6561	8.2008×10^3	3.5735×10^{-2}	3.6427×10^{-3}
Mimas	.14999	1.4306×10^4	1.1040	1.1253×10^{-1}
Enceladus	.21808	1.2626×10^4	6.7011×10^{-1}	6.8309×10^{-2}
Rhea	.71898	8.4787×10^3	1.3649×10^{-1}	1.3913×10^{-2}
Titan	2.5378	5.5686×10^3	2.5396×10^{-2}	2.5888×10^{-3}
Triton	.93533	4.3731×10^3	5.4114×10^{-2}	5.5162×10^{-3}

3. Comparison of L_2 Distance and Extent of Planetary Shadow

It is interesting to compare the distances of the apex of a planet's shadow cone and its L_2 point. The mean distance between a planet and the apex of its geometrical shadow cone is given by

$$d_s = \frac{a}{(R_\odot/R_p - 1)}, \tag{2.81}$$

where a is the semimajor axis of the planet's orbit, R_p is the planet's radius, and $R_\odot = 6.957 \times 10^5$ km (Reference 28). Equation 2.81 was used to compute the planetary shadow distances given in column 4 of

Table 2.11–Distance between the smaller finite body and a collinear point for Sun-planet systems.

Planet	1a	1b	2a	2b
	Mean distance between planet and L_1		Mean distance between planet and L_2	
	(AU)	(km)	(AU)	(km)
Mercury – 1	0.001519	2.2717×10^5	0.001523	2.2777×10^5
Mercury – 2	.001475	2.2069×10^5	.001479	2.2125×10^5
Mercury – 3	.001436	2.1488×10^5	.001440	2.1541×10^5
Venus	.006738	1.0079×10^6	.006780	1.0142×10^6
Earth	.009970	1.4916×10^6	.010037	1.5015×10^6
Earth + Moon	.010011	1.4976×10^6	.010078	1.5077×10^6
Mars	.007236	1.0824×10^6	.007259	1.0859×10^6
Jupiter	.34699	5.1909×10^7	.36314	5.4325×10^7
Saturn	.43075	6.4439×10^7	.44406	6.6431×10^7
Uranus	.46352	6.9342×10^7	.47112	7.0480×10^7
Neptune	.77931	1.1658×10^8	.79295	1.1863×10^8

Table 2.12–Distance between the smaller finite body and a collinear point for planet-satellite systems.

Satellite	1	2	3
	Mean distance between satellite and L_1 (km)	Mean distance between satellite and L_2 (km)	Radius of satellite (km)
Moon	58 020	64 516	1738
Io	9759	9912	1620
Europa	13 471	13 654	1415
Ganymede	31 866	32 511	2450
Callisto	47 942	48 770	2285
Mimas	521	522	350?
Enceladus	877	879	<470
Rhea	5776	5818	675
Titan	52 405	53 949	2475
Triton	25 918	27 251	2250

Table 2.14. The assumed values for the planetary radii listed in column 1 were obtained from Reference 28 with the exception of the following:

(1) Mercury: Reference 35.
(2) Venus: Reference 36.
(3) Mars: Mariner 4 data (Reference 37).

By comparing columns 3 and 4 of Table 2.14*, it can be seen that the L_2 point is located beyond the planetary shadow cone for Mercury, Venus, and Earth. To an observer placed at any of the L_2 points for these planets, the Sun would always be partially eclipsed. At the L_2 points of Mars, Jupiter, Saturn, Uranus, and Neptune, the Sun is totally eclipsed (neglecting atmospheric refraction). A "critical" planetary radius, which would make the length of the planetary shadow equal to the L_2 distance, is given in column 2.

Table 2.13–Distance variation between the smaller finite body and a collinear point.

Body	1*	2*	3*	4*
	Min. distance between body and L_1 (km)	Max. distance between body and L_1 (km)	Min. distance between body and L_2 (km)	Max. distance between body and L_2 (km)
Moon	5.4835×10^4	6.1205×10^4	6.0974×10^4	6.8058×10^4
Mercury – 2	1.7531×10^5	2.6607×10^5	1.7576×10^5	2.6674×10^5
Earth + Moon	1.4726×10^6	1.5227×10^6	1.4825×10^6	1.5329×10^6
Mars	9.8137×10^5	1.1835×10^6	9.8449×10^5	1.1873×10^6
Jupiter	4.9384×10^7	5.4433×10^7	5.1683×10^7	5.6967×10^7

*$d_{min} = d(1 - e)$, $d_{max} = d(1 + e)$.

Table 2.14–L_2 distance and extent of planetary shadow.

Planet	1	2	3	4
	Mean radius of planet (km)	Critical radius of planet (km)	Mean distance between planet and L_2 (km)	Mean distance between planet and apex of shadow (km)
Mercury – 1	2480	2725.6	2.2777×10^5	2.0717×10^5
Mercury – 2	2480	2647.8	2.2125×10^5	2.0717×10^5
Mercury – 3	2480	2578.3	2.1541×10^5	2.0717×10^5
Venus	6120*	6460.2	1.0142×10^6	9.6036×10^5
Earth	6371	6913.4	1.5015×10^6	1.3826×10^6
Earth + Moon	6371	6941.4	1.5077×10^6	1.3826×10^6
Mars	3390	3298.5	1.0859×10^6	1.1162×10^6
Jupiter	69750	45382.0	5.4325×10^7	8.6745×10^7
Saturn	58170	30818.1	6.6431×10^7	1.3077×10^8
Uranus	23750	16712.2	7.0480×10^7	1.0121×10^8
Neptune	22400	17800.5	1.1863×10^8	1.5030×10^8

*Radius taken to top of cloud layer.

*A comparison of the mean distances is sufficient because both distances fluctuate in the same manner for elliptical orbits.

CHAPTER III

PERTURBATIONS AND NOMINAL PATH CONTROL

The restricted three-body model for the motion of a libration-point satellite is an idealization of the true physical situation. A more realistic model must account for the gravitational perturbations of other bodies and solar radiation pressure. In this chapter, the effect of these disturbances on a libration-point satellite is considered in some detail. Quantitative results are given for a few specific cases, and the concept of nominal path control is introduced.

A. Additional Accelerations Acting on a Libration-Point Satellite

1. Gravitational Perturbations

The analysis of the motion of a libration-point satellite is more intricate when gravitational perturbations of another finite body are introduced. The addition of this fourth body affects the motion of the other finite bodies, as well as the satellite, and great care must be taken to use a proper mathematical model. A recent discussion of certain models for a "restricted four-body problem" has been given by Mohn and Kevorkian (Reference 38).

When Brown and Shook (Reference 39) calculated the perturbations of a Trojan asteroid* by Saturn, they found that the indirect effect produced by Saturn in altering Jupiter's motion was greater than its direct effect. This case is typical of perturbations of this type, and the examples given below show that direct and indirect effects are usually comparable.

2. Solar Radiation Pressure

The magnitude and direction of the acceleration caused by solar radiation pressure is somewhat random for a nonoriented satellite with an odd geometrical shape and variable reflectivity, absorptivity, and transmissibility properties. However, for an attitude-controlled satellite with a simple configuration and uniform surface properties, the variation of this acceleration is largely predictable. Although this chapter views radiation pressure as an undesirable perturbation, it will be seen in Chapters V and VI that this effect could be used advantageously for satellite position control.

The magnitude of the acceleration acting on a plane surface of mass m is given by†

*The Trojan asteroids are located in the vicinity of the equilateral-triangle points of the Sun-Jupiter system.
†It is assumed that the incident solar radiation is perpendicular to the plane surface.

$$K_p = C_p \left(\frac{A_s}{m}\right)\left(\frac{p_\oplus}{d_s^2}\right), \tag{3.1}$$

where $p_\oplus$ is the solar pressure at 1 AU from the Sun (using the solar constant given in Reference 12, $p_\oplus = 4.50 \times 10^{-6}$ newtons/m^2), d_s is the distance from the Sun in AU, A_s is the area of the plane surface, and C_p is a coefficient that depends on the surface properties. For a perfect absorber (black body), $C_p = 1$, while a value of $C_p = 2$ corresponds to a perfect reflector. The area-to-mass ratios range from about 0.001 m^2/kg for a very dense satellite to 0.1 m^2/kg for a satellite with very large solar panels. Assuming an average value of $(A_s/m) = 0.01$ m^2/kg and taking $C_p = 2$, $d_s = 1$ AU, the acceleration from radiation pressure is roughly $K_p = 9.17 \times 10^{-9}g$.

3. Thrust Control

Satellite position control is usually achieved with low-thrust devices. These devices could be cold-gas jets, ion thrustors, or some other suitable system. The thrust may be applied either continuously or discontinuously, depending on the control requirements. Detailed analyses of the controlled motion of a libration-point satellite are presented in the remaining chapters.

B. Control About Nominal Path

Although the concept introduced in this section is applicable to all the libration points, the discussion here will be limited to the collinear points. The modification of this technique for the other points is straightforward.

1. Basic Strategy

The addition of perturbation and control terms to the linearized equations of motion at the collinear points, Equation 2.48, gives

$$\ddot{x} - 2\dot{y} - (2B_L + 1)x = P_x(t) + F_{cx}, \tag{3.2a}$$

$$\ddot{y} + 2\dot{x} + (B_L - 1)y = P_y(t) + F_{cy}, \tag{3.2b}$$

and

$$\ddot{z} + B_L z = P_z(t) + F_{cz}, \tag{3.2c}$$

where $\mathbf{P}(t)$ is a periodic perturbing acceleration and $\mathbf{F}_c$ is a control acceleration. Because of the natural instability of a satellite in the vicinity of a collinear libration point, some thrust control for station keeping will always be necessary. Additional thrust control could be used to cancel the perturbing acceleration. However, it is more economical to control about a suitable periodic perturbed path. This "nominal path" is determined by simply solving for the forced response of Equation 3.2 with $\mathbf{F}_c = 0$. The forced response to a sinusoidal input is well defined, except for exact resonance, even though the uncontrolled system, is unstable. Denoting the nominal path by (x_n, y_n, z_n) and using the coordinate transformation

$$\xi = x - x_n,$$

$$\eta = y - y_n, \tag{3.3}$$

and

$$\zeta = z - z_n,$$

the equations of motion relative to the nominal path are

$$\ddot{\xi} - 2\dot{\eta} - (2B_L + 1)\xi = F_{cx},$$

$$\ddot{\eta} + 2\dot{\xi} + (B_L - 1)\eta = F_{cy}, \tag{3.4}$$

and

$$\ddot{\zeta} + B_L\zeta = F_{cz},$$

which is identical to Equation 3.2 with $\mathbf{P}(t)$ absent. This result could have been stated earlier by simply using the principle of linear superposition.

The foregoing development is an approximation that is strictly valid only so long as the nominal path is very small. Equations of motion relative to a moderately large nominal path are derived below.

2. Periodic Orbits

It is well known that families of unstable periodic orbits can exist in the vicinity of the collinear libration points (Reference 1). To satisfy certain mission constraints, it is sometimes necessary to insert a satellite into one of these orbits. For moderate amplitude orbits located in the xy-plane, a good approximation can be obtained from Equations 3.2a and 3.2b with $\mathbf{P}(t) = \mathbf{F}_c = \mathbf{0}$. If certain initial conditions are satisfied, only the oscillatory mode is excited, and the satellite will follow a periodic orbit about the libration point, as shown in Figure 3.1. The equations for this orbit are (Reference 1)

$$x_n = A_x \sin \omega_n t$$

and

$$y_n = A_y \cos \omega_n t, \tag{3.5}$$

where

$$A_x = \frac{2\omega_n}{\omega_n^2 + (2B_L + 1)} A_y \equiv kA_y \tag{3.6}$$

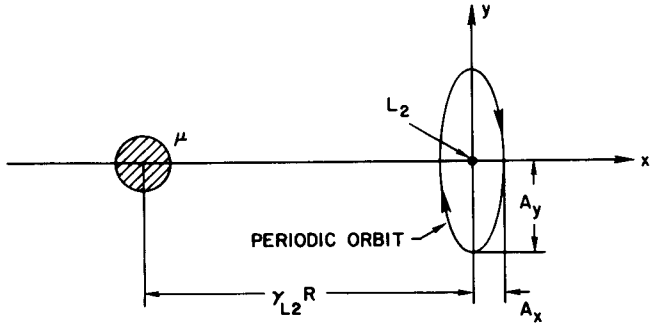

Figure 3.1–Periodic orbit around a collinear point.

and ω_n is the magnitude of an imaginary root of Equation 2.49. It should be noted here that Equation 3.5 is only a first approximation to the true orbit, and higher order corrections are introduced when nonlinearities, eccentricity, and perturbations are taken into account. The corrected orbit is still bounded, but it is only quasi-periodic.

3. Higher Order Corrections for a Periodic Orbit

The determination of the corrections to the orbit of Equation 3.5 is a tedious and lengthy

process. Fortunately, the computation of a few higher order terms is usually sufficient because the remaining small accelerations do not significantly add to the station-keeping cost. In this section, only second-order terms are considered. Although the corrections may be quite small, the station-keeping cost could be significantly increased if they are disregarded.

The method of successive approximations (Reference 40) can be used to determine the second-order correction to a periodic orbit around a collinear point. The equations of the corrected orbit to second order can be written in the form

$$x_n = x_{n1} + x_{n2}$$

and

$$y_n = y_{n1} + y_{n2}, \tag{3.7}$$

where x_{n1} and y_{n1} are given by Equation 3.5. That is,

$$x_{n1} = A_{x1} \sin \omega_n t$$

and

$$y_{n1} = A_{y1} \cos \omega_n t \tag{3.8}$$

with $A_{x1} = kA_{y1}$. Substitution of Equation 3.7 into Equations 2.43a and 2.43b with $\mathbf{P}(t)$ included and deletion of all terms higher than second order yield two coupled linear differential equations for x_{n2} and y_{n2}. A_{y1}, ρ, ν, and $\mathbf{P}(t)$ are treated as first-order quantities, and coupling between the eccentricity and gravitational perturbations is neglected. With these restrictions, the second-order effects of nonlinearity, eccentricity, and perturbations can be treated separately. An analysis of this type is usually adequate for order of magnitude estimates of the different effects.

Frequency corrections are also present and can be computed by expressing the frequency as

$$\omega_n = \omega_{n0} + \omega_{n1} + \omega_{n2} + \ldots . \tag{3.9}$$

Fortunately, $\omega_{n1} = 0$ for the cases considered below, and the frequency is well approximated by $\omega_n = \omega_{n0}$.

Response to a periodic input

It will be necessary to calculate the forced response to an input of the form

$$\mathbf{P}(t) = K_x \cos(\omega t + \phi)\mathbf{i} + K_y \sin(\omega t + \phi)\mathbf{j}.$$

The linearized equations of motion near a collinear point with this input are

$$\ddot{x} - 2\dot{y} - (2B_L + 1)x = K_x \cos(\omega t + \phi)$$

and

$$\ddot{y} + 2\dot{x} + (B_L - 1)y = K_y \sin(\omega t + \phi). \tag{3.10}$$

A particular solution of Equation 3.10 can be written as

$$x_p = A_x \cos(\omega t + \phi)$$

and

$$y_p = A_y \sin(\omega t + \phi), \tag{3.11}$$

where

$$\begin{bmatrix} A_x \\ A_y \end{bmatrix} = \frac{\begin{bmatrix} \left[-\omega^2 + (B_L - 1)\right] & 2\omega \\ 2\omega & \left[-\omega^2 - (2B_L + 1)\right] \end{bmatrix} \begin{bmatrix} K_x \\ K_y \end{bmatrix}}{\left[\omega^4 + (B_L - 2)\omega^2 - (2B_L + 1)(B_L - 1)\right]} \tag{3.12}$$

This result will be used repeatedly below.

Nonlinear correction

Employing the procedure outlined above, it can be deduced that the differential equations for the nonlinear correction are

$$\ddot{x}_{n2} - 2\dot{y}_{n2} - (2B_L + 1)x_{n2} = C_x + K_x \cos 2\omega_n t$$

and (3.13)

$$\ddot{y}_{n2} + 2\dot{x}_{n2} + (B_L - 1)y_{n2} = K_y \sin 2\omega_n t,$$

where

$$C_x = \pm\frac{3}{2}C_L\left(\frac{1}{2} - k^2\right)A_{y1}^2, \tag{3.14}$$

$$K_x = \pm\frac{3}{2}C_L\left(\frac{1}{2} + k^2\right)A_{y1}^2, \tag{3.15}$$

and

$$K_y = \pm\frac{3}{2}C_L k A_{y1}^2. \tag{3.16}$$

Therefore

$$x_{n2} = x_{c2} + A_{x2} \cos 2\omega_n t$$

and (3.17)

$$y_{n2} = A_{y2} \sin 2\omega_n t,$$

where A_{x2} and A_{y2} are computed by making use of Equations 3.10 to 3.12, and $x_{c2} = -C_x/(2B_L + 1)$. As an example, consider the L_2 point of the Earth-Moon system. For this point, $B_{L2} = 3.19042$, $C_{L2} = 15.8451$, $\omega_n = 1.86265$, $k = 0.343336$, and

$$C_x = 9.0821\ A_{y1}^2, \qquad x_{c2} = -1.2305\ A_{y1}^2,$$

$$K_x = 14.686\ A_{y1}^2, \qquad A_{x2} = -0.57443\ A_{y1}^2,$$

$$K_y = 8.1603\ A_{y1}^2, \qquad A_{y2} = -0.33203\ A_{y1}^2.$$

Choosing $A_{y1} = 0.02 = 7688.1$ km, these relationships give

$$C_x = 1.0085 \times 10^{-6} g, \qquad x_{c2} = -189.20 \text{ km},$$

$$K_x = 1.6307 \times 10^{-6} g, \qquad A_{x2} = -88.33 \text{ km},$$

$$K_y = 9.0617 \times 10^{-7} g, \qquad A_{y2} = -51.05 \text{ km},$$

and $A_{x1} = 0.343336$ $A_{y1} = 2639.6$ km.

It should be mentioned that Plummer (References 41 and 42) has calculated the nonlinear corrections to third order for all of the collinear points. Unfortunately, Plummer's solutions are limited to the case where $\mu = 1/11$.

Eccentricity correction

For the eccentricity correction, the differential equations are

$$\ddot{x}_{n2} - 2\dot{y}_{n2} - (2B_L + 1)x_{n2} = 2\nu\dot{y}_{n1} + \dot{\nu}y_{n1} + (2\nu - 6B_L\rho)x_{n1}$$

and (3.18)

$$\ddot{y}_{n2} + 2\dot{x}_{n2} + (B_L - 1)y_{n2} = -2\nu\dot{x}_{n1} - \dot{\nu}x_{n1} + (2\nu + 3B_L\rho)y_{n1},$$

where the expressions for ρ and ν are obtained from Equations 2.5 and 2.6. Taking $\phi = 0$ and neglecting terms of $O(e^2)$, these quantities are given by

$$\rho = -e \cos t$$

and (3.19)

$$\nu = 2e \cos t.$$

Using Equations 3.6, 3.8, and 3.19, Equation 3.18 becomes

$$\ddot{x}_{n2} - 2\dot{y}_{n2} - (2B_L + 1)x_{n2} = K_x \sin(\omega_n + 1)t + K'_x \sin(\omega_n - 1)t$$

and (3.20)

$$\ddot{y}_{n2} + 2\dot{x}_{n2} + (B_L - 1)y_{n2} = K_y \cos(\omega_n + 1)t + K'_y \cos(\omega_n - 1)t,$$

where

$$K_x = e\left[-2\omega_n - 1 + k(3B_L + 2)\right]A_{y1}, \tag{3.21}$$

$$K'_x = -e\left[2\omega_n - 1 - k(3B_L + 2)\right]A_{y1}, \tag{3.22}$$

$$K_y = -e\left[k(2\omega_n + 1) + \left(\frac{3}{2}B_L - 2\right)\right]A_{y1}, \tag{3.23}$$

and

$$K'_y = -e\left[k(2\omega_n - 1) + \left(\frac{3}{2}B_L - 2\right)\right]A_{y1}. \tag{3.24}$$

The solutions can be written in the form

$$x_{n2} = A_{x2} \sin(\omega_n + 1)t + A'_{x2} \sin(\omega_n - 1)t$$

and

$$y_{n2} = A_{y2} \cos (\omega_n + 1)t + A'_{y2} \cos (\omega_n - 1)t, \tag{3.25}$$

and A_{x2}, A'_{x2}, A_{y2}, and A'_{y2} are again determined by using Equations 3.10 to 3.12. Returning to the example at the L_2 point of the Earth-Moon system (e = 0.05490), elementary calculations give

$$K_x = -0.041311\ A_{y1}, \qquad A_{x2} = 0.026893\ A_{y1},$$

$$K'_x = 0.068489\ A_{y1}, \qquad A'_{x2} = -0.030659\ A_{y1},$$

$$K_y = -0.24200\ A_{y1}, \qquad A_{y2} = 0.065947\ A_{y1},$$

$$K'_y = -0.20430\ A_{y1}, \qquad A'_{y2} = -0.10469\ A_{y1},$$

and for A_{y1} = 0.02 = 7688.1 km,

$$K_x = -2.2937 \times 10^{-7} g, \qquad A_{x2} = 206.76 \text{ km},$$

$$K'_x = 3.8027 \times 10^{-7} g, \qquad A'_{x2} = -235.71 \text{ km},$$

$$K_y = -1.3436 \times 10^{-6} g, \qquad A_{y2} = 507.01 \text{ km},$$

$$K'_y = -1.1343 \times 10^{-6} g, \qquad A'_{y2} = -804.84 \text{ km}.$$

A comparison shows that the amplitudes of the eccentricity corrections are much larger than the amplitudes of the nonlinear corrections. It is shown below that these eccentricity corrections also dominate corrections caused by the Sun's gravitational field and radiation pressure.

Effect of gravitational perturbations and solar radiation pressure

Because the analysis of gravitational perturbations is slightly different for every libration point, a generalized result for periodic orbit corrections cannot be given. However, specific cases are readily analyzed, and the effect of the Sun's perturbation on a periodic orbit around a collinear point of the Earth-Moon system is described in section C of this chapter.

A general result for solar radiation pressure is even less probable because this effect is highly dependent on the spacecraft configuration and orientation. Nevertheless, a highly restricted example is examined here for illustrative purposes. Consider a satellite near the L_2 point of the Earth-Moon system. The major contribution to the satellite's cross-sectional area is given by a high-gain antenna with a diameter of 3 m (A_s = 7.0686 m^2). If the antenna is always directed toward the Moon as shown in Figure 3.2, then the angle ψ of the incident solar radiation will vary sinusoidally. Assuming that all of the incident radiation is reflected specularly, the instantaneous acceleration acting on the spacecraft is (Reference 43)

$$P_x = \pm K_p \cos^2 \psi, \tag{3.26}$$

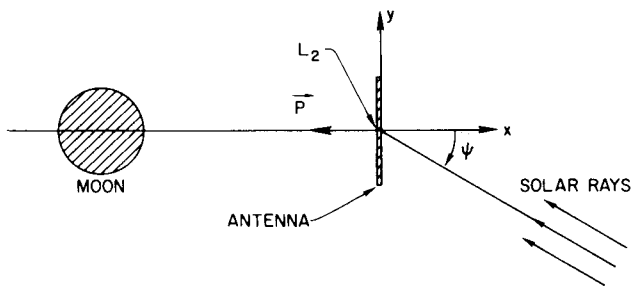

Figure 3.2–Geometry for radiation pressure example.

where K_p is given by Equation 3.1, with $C_p = 2$. For a satellite mass $m = 200$ kg, the average acceleration is $|\overline{P_x}| = K_p/2 = 1.62 \times 10^{-8} g$. Accelerations of this magnitude may simply be canceled by thrust control.

4. Linearized Equations of Motion Relative to a Nominal Path

A nominal path can usually be represented as a series of successive approximations of the form

$$\begin{aligned} x_n &= x_{n1} + x_{n2} + x_{n3} + \ldots, \\ y_n &= y_{n1} + y_{n2} + y_{n3} + \ldots, \\ z_n &= z_{n1} + z_{n2} + z_{n3} + \ldots, \end{aligned} \tag{3.27}$$

and

where the second subscript denotes the order of the term. The equations of motion relative to the nominal path can be found by substituting Equation 3.3 into Equation 2.43. Only terms involving the coordinates (ξ, η, ζ) will be present because Equation 3.27 is a solution of Equation 2.43 with $\mathbf{P}(t)$ included. Assuming that ρ and ν are negligible when compared to $3C_L x_{n1}$, etc., the linearized equations of motion are approximately*

$$\begin{aligned} \ddot{\xi} - 2\dot{\eta} - (2B_L + 1)\xi &= \mp 3C_L\left[2x_{n1}\xi - y_{n1}\eta - z_{n1}\zeta\right] + F_{cx}, \\ \ddot{\eta} + 2\dot{\xi} + (B_L - 1)\eta &= \pm 3C_L\left[x_{n1}\eta + y_{n1}\xi\right] + F_{cy}, \\ \ddot{\zeta} + B_L\zeta &= \pm 3C_L\left[x_{n1}\zeta + z_{n1}\xi\right] + F_{cz}. \end{aligned} \tag{3.28}$$

and

When the nominal path is very small, Equation 3.28 reduces to Equation 3.4.

For a quasi-periodic orbit, the first-order terms for the nominal path are given by Equation 3.5. If the satellite is also performing an out-of-plane oscillation, it is obvious from Equation 2.43c that

$$z_{n1} = A_{z1} \cos(\omega_z t + \alpha_0), \tag{3.29}$$

where $\omega_z = \sqrt{B_L}$ and α_0 is a phase angle. Substitution of these first-order terms into Equation 3.28 gives

$$\begin{aligned} \ddot{\xi} - 2\dot{\eta} - (2B_L + 1)\xi = \mp 3C_L\Big\{&2\left[A_{x1} \sin \omega_n t\right]\xi - \left[A_{y1} \cos \omega_n t\right]\eta \\ &- \left[A_{z1} \cos(\omega_z t + \alpha_0)\right]\zeta\Big\} + F_{cx}, \end{aligned}$$

*As in Chapter II, the upper sign holds at L_2, and the lower sign at L_1.

$$\ddot{\eta} + 2\dot{\xi} + (B_L - 1)\eta = \pm 3C_L\left\{\left[A_{x1}\sin\omega_n t\right]\eta + \left[A_{y1}\cos\omega_n t\right]\xi\right\} + F_{cy}, \tag{3.30}$$

and

$$\ddot{\zeta} + B_L\zeta = \pm 3C_L\left\{\left[A_{x1}\sin\omega_n t\right]\zeta + \left[A_{z1}\cos(\omega_z t + \alpha_0)\right]\xi\right\} + F_{cz}.$$

C. Examples of Gravitational Perturbations

1. Solar Perturbation Near the Earth-Moon Collinear Points

The effect of the Sun's perturbation on a satellite at a collinear point of the Earth-Moon system was first investigated by Colombo (References 3 and 44). He demonstrated that, to first order, the acceleration produced by the direct effect of the Sun is completely canceled by the indirect effect of the Sun on the Moon. A more complete derivation of Colombo's solution has been given by Nicholson (Reference 45), who also examined the forced motion caused by the higher order terms.* It should be emphasized that Colombo's solution is valid only *at* the libration point, and cannot be applied to a satellite following a periodic orbit around the point.

To calculate the effect of the Sun's perturbation on a periodic orbit, a somewhat different approach is advisable. The method presented in this section uses the lunar theory of De Pontecoulant to account for the Sun's indirect effect. This method is first shown to be in agreement with Colombo's result at the libration point, and then used to determine the correction to a periodic orbit around a collinear point. Because the mean inclination of the Moon's orbital plane to the ecliptic is only about 5°, and the eccentricities of the orbits of the Earth and the Moon are $e' = 0.01673$ and $e = 0.05490$, respectively, the analysis given below will be limited to zero-eccentricity, coplanar orbits.

De Pontecoulant's expressions for the motion of the Moon

A complete listing of De Pontecoulant's results for the motion of the Moon is given in Reference 46, and an abbreviated version can be found in Reference 47. Literally hundreds of terms are involved in these expressions, but if it is assumed that $e = e' = 0$ and three-dimensional effects are neglected, the formulas reduce to

$$\rho = -\frac{1}{6}m^2 + \frac{331}{288}m^4 - \left[m^2 + \frac{19}{6}m^3 + \frac{125}{18}m^4\right]\cos 2\omega_s t - \frac{3}{8}m^4\cos 4\omega_s t$$
$$+ \left[\frac{15}{16}m + \frac{81}{16}m^2\right]\frac{a}{a'}\cos\omega_s t - \frac{25}{64}m^2\frac{a}{a'}\cos 3\omega_s t + O(m^5) \tag{3.31}$$

and

$$\nu = \left[\frac{11}{4}m^2 + \frac{85}{12}m^3 + \frac{539}{36}m^4\right]\cos 2\omega_s t + \frac{201}{64}m^4\cos 4\omega_s t$$
$$- \left[\frac{15}{8}m + \frac{39}{4}m^2\right]\frac{a}{a'}\cos\omega_s t + \frac{45}{32}m^2\frac{a}{a'}\cos 3\omega_s t + O(m^5), \tag{3.32}$$

*The magnitude of the acceleration from the higher order terms is approximately $2 \times 10^{-9} g$. A nominal path calculation is unnecessary here because the magnitude of this acceleration is comparable to random solar radiation pressure effects.

where m is the ratio of the mean motions of the Earth and the Moon ($m = n'/n = 0.07480133$), a/a' is the ratio of the semimajor axes of the Earth and the Moon [$a/a' = 0.002559 \sim O(m^2)$], $\omega_s = 1 - m = 0.92519867$, and $t = 0$ corresponds to new Moon. Differentiation of Equations 3.31 and 3.32 gives

$$\dot{\rho} = \left[2m^2 + \frac{13}{3}m^3 + \frac{68}{9}m^4\right] \sin 2\omega_s t + \frac{3}{2}m^4 \sin 4\omega_s t - \left[\frac{15}{16}m + \frac{33}{8}m^2\right]\frac{a}{a'} \sin \omega_s t + \frac{75}{64}m^2\frac{a}{a'} \sin 3\omega_s t + O(m^5), \tag{3.33}$$

$$\ddot{\rho} = \left[4m^2 + \frac{14}{3}m^3 + \frac{58}{9}m^4\right] \cos 2\omega_s t + 6m^4 \cos 4\omega_s t - \left[\frac{15}{16}m + \frac{51}{16}m^2\right]\frac{a}{a'} \cos \omega_s t + \frac{225}{64}m^2\frac{a}{a'} \cos 3\omega_s t + O(m^5), \tag{3.34}$$

and

$$\dot{\nu} = -\left[\frac{11}{2}m^2 + \frac{26}{3}m^3 + \frac{142}{9}m^4\right] \sin 2\omega_s t - \frac{201}{16}m^4 \sin 4\omega_s t + \left[\frac{15}{8}m + \frac{63}{8}m^2\right]\frac{a}{a'} \sin \omega_s t - \frac{135}{32}m^2\frac{a}{a'} \sin 3\omega_s t + O(m^5). \tag{3.35}$$

Derivation of direct solar effect

The geometry for the direct solar perturbation in the vicinity of a collinear point is shown in Figure 3.3. The contribution of this direct solar effect to the effective potential energy (for motion relative to the Earth) is

$$U_D = -M_\odot\left[\frac{1}{|\mathbf{r}_s - \mathbf{r}|} - \frac{\mathbf{r}_s \cdot \mathbf{r}}{r_s^3}\right], \tag{3.36}$$

where

$$\mathbf{r} = \left[(1 \pm \gamma_L)(1 + \rho) + x\right]\mathbf{i} + y\mathbf{j}, \tag{3.37}$$

$$\mathbf{r}_s = r_s\left[\cos \omega_s t\mathbf{i} - \sin \omega_s t\mathbf{j}\right], \tag{3.38}$$

and $M_\odot$ is the mass of the Sun. Since $r_s \gg r$, Equation 3.36 can be expanded in a power series

$$U_D = -\frac{M_\odot}{r_s}\left\{1 + \left[\frac{3}{2}\left(\frac{\mathbf{r}_s \cdot \mathbf{r}}{r_s^2}\right)^2 - \frac{1}{2}\left(\frac{r}{r_s}\right)^2\right] + \left[\frac{5}{2}\left(\frac{\mathbf{r}_s \cdot \mathbf{r}}{r_s^2}\right)^3 - \frac{3}{2}\left(\frac{\mathbf{r}_s \cdot \mathbf{r}}{r_s^2}\right)\left(\frac{r}{r_s}\right)^2\right] + \ldots\right\}. \tag{3.39}$$

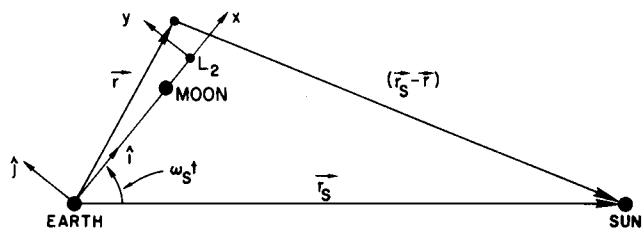

Figure 3.3–Geometry for direct solar perturbation near a collinear point of the Earth-Moon system.

Therefore, the acceleration can be written

$$\mathbf{P}_D = -\nabla U_D = m^2 r\left\{\left[3(\hat{\mathbf{r}}\cdot\hat{\mathbf{r}}_s)\hat{\mathbf{r}}_s - \hat{\mathbf{r}}\right] + \left(\frac{r}{r_s}\right)\left[\frac{15}{2}(\hat{\mathbf{r}}\cdot\hat{\mathbf{r}}_s)^2\hat{\mathbf{r}}_s - 3(\hat{\mathbf{r}}\cdot\hat{\mathbf{r}}_s)\hat{\mathbf{r}} - \frac{3}{2}\hat{\mathbf{r}}_s\right] + \ldots\right\}, \tag{3.40}$$

where $M_\odot/r_s^3 = m^2$. The components of $\mathbf{P}_D$ are approximately

$$P_{xD} = \mathbf{P}_D \cdot \mathbf{i} \cong m^2 r\left\{\frac{1}{2}(3\cos 2\omega_s t + 1) - \frac{3}{2}\left(\frac{y}{r}\right)\sin 2\omega_s t + \left(\frac{r}{r_s}\right)\left[\frac{3}{8}(3\cos\omega_s t + 5\cos 3\omega_s t) - \frac{3}{4}\left(\frac{y}{r}\right)(\sin\omega_s t + 5\sin 3\omega_s t)\right]\right\} \tag{3.41}$$

and

$$P_{yD} = \mathbf{P}_D \cdot \mathbf{j} \cong m^2 r\left\{-\frac{3}{2}\sin 2\omega_s t + \frac{1}{2}\left(\frac{y}{r}\right)(1 - 3\cos 2\omega_s t) - \left(\frac{r}{r_s}\right)\left[\frac{3}{8}(\sin\omega_s t + 5\sin 3\omega_s t) - \frac{3}{4}\left(\frac{y}{r}\right)(\cos\omega_s t - 5\cos 3\omega_s t)\right]\right\}. \tag{3.42}$$

Cancellation of first-order terms at a collinear point

The indirect solar perturbation enters through ρ and ν. From Equations 2.43a and 2.43b, it can be seen that the indirect acceleration at a collinear point is approximately

$$P_{xI} \cong -(1 \pm \gamma_L)(\ddot{\rho} - 2\nu - 3\rho) \tag{3.43}$$

and

$$P_{yI} \cong -(1 \pm \gamma_L)(2\dot{\rho} + \dot{\nu}). \tag{3.44}$$

To be in harmony with Colombo's solution, it is only necessary to show that all acceleration terms to $O(m^3)$ vanish. The linear approximations in Equations 3.43 and 3.44 are sufficiently accurate for this purpose. To the same order of approximation, Equations 3.41 and 3.42 are

$$P_{xD} \cong \frac{1}{2}m^2(1 \pm \gamma_L)(3\cos 2\omega_s t + 1) \tag{3.45}$$

and

$$P_{yD} \cong -\frac{3}{2}m^2(1 \pm \gamma_L)\sin 2\omega_s t. \tag{3.46}$$

Substituting Equations 3.31 to 3.35 [keeping *only* terms to $O(m^3)$] into Equations 3.43 and 3.44, it is found that $P_{xI} + P_{xD} = 0$ and $P_{yI} + P_{yD} = 0$ to $O(m^3)$.*

Periodic orbit correction

Using Equations 2.43a, 2.43b, 3.41, and 3.42 and neglecting terms of $O(m^4)$, the linearized equations of motion in the vicinity of a collinear point are

*In an earlier paper (Reference 7), this author reached an erroneous conclusion regarding this cancellation because of inappropriate expressions for ρ and ν.

$$\ddot{x} - 2\dot{y} - (2B_L + 1)x = \left[2\nu - 6B_L\rho + \frac{m^2}{2}(1 + 3\cos 2\omega_s t)\right] x + \left[\dot{\nu} - \frac{3}{2}m^2 \sin 2\omega_s t\right] y + 2\nu\dot{y}$$

and (3.47)

$$\ddot{y} + 2\dot{x} + (B_L - 1)y = -\left[\dot{\nu} + \frac{3}{2}m^2 \sin 2\omega_s t\right] x + \left[2\nu + 3B_L\rho + \frac{m^2}{2}(1 - 3\cos 2\omega_s t)\right] y - 2\nu\dot{x}.$$

As before, the first approximation to a periodic orbit around a collinear point is given by Equation 3.8. A frequency correction to this periodic orbit can be obtained from Equation 3.47. The constant coefficients of $O(m^2)$ in Equation 3.47 lead to a modified characteristic equation (cf. Equation 2.49)

$$s^4 - \left[(B_L - 2) + \frac{m^2}{2}(B_L + 2)\right] s^2 - (2B_L + 1)(B_L - 1)\left(1 + \frac{m^2}{2}\right) = 0. \tag{3.48}$$

For the L_2 point, the modified characteristic equation yields a corrected frequency of $\omega_n = 1.86247$. However, because $\omega_{n0} = 1.86265$, this correction is usually negligible.

The second-order correction to the periodic orbit is found by employing the methods of Section B.3 of this chapter. Although the expressions for ρ and ν in Equations 3.31 and 3.32 contain periodic terms with frequencies ω_s and $2\omega_s$ when quantities of $O(m^3)$ are retained, only terms of frequency $2\omega_s$ are considered in this section. This should be sufficient for an order of magnitude estimate of the correction. The differential equations for the solar perturbation correction are

$$\ddot{x}_{n2} - 2\dot{y}_{n2} - (2B_L + 1)x_{n2} = K_x \sin(2\omega_s + \omega_n)t + K'_x \sin(\omega_n - 2\omega_s)t$$

and (3.49)

$$\ddot{y}_{n2} + 2\dot{x}_{n2} + (B_L - 1)y_{n2} = K_y \cos(2\omega_s + \omega_n)t + K'_y \cos(\omega_n - 2\omega_s)t,$$

where

$$K_x = \left\{k\left[\nu_3 - 3B_L\rho_3 + \frac{3}{4}m^2\right] - \nu_3\omega_n + \frac{1}{2}\left[\dot{\nu}_3 - \frac{3}{2}m^2\right]\right\} A_{y1}, \tag{3.50}$$

$$K'_x = \left\{k\left[\nu_3 - 3B_L\rho_3 + \frac{3}{4}m^2\right] - \nu_3\omega_n - \frac{1}{2}\left[\dot{\nu}_3 - \frac{3}{2}m^2\right]\right\} A_{y1}, \tag{3.51}$$

$$K_y = \left\{k\left[\frac{1}{2}\left(\dot{\nu}_3 + \frac{3}{2}m^2\right) - \nu_3\omega_n\right] + \left[\nu_3 + \frac{3}{2}B_L\rho_3 - \frac{3}{4}m^2\right]\right\} A_{y1}, \tag{3.52}$$

and

$$K'_y = \left\{-k\left[\frac{1}{2}\left(\dot{\nu}_3 + \frac{3}{2}m^2\right) + \nu_3\omega_n\right] + \left[\nu_3 + \frac{3}{2}B_L\rho_3 - \frac{3}{4}m^2\right]\right\} A_{y1}, \tag{3.53}$$

with

$$\rho_3 \equiv -\left(m^2 + \frac{19}{6}m^3\right),$$

$$\nu_3 \equiv \left(\frac{11}{4}m^2 + \frac{85}{12}m^3\right),$$

and

$$\dot{\nu}_3 \equiv -\left(\frac{11}{2}m^2 + \frac{26}{3}m^3\right).$$

Particular solutions for these differential equations are

$$x_{n2} = A_{x2} \sin(2\omega_s + \omega_n)t + A'_{x2} \sin(\omega_n - 2\omega_s)t$$

and

$$y_{n2} = A_{y2} \cos(2\omega_s + \omega_n)t + A'_{y2} \cos(\omega_n - 2\omega_s)t. \tag{3.54}$$

Once again, consider the example of Section B.3 of this chapter. Using the values

$$\rho_3 = -0.00692059, \qquad \nu_3 = 0.0183515,$$

$$\dot{\nu}_3 = -0.0344011, \qquad \omega_s = 0.925199,$$

$$m = 0.07480133, \qquad B_{L2} = 3.19042,$$

$$\omega_n = 1.86265, \qquad k = 0.343336,$$

it is found that

$$K_x = -0.025096\ A_{y1}, \qquad A_{x2} = 0.0029012\ A_{y1},$$

$$K'_x = 0.017698\ A_{y1}, \qquad A'_{x2} = -0.0024375\ A_{y1},$$

$$K_y = -0.035165\ A_{y1}, \qquad A_{y2} = 0.0048903\ A_{y1},$$

$$K'_y = -0.026236\ A_{y1}, \qquad A'_{y2} = -0.011951\ A_{y1},$$

and for $A_{y1} = 0.02 = 7688.1$ km

$$K_x = -1.3934 \times 10^{-7} g, \qquad A_{x2} = 22.30 \text{ km},$$

$$K'_x = 9.8264 \times 10^{-8} g, \qquad A'_{x2} = -18.74 \text{ km},$$

$$K_y = -1.9524 \times 10^{-7} g, \qquad A_{y2} = 37.60 \text{ km},$$

$$K'_y = -1.4567 \times 10^{-7} g, \qquad A'_{y2} = -91.88 \text{ km}.$$

Although these corrections are small, the solar perturbation terms should be included in periodic orbit calculations because accelerations of $10^{-7} g$ are not insignificant.

2. Effect of the Moon at the Sun-Earth Collinear Points

The geometry for the Sun-Earth-Moon system is depicted in Figure 3.4. Consider a point O that is collinear with the Earth-Moon barycenter B and the Sun. The distance r_{BO} is determined by assuming that the total mass of the Earth and Moon are concentrated at B, and then taking r_{BO} as the libration-point distance γ_L for $\mu = (m_1 + m_2)/(m_1 + m_2 + m_3)$. Does the point O lie closer to an equilibrium solution in the Sun-Earth-Moon system than the classical Sun-Earth collinear libration point? This question can be resolved by finding the perturbed path (dynamic equilibrium point or "nominal path") for a satellite in the vicinity of the point O. If the maximum radius of the perturbed path relative to O is smaller than the distance from O to the classical collinear point, then it is more appropriate to consider O to be a collinear libration point of the Sun-Earth-Moon system.

The accelerations relative to an inertial reference system can be obtained with the aid of Figure 3.4. Defining $\mathbf{r}_{ij} \equiv \mathbf{r}_j - \mathbf{r}_i$, these accelerations are

$$\ddot{\mathbf{r}}_O = \frac{m_1\mathbf{r}_{O1}}{r_{O1}^3} + \frac{m_2\mathbf{r}_{O2}}{r_{O2}^3} + \frac{m_3\mathbf{r}_{O3}}{r_{O3}^3}, \tag{3.55}$$

$$\ddot{\mathbf{r}}_1 = \frac{m_2\mathbf{r}_{12}}{r_{12}^3} + \frac{m_3\mathbf{r}_{13}}{r_{13}^3}, \tag{3.56}$$

$$\ddot{\mathbf{r}}_2 = -\frac{m_1\mathbf{r}_{12}}{r_{12}^3} + \frac{m_3\mathbf{r}_{23}}{r_{23}^3}, \tag{3.57}$$

and

$$\ddot{\mathbf{r}}_3 = -\frac{m_1\mathbf{r}_{13}}{r_{13}^3} - \frac{m_2\mathbf{r}_{23}}{r_{23}^3}. \tag{3.58}$$

Using the definition of the barycenter ($m_1\mathbf{r}_{B1} + m_2\mathbf{r}_{B2} = 0$), it is found that

$$\mathbf{r}_B = \mathbf{r}_2 - \mathbf{r}_{B2} = \mathbf{r}_2 - \frac{m_1}{m_1 + m_2}(\mathbf{r}_2 - \mathbf{r}_1) = \frac{m_2}{m_1 + m_2}\mathbf{r}_2 + \frac{m_1}{m_1 + m_2}\mathbf{r}_1. \tag{3.59}$$

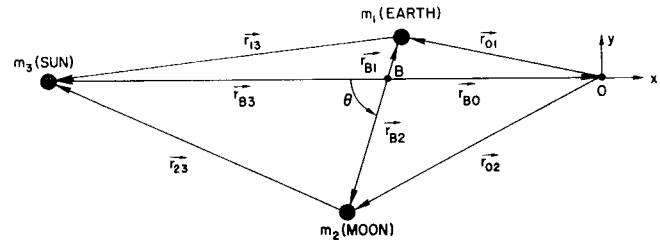

Figure 3.4–Geometry for a collinear point in the Sun-Earth-Moon system.

Differentiating Equation 3.59 and substituting Equations 3.56 and 3.57 gives

$$\ddot{\mathbf{r}}_B = m_3\left[\frac{m_1\mathbf{r}_{13}}{(m_1 + m_2)r_{13}^3} + \frac{m_2\mathbf{r}_{23}}{(m_1 + m_2)r_{23}^3}\right]. \tag{3.60}$$

This relation, along with Equation 3.58, leads to*

*This result is obtained by keeping only the first term in an expansion where the ratio of the second term to the first term is about 8×10^{-8}.

$$\ddot{\mathbf{r}}_{B3} = \ddot{\mathbf{r}}_3 - \ddot{\mathbf{r}}_B = -\frac{m_1 + m_2 + m_3}{m_1 + m_2}\left[\frac{m_1\mathbf{r}_{13}}{r_{13}^3} + \frac{m_2\mathbf{r}_{23}}{r_{23}^3}\right] \cong -\frac{(m_1 + m_2 + m_3)}{r_{B3}^3}\mathbf{r}_{B3}. \tag{3.61}$$

Making use of Equations 3.55, 3.60, and 3.61, it is now possible to give the acceleration of a satellite at O relative to the Sun as

$$\ddot{\mathbf{r}}_{3O} = \ddot{\mathbf{r}}_{BO} - \ddot{\mathbf{r}}_{B3} = \ddot{\mathbf{r}}_O - \ddot{\mathbf{r}}_B - \ddot{\mathbf{r}}_{B3} = -\frac{m_3\mathbf{r}_{3O}}{r_{3O}^3} + \frac{(m_1 + m_2 + m_3)}{r_{B3}^3}\mathbf{r}_{B3} - \frac{1}{r_{O1}^3}(m_2\mathbf{r}_{B2} + m_1\mathbf{r}_{BO})$$

$$+\frac{m_2}{r_{O2}^3}(\mathbf{r}_{B2} - \mathbf{r}_{BO}) - \frac{m_3}{(m_1 + m_2)r_{13}^3}(m_1\mathbf{r}_{B3} + m_2\mathbf{r}_{B2}) - \frac{m_3m_2}{(m_1 + m_2)r_{23}^3}(\mathbf{r}_{B3} - \mathbf{r}_{B2}). \tag{3.62}$$

Neglecting terms of $O(r_{B2}/r_{BO})^4$, ($r_{B2}/r_{BO} \cong 1/4$), a moderate amount of algebra reduces Equation 3.62 to

$$\ddot{\mathbf{r}}_{3O} \cong -\frac{m_3\mathbf{r}_{3O}}{r_{3O}^3} - (m_1 + m_2)\left[\frac{\mathbf{r}_{BO}}{r_{BO}^3} - \frac{\mathbf{r}_{B3}}{r_{B3}^3}\right] + \mathbf{P}, \tag{3.63}$$

where

$$\mathbf{P} = \frac{m_2}{r_{BO}^3}\left\{\left[3\frac{\mathbf{r}_{B2}\cdot\mathbf{r}_{BO}}{r_{BO}^2} - \frac{3}{2}\left(\frac{r_{B2}}{r_{BO}}\right)^2 + \frac{15}{2}\left(\frac{\mathbf{r}_{B2}\cdot\mathbf{r}_{BO}}{r_{BO}^2}\right)^2\right]\mathbf{r}_{B2} + \left[\frac{3}{2}\left(\frac{r_{B2}}{r_{BO}}\right)^2\right.\right.$$

$$\left.\left. - \frac{15}{2}\left(\frac{\mathbf{r}_{B2}\cdot\mathbf{r}_{BO}}{r_{BO}^2}\right)^2 + \frac{15}{2}\left(\frac{r_{B2}}{r_{BO}}\right)^2\left(\frac{\mathbf{r}_{B2}\cdot\mathbf{r}_{BO}}{r_{BO}^2}\right) - \frac{35}{2}\left(\frac{\mathbf{r}_{B2}\cdot\mathbf{r}_{BO}}{r_{BO}^2}\right)^3\right]\mathbf{r}_{BO}\right\}. \tag{3.64}$$

Since $r_{BO} = \gamma_L$, it is immediately obvious from Equation 3.63 that $\ddot{\mathbf{r}}_{3O} = \mathbf{P}$.

For the remainder of the analysis, the orbital eccentricities and the inclination of the Earth-Moon orbit to the ecliptic are neglected. Essentially nothing is lost here because this approximation is consistent with the deletion of terms of $O(r_{B2}/r_{BO})^4$. Using $\mathbf{r}_{B2}\cdot\mathbf{r}_{BO} = \mp r_{B2}r_{BO}\cos\theta$ (upper sign for L_2; lower sign for L_1), the linearized equations of motion relative to O become

$$\ddot{x} - 2\dot{y} - (2B_L + 1)x = P_x$$

and $$\tag{3.65}$$

$$\ddot{y} + 2\dot{x} + (B_L - 1)y = P_y,$$

where

$$P_x = \frac{m_2}{r_{BO}^2}\left(\frac{r_{B2}}{r_{BO}}\right)^2\left\{\mp\frac{3}{4}[1 + 3\cos 2\theta] + \frac{1}{2}[3\cos\theta + 5\cos 3\theta]\left(\frac{r_{B2}}{r_{BO}}\right)\right\}, \tag{3.66}$$

$$P_y = \frac{3}{2}\frac{m_2}{r_{BO}^2}\left(\frac{r_{B2}}{r_{BO}}\right)^2\left\{\pm\sin 2\theta - \frac{1}{4}[\sin\theta + 5\sin 3\theta]\left(\frac{r_{B2}}{r_{BO}}\right)\right\}, \tag{3.67}$$

and $\theta = nt$ ($n = 13.369$). A particular solution of Equation 3.65 is the perturbed path

$$x_n = x_c + A_x \cos\theta + A'_x \cos 2\theta + A''_x \cos 3\theta$$

and

$$y_n = A_y \sin\theta + A'_y \sin 2\theta + A''_y \sin 3\theta. \tag{3.68}$$

For the perturbed path at the L_2 point,

$$m_2 = 3.7397 \times 10^{-8}, \qquad B_{L2} = 3.9405,$$

$$r_{BO} = 1.0078 \times 10^{-2}, \qquad \left(\frac{r_{B2}}{r_{BO}}\right) = 0.25187,$$

$$K \equiv \frac{m_2}{r_{BO}^2}\left(\frac{r_{B2}}{r_{BO}}\right)^2 = 2.5358 \times 10^{-5} = 1.4120 \times 10^{-8} g,$$

$$x_c = 295.10 \text{ km},$$

$$A_x = -7.47 \text{ km}, \qquad A_y = 3.01 \text{ km},$$

$$A'_x = 11.47 \text{ km}, \qquad A'_y = -8.22 \text{ km},$$

$$A''_x = -1.41 \text{ km}, \qquad A''_y = 1.10 \text{ km}.$$

The constant term x_c represents a shift along the x-axis to a new point O'. Relative to O', the maximum distance to the perturbed path is about 20 km. Therefore, the point O' is never further than about 20 km from a dynamic "equilibrium" point of the restricted four-body problem (Sun, Earth, Moon, and satellite).

3. Jupiter's Effect at the Sun-Earth Isosceles-Triangle Points

A satellite moving in the Earth's orbit around the Sun will be perturbed by several bodies, e.g., Earth, Moon, or Jupiter. The relative importance of the different effects may be quite variable, depending on the distance of the satellite from the Earth. In Chapter II, the Earth's effect was considered, and artificial libration points were created by canceling this effect with a constant thrust acceleration. The principal objective of this section is to obtain an estimate of Jupiter's effect at these artificial libration points (isosceles-triangle points) when the satellite is relatively close to the Earth.

The geometry for Jupiter's perturbation at a Sun-Earth isosceles-triangle point is shown in Figure 3.5. Neglecting some small indirect effects, Jupiter's perturbative acceleration is

$$\mathbf{P}_J = M_J \left[\frac{\mathbf{r}}{r^3} - \frac{\mathbf{r}_E}{r_E^3}\right]. \tag{3.69}$$

Assuming that (a/r) is small, Equation 3.69 becomes

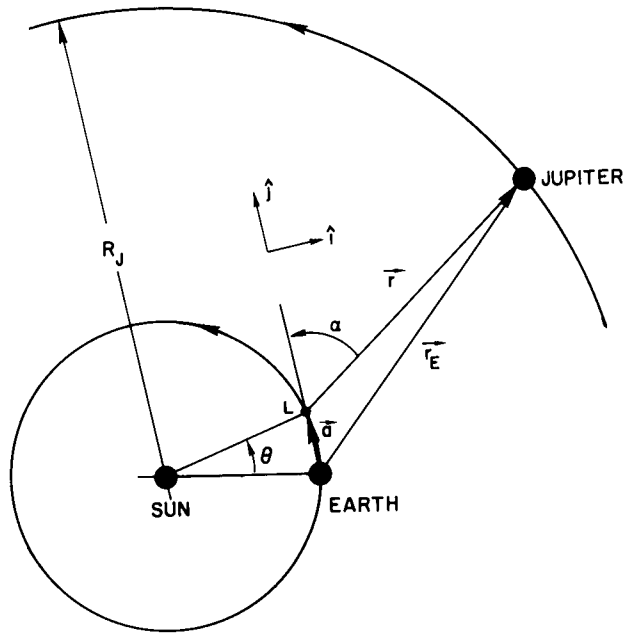

Figure 3.5–Geometry for Jupiter's perturbation at a Sun-Earth isosceles-triangle point.

$$\mathbf{P}_J \cong \frac{M_J}{r^3}\left[-\mathbf{a} + 3\frac{\mathbf{r}\cdot\mathbf{a}}{r^2}\mathbf{r}\right], \tag{3.70}$$

and the components are given by

$$P_{Jx} = \mathbf{P}_J \cdot \mathbf{i} = \frac{3}{2}\frac{M_J}{r^2}\left(\frac{a}{r}\right)\sin 2\alpha \tag{3.71}$$

and

$$P_{Jy} = \mathbf{P}_J \cdot \mathbf{j} = \frac{1}{2}\frac{M_J}{r^2}\left(\frac{a}{r}\right)[1 + 3\cos 2\alpha]. \tag{3.72}$$

The magnitude of Jupiter's acceleration is

$$|\mathbf{P}_J| = \frac{1}{2}\frac{M_J}{r^2}\left(\frac{a}{r}\right)[10 + 6\cos 2\alpha]^{1/2}. \tag{3.73}$$

For $\theta = 10°$ and $\alpha = 90°$, rough calculations give $|\mathbf{P}_J| \cong 1.35 \times 10^{-9} g$ (this value is relatively constant for $0° < \alpha < 180°$). Because the thrust acceleration at $\theta = 10°$ is $|\mathbf{F}_c| \cong 6.02 \times 10^{-8} g$, Jupiter's perturbation can be ignored when $\theta < 10°$.

4. Solar Effect at the Earth-Moon Equilateral-Triangle Points

The analysis of the uncontrolled motion of a satellite in the vicinity of the Sun-perturbed Earth-Moon equilateral-triangle points represents one of the most difficult problems in celestial mechanics. In the past few years, several papers, e.g., see References 48 to 55, have appeared on this subject. A recent analytical study by Schechter (Reference 54) is probably the most productive to date, and some of his conclusions have been verified by the numerical work of Kolenkiewicz and Carpenter (Reference 55). However, the general problem remains unsolved because the important effect of the lunar eccentricity was not considered in Schechter's study.

CHAPTER IV

LINEAR FEEDBACK CONTROL

After a satellite has been injected into the vicinity of a libration point, a translation control system can be used to eliminate the initial errors. This control system can also be used for station keeping. To implement this control, closed-loop guidance laws (feedback control logic) will be needed. In this chapter, *simple* linear feedback control laws are developed for the collinear and equilateral-triangle points. Although the control acceleration is treated as if it were continuous, this assumption is not overly restrictive because a pulsed control will behave essentially like a continuous control if the frequency of the pulse control is much higher than any of the natural frequencies of the system.*

For motion in the immediate vicinity of a libration point, the linearized equations of motion are sufficiently accurate. These equations will contain periodic coefficients if eccentricity is present or if the satellite is following a nominal path. In many instances, these effects are small and can be neglected. However, to obtain some estimate of the importance of these periodic coefficients, Floquet stability investigations for some representative cases are included here.

A. Collinear Points

For small eccentricities, the linearized equations of motion at a collinear point (or relative to a *small* nominal path about the point) are approximately (from Equation 3.4)†

$$\ddot{x} - 2\dot{y} - (2B_L + 1)x = F_{cx}, \tag{4.1a}$$

$$\ddot{y} + 2\dot{x} + (B_L - 1)y = F_{cy}, \tag{4.1b}$$

and

$$\ddot{z} + B_L z = F_{cz}. \tag{4.1c}$$

The z-axis motion is bounded and can be damped by simply taking $F_{cz} = -k_1'\dot{z}$, where the feedback gain $k_1' > 0$. The control synthesis for the unstable xy-motion is less obvious, but it can be accomplished with classical methods [Routh criterion (Reference 56) and root locus (Reference 57)].

*The continuous approximation is probably adequate if the pulsing rate is greater than 10 times any of the natural frequencies of the system.

†For the equations relative to a nominal path, the variables (ξ, η, ζ) should be used ($\xi = x - x_n$, etc.). However, this distinction will be overlooked when the equations have the same form.

1. Routh Stability Conditions

For a radial-axis (x-axis) control using only range and range-rate (x and $\dot{x}$) feedback, the control is

$$F_{cx} = -k_1\dot{x} - k_2x$$

and

$$F_{cy} = 0. \tag{4.2}$$

This leads to the characteristic equation

$$s^4 + k_1s^3 + \left[k_2 - (B_L - 2)\right]s^2 + k_1(B_L - 1)s + \left[k_2 - (2B_L + 1)\right](B_L - 1) = 0. \tag{4.3}$$

From Routh's criterion, the necessary and sufficient conditions for asymptotic stability are

$$k_1 > 0$$

and

$$k_2 > (2B_L + 1). \tag{4.4}$$

It is shown in the next section that, for certain values of k_1 and k_2, more damping can be obtained by adding some positive y-feedback. For this case

$$F_{cx} = -k_1\dot{x} - k_2x + k_4y$$

and

$$F_{cy} = 0, \tag{4.5}$$

and the characteristic equation is*

$$s^4 + k_1s^3 + \left[k_2 - (B_L - 2)\right]s^2 + \left[k_1(B_L - 1) + 2k_4\right]s + \left[k_2 - (2B_L + 1)\right](B_L - 1) = 0. \tag{4.6}$$

The Routh conditions are

$$k_1 > 0, \quad k_2 > 2B_L + 1,$$

$$k_1(B_L - 1) + 2k_4 > 0, \tag{4.7}$$

and

$$2k_1^2(B_L - 1) - k_4\left\{k_1\left[3B_L - (k_2 + 4)\right] + 2k_4\right\} > 0.$$

If cross-axis (y-axis) control is used, it is necessary to feed back all of the state variables for stability. This control can be written

$$F_{cx} = 0$$

and

$$F_{cy} = -k_5\dot{x} - k_6x - k_7\dot{y} + k_8y. \tag{4.8}$$

*The same characteristic equation is obtained with the dual-axis control, $F_{cx} = -k_1\dot{x} - k_2x$, $F_{cy} = -k_6x$, with k_6 replacing k_4.

The characteristic equation is given by*

$$s^4 + k_7 s^3 + \left[2k_5 - k_8 - (B_L - 2)\right]s^2 + \left[2k_6 - k_7(2B_L + 1)\right]s + \left[k_8 - (B_L - 1)\right](2B_L + 1) = 0, \qquad (4.9)$$

and the Routh conditions are

$$k_7 > 0, \quad 2k_5 > k_8 + (B_L - 2),$$

$$2k_6 > k_7(2B_L + 1), \quad k_8 > (B_L - 1), \qquad (4.10)$$

and

$$k_6\left\{k_7\left[2k_5 - k_8 + (3B_L + 4)\right] - 2k_6\right\} - k_7^2(k_5 + 2)(2B_L + 1) > 0.$$

2. Root Loci and Closed-Loop Response

The preceding section has shown that it is possible to obtain a stable radial-axis control that requires only range and range-rate measurements. However, it is still necessary to select the gains k_1 and k_2 for a satisfactory response. A simple method for determining these gains is to use root-locus plots. Taking $k_1 = 0$ and writing Equation 4.3 in the form

$$\frac{k_2\left[s^2 + (B_L - 1)\right]}{s^4 - (B_L - 2)s^2 - (2B_L + 1)(B_L - 1)} = -1 \qquad (4.11)$$

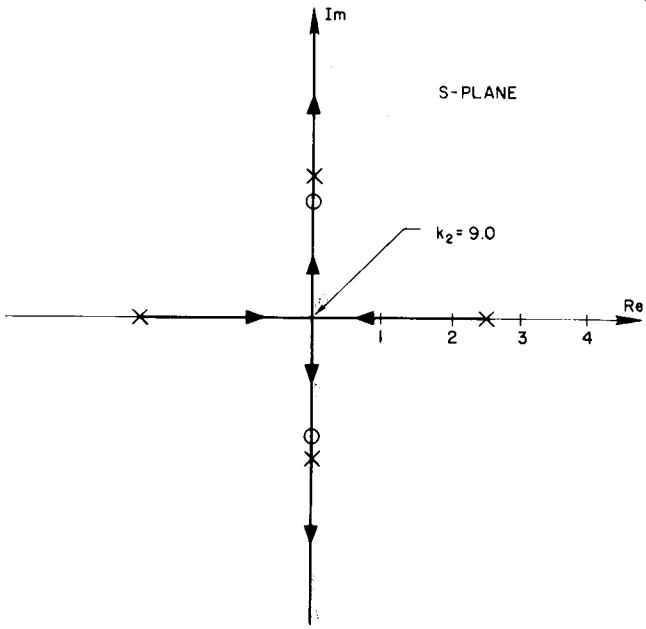

Figure 4.1—Root-locus plot for Equation 4.11. Gain is k_2, and $B_L = 4$.

leads to the root-locus plot of Figure 4.1. It is seen that neutral stability is obtained when $k_2 > (2B_L + 1)$. When $k_1 \neq 0$, Equation 4.3 can be written

$$\frac{k_1 s\left[s^2 + (B_L - 1)\right]}{s^4 + \left[k_2 - (B_L - 2)\right]s^2 + (B_L - 1)\left[k_2 - (2B_L + 1)\right]} = -1. \qquad (4.12)$$

The root loci of Equation 4.12 and some corresponding response diagrams† are depicted in Figures 4.2 to 4.7 for three values of k_2. Inspection of these figures shows that, for $B_L = 4$, a well-damped response can be achieved by taking $k_1 = 4.0$ and $k_2 = 12.0$ (note that $k_1 = \frac{1}{3}k_2$).

It is obvious that the response will be underdamped whenever k_2 is too large. However, when the radial-axis control is augmented with positive $\dot{y}$-feedback, it is possible to obtain more damping.

*This characteristic equation can also be obtained with the dual-axis control, $F_{cx} = k_3\dot{y} + k_4 y$, $F_{cy} = -k_7\dot{y} + k_8 y$, with k_3 and k_4 replacing k_5 and k_6, respectively.

†The response diagrams were obtained from a TR-48 analog computer simulation.

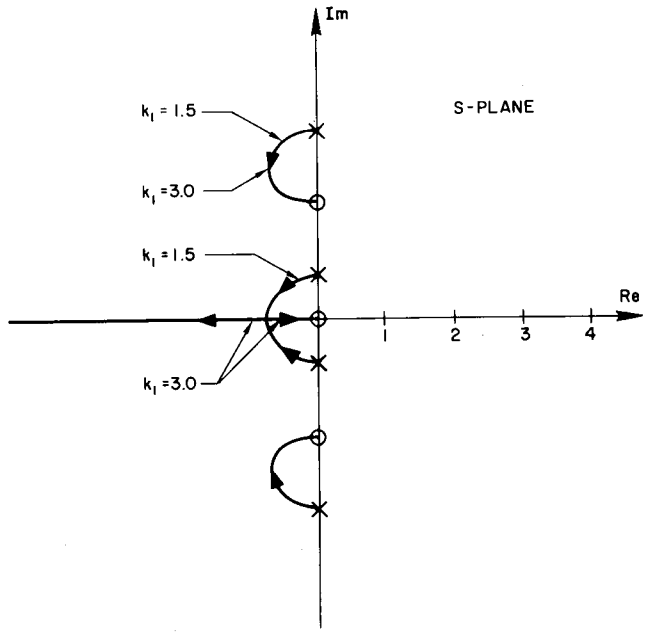

Figure 4.2–Left, root-locus plot for Equation 4.12. Gain is k_1, $k_2 = 10$, and $B_L = 4$.

Figure 4.3–Below, response with radial-axis control of Equation 4.2, y versus x, $k_2 = 10$, $B_L = 4$, and $\dot{x}(0) = \dot{y}(0) = 0$.

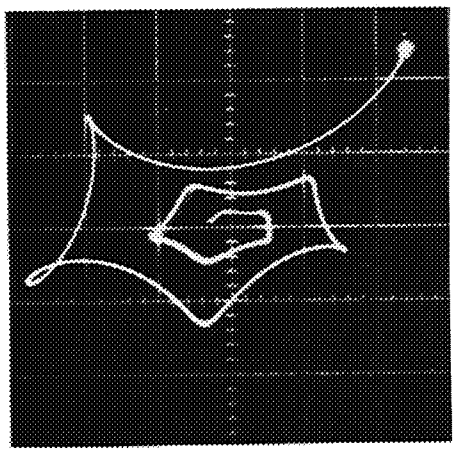

$k_1 = 0.5$.

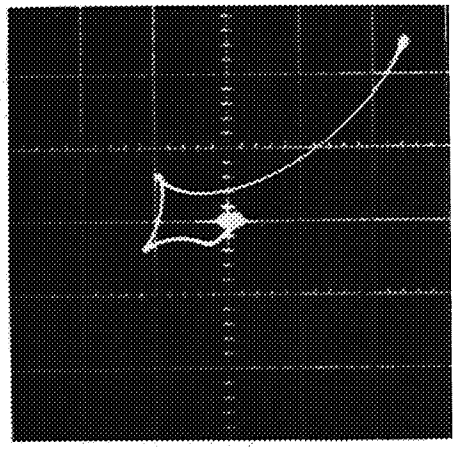

$k_1 = 1.5$.

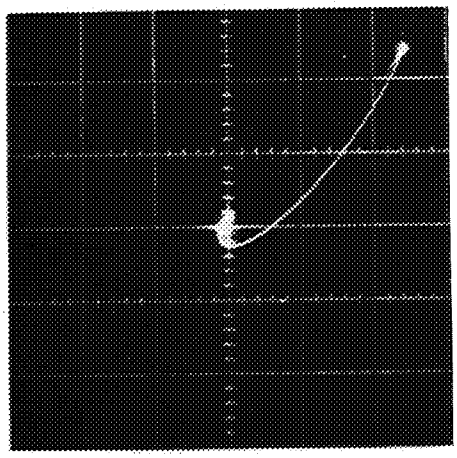

$k_1 = 3$.

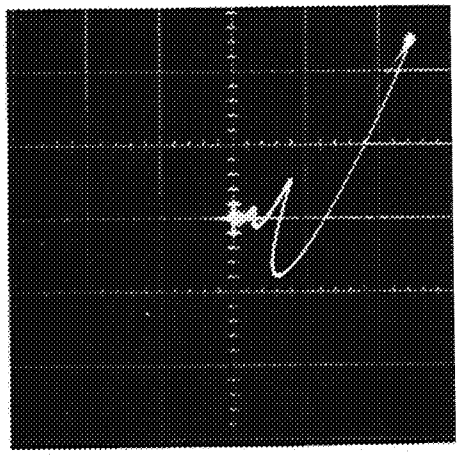

$k_1 = 5$.

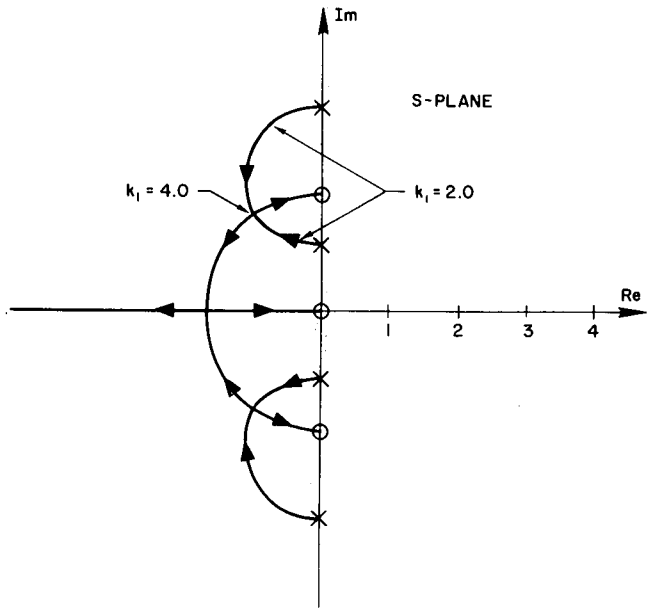

Figure 4.4–Left, root-locus plot for Equation 4.12. Gain is k_1, $k_2 = 12$, and $B_L = 4$.

Figure 4.5–Below, response with radial-axis control of Equation 4.2, y versus x, $k_2 = 12$, $B_L = 4$, and $\dot{x}(0) = \dot{y}(0) = 0$.

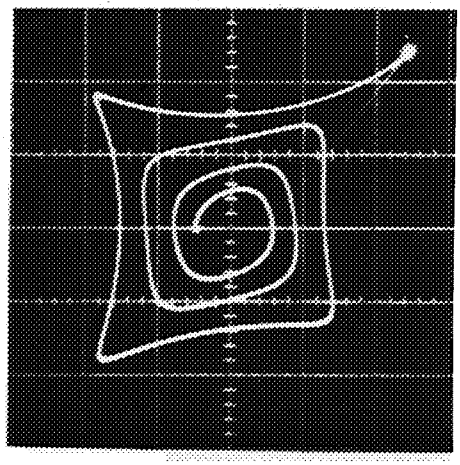

$k_1 = 0.5$.

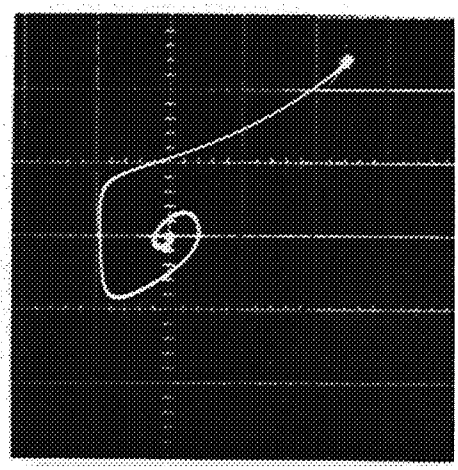

$k_1 = 2$.

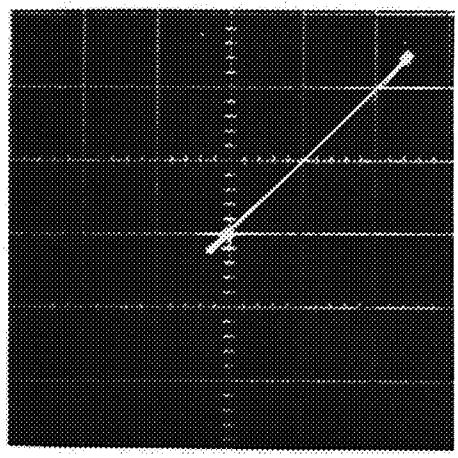

$k_1 = 4$.

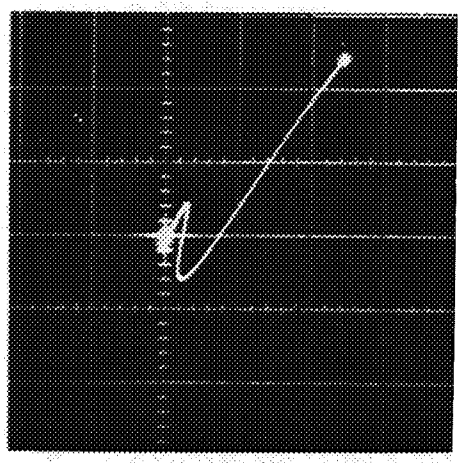

$k_1 = 6$.

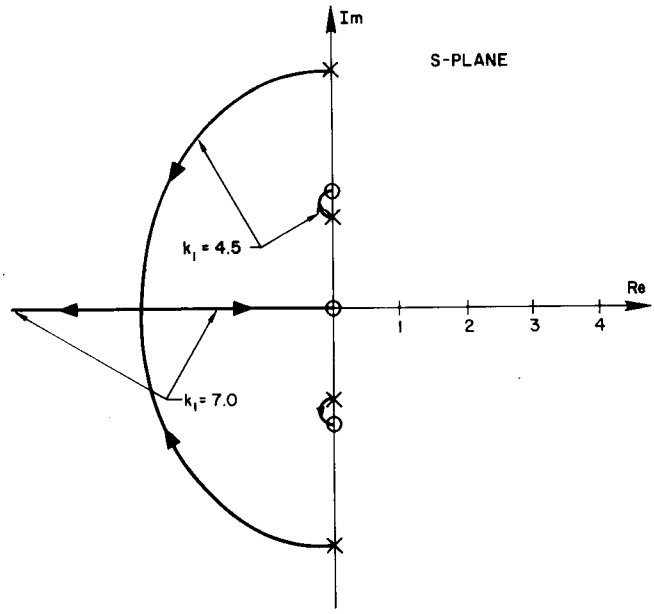

Figure 4.6–Left, root-locus plot for Equation 4.12. Gain is k_1, $k_2 = 16$, and $B_L = 4$.

Figure 4.7–Below, response with radial-axis control of Equation 4.2, y versus x, $k_2 = 16$, $B_L = 4$, and $\dot{x}(0) = \dot{y}(0) = 0$.

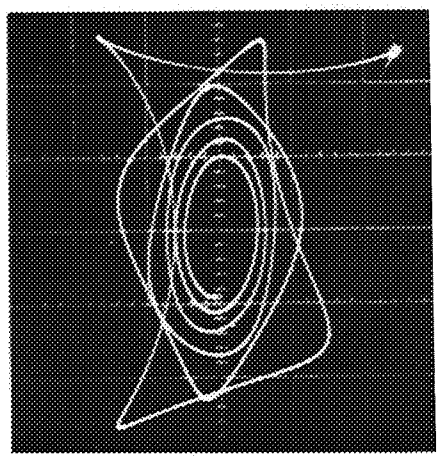

$k_1 = 0.5$.

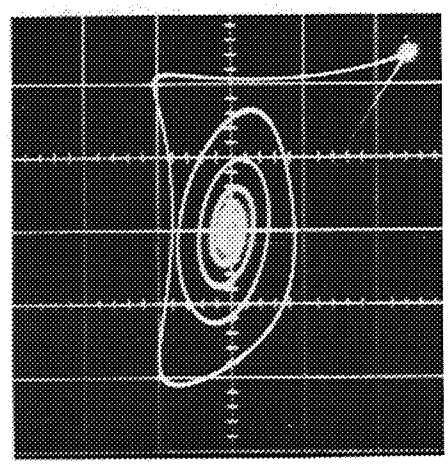

$k_1 = 1.5$.

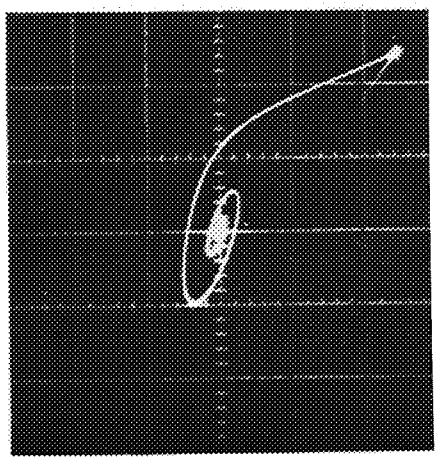

$k_1 = 4.5$.

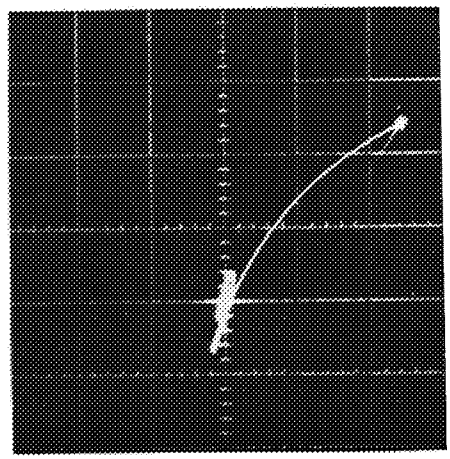

$k_1 = 7$.

This can be seen at once by comparing Figures 4.7 and 4.8 (note instability at $k_1 = 0.5$ in Figure 4.8.) An explanation for this behavior can be found by writing Equation 4.9 as

$$\frac{2k_4 s}{s^4 + k_1 s^3 + \left[k_2 - (B_L - 2)\right]s^2 + k_1(B_L - 1)s + (B_L - 1)\left[k_2 - (2B_L + 1)\right]} = -1 \tag{4.13}$$

and examining the resulting root-locus plot given in Figure 4.9. It can be seen that the damping will be increased for small values of k_4, but instability can occur if k_4 becomes too large.

3. Floquet Stability Investigations

In some instances, the magnitudes of the periodic coefficients in the linearized equations of motion are appreciable. Therefore, the effects of these coefficients on the stability of the closed-loop system should be examined. If the effects from the eccentricity and the amplitude of a nominal path are analyzed

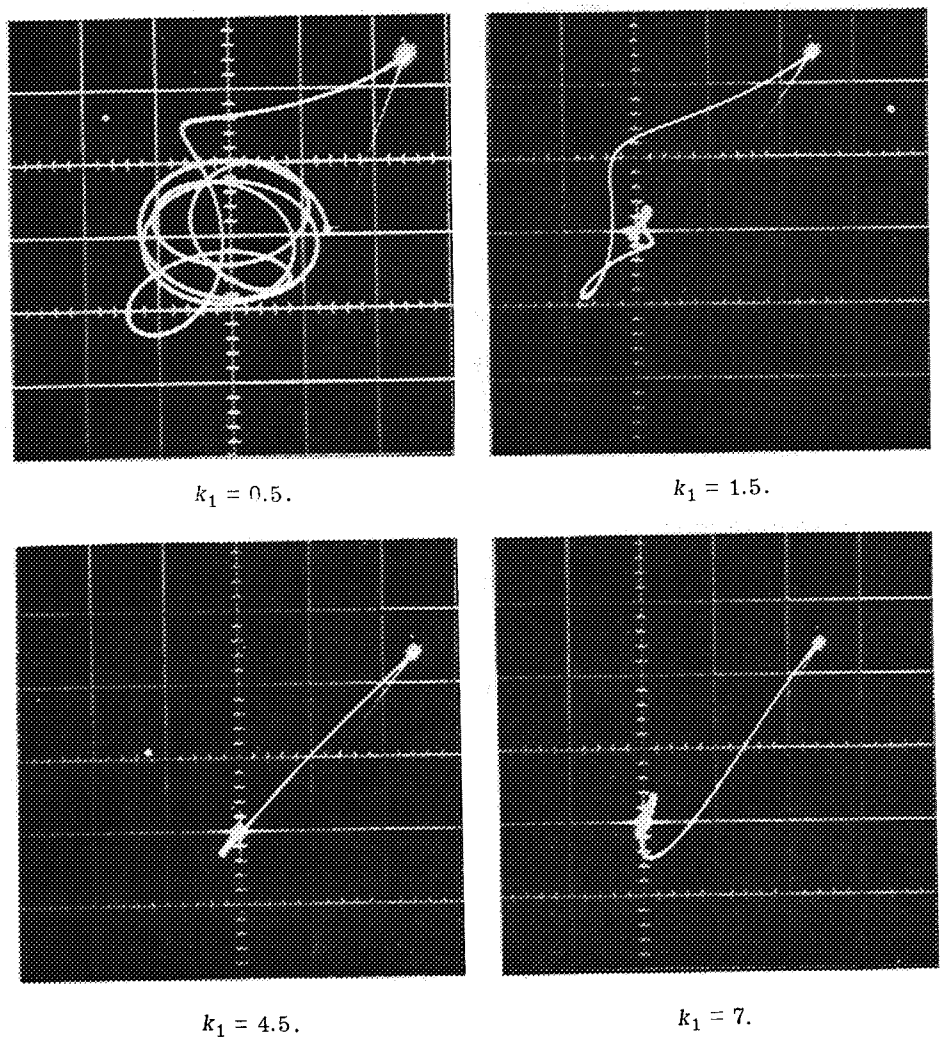

$k_1 = 0.5$. $k_1 = 1.5$.

$k_1 = 4.5$. $k_1 = 7$.

Figure 4.8–Response with radial-axis control of Equation 4.5, y versus x, $k_2 = 16$, $k_4 = 3.5$, $B_L = 4$, and $\dot{x}(0) = \dot{y}(0) = 0$.

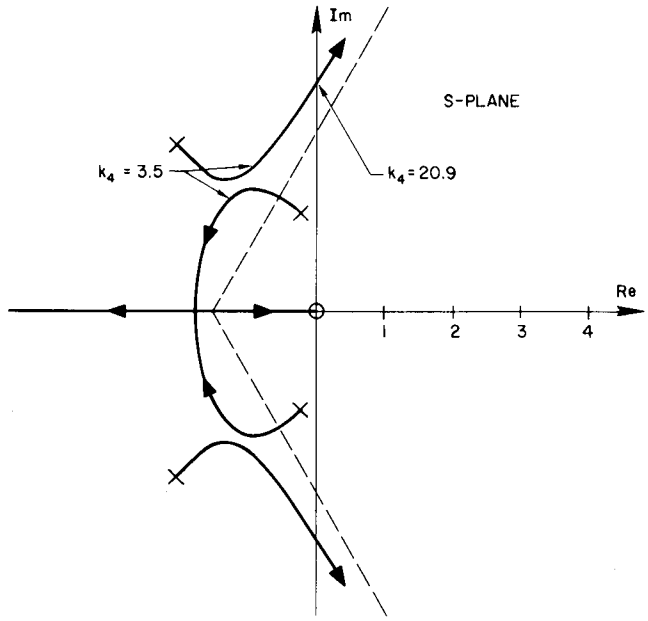

Figure 4.9—Root-locus plot for Equation 4.13. Gain is k_4, $k_1 = 4.5$, $k_2 = 16$, and $B_L = 4$.

separately,* this examination can be performed in an efficient manner by making use of Floquet theory (Reference 58).

The linearized equations of motion can be written in the matrix form

$$\dot{X}(t) = F(t)X(t). \tag{4.14}$$

For a two-dimensional analysis (fourth-order system), $X(t)$ is a 4×1 state vector and $F(t)$ is a 4×4 periodic matrix [i.e., $F(t) = F(t + T)$]. To implement Floquet's theory, it is first necessary to define a 4×4 matrix $H(t)$ by

$$\dot{H}(t) = F(t)H(t)$$

and

$$H(0) = I \quad \text{(unit matrix)}. \tag{4.15}$$

Equation 4.15 is integrated numerically to obtain $H(T)$, and the following characteristic equation is formed

$$\det [H(T) - \lambda I] = 0. \tag{4.16}$$

On the assumption that the roots λ_j ($j = 1, 2, 3, 4$) of Equation 4.16 are distinct, Floquet's theorem states that all solutions of Equation 4.14 are bounded if and only if

$$|\lambda_j| \leq 1 \quad j = 1, 2, 3, 4. \tag{4.17}$$

Eccentricity effect

From Equations 2.43 and 4.2, the linearized equations of motion at a collinear point with radial-axis control are

$$\ddot{x} - 2(1 + \nu)\dot{y} - (2B_L + 1)x = (2\nu - 6B_L\rho)x + \dot{\nu}y - k_1\dot{x} - k_2x$$

and

$$\ddot{y} + 2(1 + \nu)\dot{x} + (B_L - 1)y = -\dot{\nu}x + (2\nu + 3B_L\rho)y. \tag{4.18}$$

Neglecting terms of $O(e^2)$ (cf. Equation 3.19),

$$\rho = -e \cos t$$

and

$$\nu = 2e \cos t. \tag{4.19}$$

Therefore, $T = 2\pi$, and

*In general, some coupling is present.

$$X(t) = \begin{bmatrix} x(t) \\ \dot{x}(t) \\ y(t) \\ \dot{y}(t) \end{bmatrix}, \tag{4.20}$$

$$F(t) = \begin{bmatrix} 0 & 1 & 0 & 0 \\ F_{21} & -k_1 & F_{23} & F_{24} \\ 0 & 0 & 0 & 1 \\ F_{41} & F_{42} & F_{43} & 0 \end{bmatrix}, \tag{4.21}$$

$$F_{21} = \left[(2B_L + 1) - k_2 + 2e(2 + 3B_L) \cos t\right], \tag{4.22}$$

$$F_{23} = -F_{41} = -2e \sin t, \tag{4.23}$$

$$F_{24} = -F_{42} = 2(1 + 2e \cos t), \tag{4.24}$$

and

$$F_{43} = -\left[(B_L - 1) + e(3B_L - 4) \cos t\right]. \tag{4.25}$$

When Equations 4.20 to 4.25 are substituted into Equation 4.14, and when the aforementioned procedure is carried out, the instability regions of the parameter space (k_1, k_2) are determined. Instability charts for the collinear points of the Earth-Moon system are given in Figure 4.10.

Two interesting features of these charts should be pointed out. By analogy with the constant coefficient system, Equation 4.22 suggests that the periodic coefficient system may be stable if

$$k_2 > (2B_L + 1) + 2e(2 + 3B_L). \tag{4.26}$$

For the Earth-Moon system, Equation 4.26 gives $\left(k_2\right)_{L1} > 13.19$ and $\left(k_2\right)_{L2} > 8.65$. When these inequalities are satisfied, the larger instability regions of Figure 4.10 are excluded. The remaining points of instability can be explained by resonance. The value of k_2 for closed-loop resonance of the constant coefficient system can be found from Equation 4.3. For $k_1 = 0$, this value of k_2 is given by

$$k_2 = \frac{(2B_L + 1)(B_L - 1) - (B_L - 2)\omega^2 - \omega^4}{(B_L - 1) - \omega^2}. \tag{4.27}$$

When $\omega = 1$, the critical values of k_2 in the Earth-Moon system are $\left(k_2\right)_{L1} = 13.57$ and $\left(k_2\right)_{L2} = 11.74$. Figure 4.10 shows that points of instability are located in the vicinity of these critical values.

It is tempting to assume that Equations 4.26 and 4.27 can be used to find the principal instability regions for any system. At the L_2 point of the Sun-Mercury system, Equation 4.26 gives $k_2 > 14.68$,

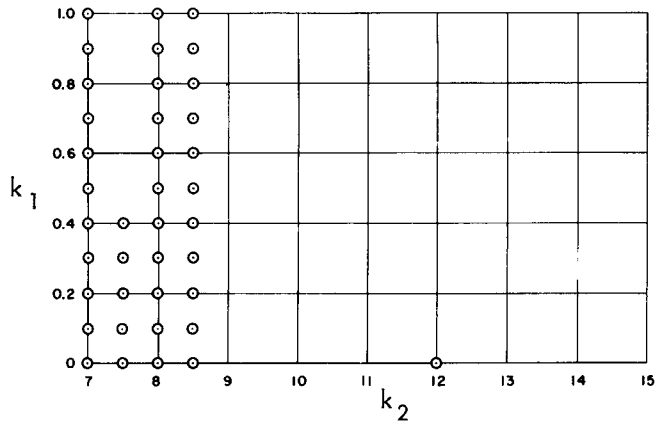

L_1 point (B_{L1} = 5.14760).

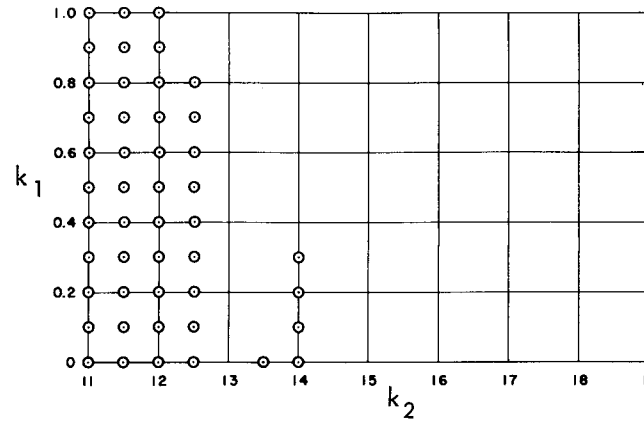

L_2 point (B_{L2} = 3.19042).

Figure 4.10–Instability charts for controlled motion, with radial-axis control of Equation 4.2, at the collinear points of the Earth-Moon system. e = 0.05490, and ⊙ – unstable.

and Equation 4.27 yields $k_2 = 11.98$. A comparison of these values with the instability chart of Figure 4.11 shows that a more sophisticated interpretation is needed for larger eccentricities.

Motion relative to a periodic orbit

If eccentricity terms are neglected, the linearized equations of motion relative to a periodic orbit around a collinear point with radial-axis control are (see Equations 3.30 and 4.2)

$$\ddot{\xi} - 2\dot{\eta} - (2B_L + 1)\xi = \mp 3C_L A_{y1}\left[2k(\sin \omega_n t)\xi - (\cos \omega_n t)\eta\right] - k_1\dot{\xi} - k_2\xi$$

and (4.28)

$$\ddot{\eta} + 2\dot{\xi} + (B_L - 1)\eta = \pm 3C_L A_{y1}\left[k(\sin \omega_n t)\eta + (\cos \omega_n t)\xi\right] .$$

In this case, $T = 2\pi/\omega_n$, and

$$X(t) = \begin{bmatrix} \xi(t) \\ \dot{\xi}(t) \\ \eta(t) \\ \dot{\eta}(t) \end{bmatrix}, \tag{4.29}$$

$$F(t) = \begin{bmatrix} 0 & 1 & 0 & 0 \\ F_{21} & -k_1 & F_{23} & 2 \\ 0 & 0 & 0 & 1 \\ F_{41} & -2 & F_{43} & 0 \end{bmatrix}, \tag{4.30}$$

$$F_{21} = \left[(2B_L + 1) - k_2 \mp 6C_L k A_{y1} \sin \omega_n t\right], \tag{4.31}$$

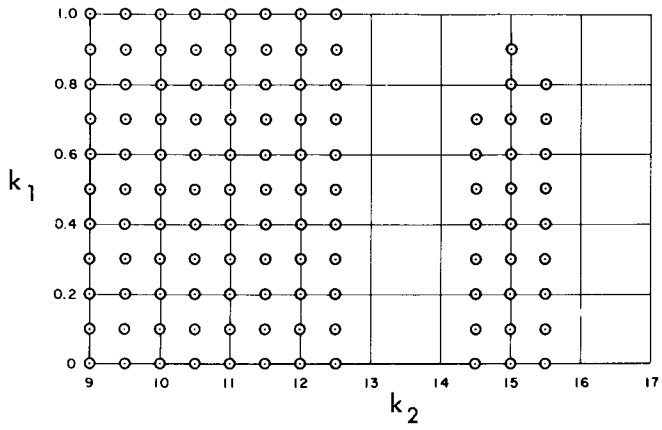

Figure 4.11–Instability chart for controlled motion, with radial-axis control of Equation 4.2, at the L_2 point of the Sun-Mercury system. $B_{L2} = 3.9772$, $e = 0.20563$, and $\odot$ – unstable.

$$F_{23} = F_{41} = \pm 3C_L A_{y1} \cos \omega_n t, \tag{4.32}$$

and

$$F_{43} = -\left[(B_L - 1) \mp 3C_L k A_{y1} \sin \omega_n t\right]. \tag{4.33}$$

The instability regions of the parameter space (A_{y1}, k_1, k_2) can be obtained by substituting Equations 4.29 to 4.33 into Equation 4.14 and following the procedure given earlier. Instability charts for the L_2 point of the Earth-Moon system are given in Figure 4.12 for six values of the gain k_1. For a lightly damped system ($k_1 = 0.1$), the region of instability is rather large. However, the size of this region shrinks quite rapidly as the damping is increased. At $k_1 = 2.5$, it has almost disappeared from the parameter space of Figure 4.12. For $\omega = \omega_n/2 = 0.931325$, Equation 4.27 gives $k_2 = 10.87$. Thus, the instability region of Figure 4.12 is caused by a subharmonic resonance at $\omega = \omega_n/2$ as might be expected from the form of $F(t)$.

B. Equilateral-Triangle Points

If eccentricity is neglected, the linearized equations of motion at an equilateral-triangle point are (from Equation 2.62)

$$\ddot{x}' - 2\dot{y}' - \alpha x' = F_{cx'}, \tag{4.34a}$$

$$\ddot{y}' + 2\dot{x}' - \beta y' = F_{cy'}, \tag{4.34b}$$

and

$$\ddot{z}' + z' = F_{cz'}. \tag{4.34c}$$

Once again, the z'-axis motion can be damped by using the control $F_{cz'} = -k_1'\dot{z}'$ with $k_1' > 0$. As shown in Chapter II, for $\mu < 0.03852\ldots$, the coupled motion in the x'y'-plane is neutrally stable when $F_{cx'} = F_{cy'} = 0$. In this section, a simple *single-axis* feedback control is designed; this control will provide adequate damping for the oscillatory motion.*

1. Routh Stability Conditions

Damping can be accomplished with the radial-axis (x'-axis) control

$$F_{cx'} = -k_1\dot{x}' + k_4 y'$$

and

$$F_{cy'} = 0. \tag{4.35}$$

*Fleming (Reference 5) has designed a dual-axis feedback control to perform the same task.

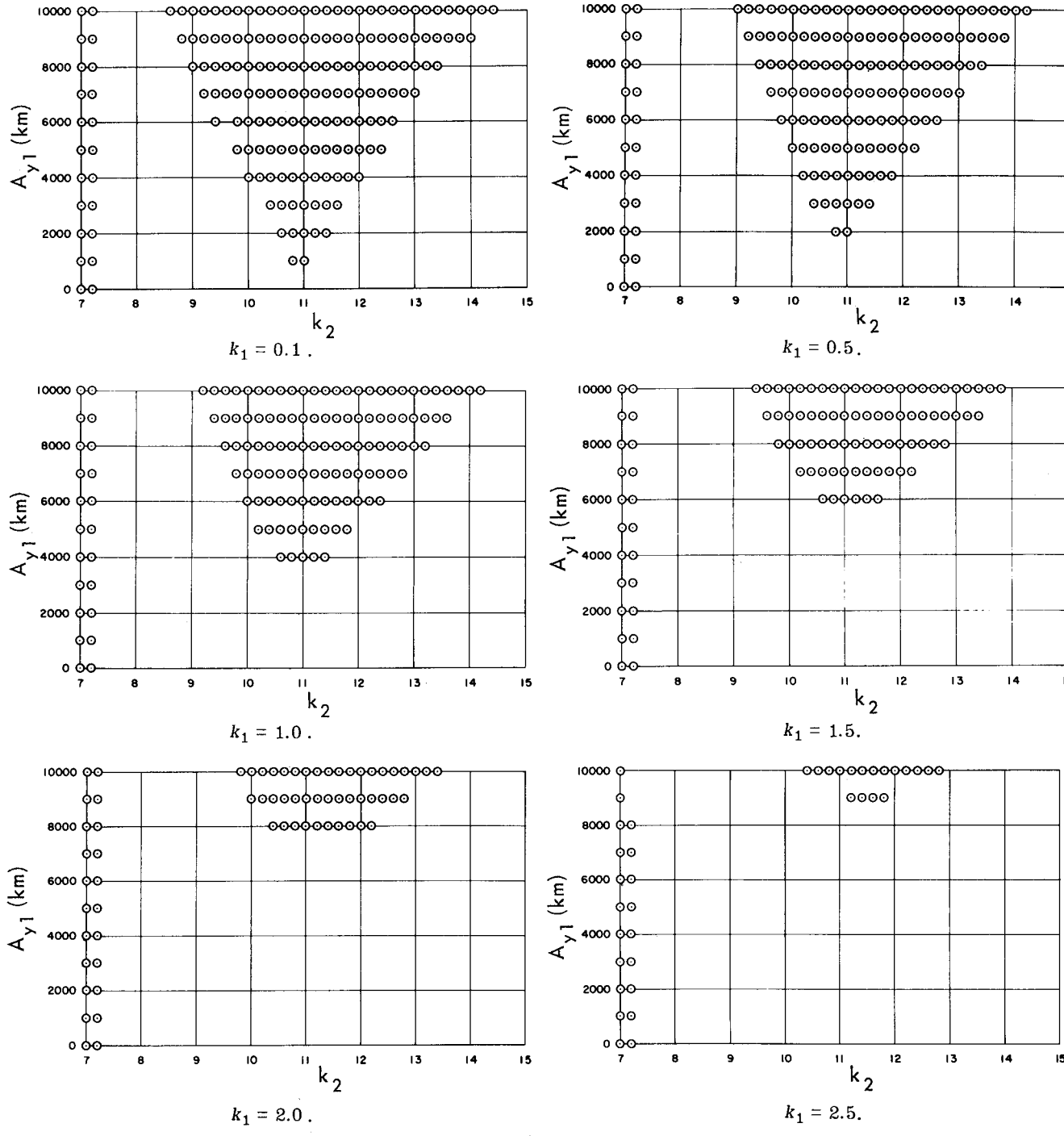

Figure 4.12–Instability charts for controlled motion, with radial-axis control of Equation 4.2, relative to a periodic orbit around the L_2 point of the Earth-Moon system. ⊙ – unstable.

With this control, the characteristic equation becomes*

$$s^4 + k_1 s^3 + s^2 + (2k_4 - k_1\beta)s + a\beta = 0, \tag{4.36}$$

*The dual-axis control, $F_{cx'} = -k_1\dot{x}'$, $F_{cy'} = -k_6 x'$, yields the same characteristic equation, with k_6 replacing k_4.

and the Routh conditions are

$$k_1 > 0, \quad 2k_4 > k_1\beta,$$

and

$$k_1\left[k_4(1 + 2\beta) - 2k_1\beta\right] > 2k_4^2. \tag{4.37}$$

The damping can also be obtained with the cross-axis (y'-axis) control

$$F_{cx'} = 0$$

and

$$F_{cy'} = -k_6x' - k_7\dot{y}'. \tag{4.38}$$

For this case, the characteristic equation is*

$$s^4 + k_7s^3 + s^2 + (2k_6 - k_7\alpha)s + \alpha\beta = 0, \tag{4.39}$$

and the Routh conditions are

$$k_7 > 0, \quad 2k_6 > k_7\alpha,$$

and

$$k_7\left[k_6(1 + 2\alpha) - 2k_7\alpha\right] > 2k_6^2. \tag{4.40}$$

Notice that Equation 4.40 has the same form as Equation 4.37, with α replacing β.

2. Root Loci and Closed-Loop Response

Because of the similarity of Equations 4.36 and 4.39, the root-locus plots for both the radial-axis and the cross-axis controls are equivalent. Therefore, only the radial-axis control of Equation 4.35 is considered here. To obtain quantitative results, the parameters α and β (see Equations 2.63 and 2.64) are computed for the Earth-Moon system, and

$$\alpha = 2.97275, \quad \beta = 0.02725. \tag{4.41}$$

If $k_4 = 0$, Equation 4.36 can be written as

$$\frac{k_1s(s^2 - \beta)}{s^4 + s^2 + \alpha\beta} = -1, \tag{4.42}$$

and the root-locus plot of Figure 4.13 is obtained. By choosing appropriate values for k_1 and k_4, the unstable roots are taken into the left half of the plane. This can be seen graphically by writing Equation 4.36 as

$$\frac{2k_4s}{s^4 + k_1s^3 + s^2 - k_1\beta s + \alpha\beta} = -1 \tag{4.43}$$

*The dual-axis control, $F_{cx'} = k_4y'$, $F_{cy'} = -k_7\dot{y}'$, yields the same characteristic equation, with k_4 replacing k_6.

and inspecting a root-locus plot for a fixed value of k_1. For $k_1 = 2.0$, the root-locus plot of Equation 4.43 is given in Figure 4.14. The Routh conditions of Equation 4.37 show that asymptotic stability is obtained when

$$0.05808 < \frac{k_4}{k_1} < 0.4692. \tag{4.44}$$

In Figure 4.15, the closed-loop response for $k_1 = 2.0$ and $k_4 = 0.25$ is compared with the uncontrolled motion.

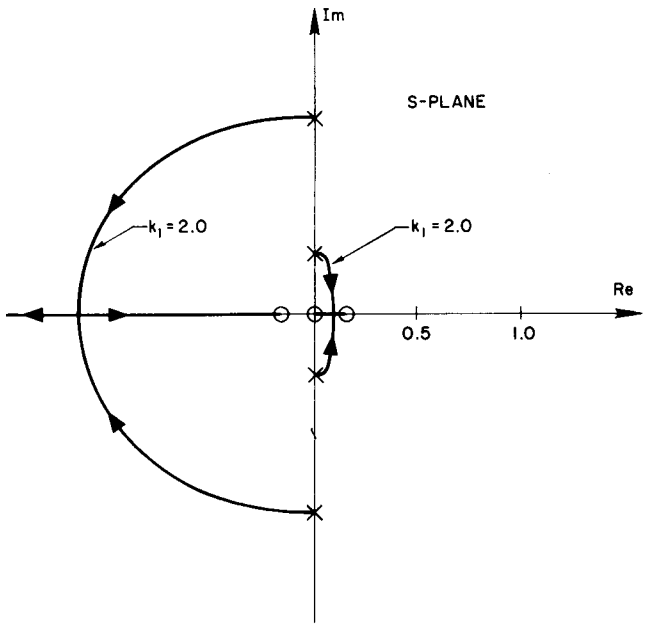

Figure 4.13–Root-locus plot for Equation 4.42. Gain is k_1, $\alpha = 2.97275$, and $\beta = 0.02725$.

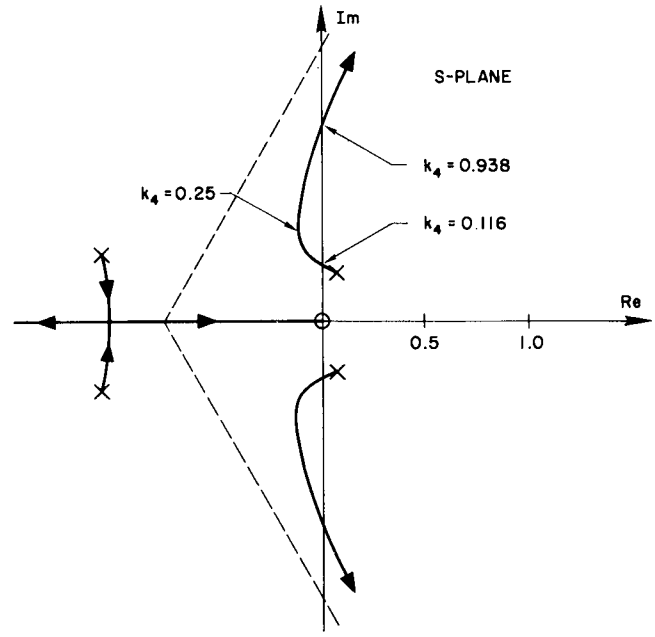

Figure 4.14–Root-locus plot for Equation 4.43. Gain is k_4, $k_1 = 2.0$, $\alpha = 2.97275$, and $\beta = 0.02725$.

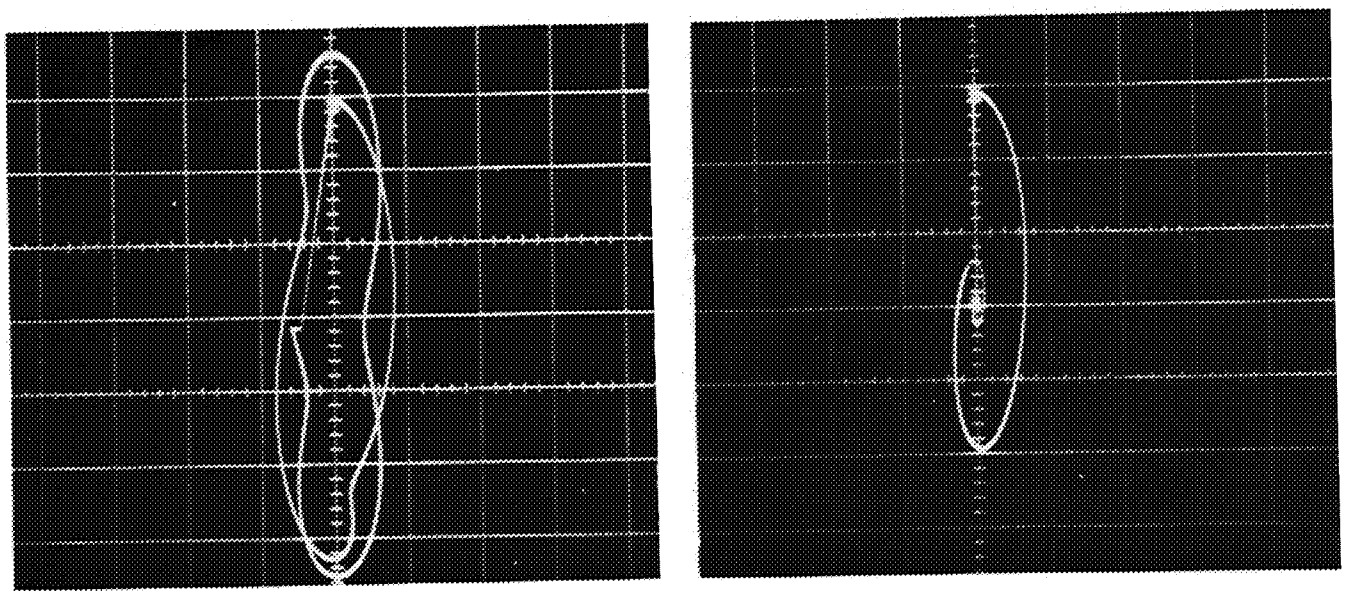

Without control.

With radial-axis control of Equation 4.35, $k_1 = 2.0$ and $k_4 = 0.25$.

Figure 4.15–Response at the equilateral-triangle points, y' versus x'. $\alpha = 2.97275$, $\beta = 0.02725$, and $\dot{x}'(0) = x'(0) = \dot{y}'(0) = 0$.

CHAPTER V

STATION KEEPING

Several methods for satellite station keeping in the vicinity of a collinear libration point are examined in Chapters V to VII. An on-off control system is analyzed in Chapter VI, and an unconventional method is investigated in Chapter VII. In the present chapter, the radial-axis control of Equation 4.2 is treated. General analytical relationships for the control requirements are formulated, and a solar sail control technique is also presented.

As noted earlier, station-keeping problems for libration-point satellites have not received very much attention. On the other hand, station-keeping techniques for synchronous satellites of the Earth (24-hour satellites) have been thoroughly analyzed (References 59 to 63), and a large reservoir of practical experience has been acquired (References 64 to 66). This knowledge could be very useful in the design of propulsion systems, sensors, attitude control systems, etc., for libration-point satellites.

A. Average Control-Acceleration Requirements

Realistic estimates of station-keeping costs are needed for feasibility studies of libration-point satellite missions. In this section, some general expressions for these costs are derived. To establish a basis for comparison, note that the average control accelerations for synchronous satellites are about $1.5 \times 10^{-7} g$ (1 fps/yr $\cong 1 \times 10^{-9} g$) for north-south station keeping, and about one-tenth of this value for east-west station keeping (Reference 63).

1. Cost Estimates for Noise Inputs

The station-keeping cost for a satellite that is following a nominal path around a collinear libration point is a function of measurement noise, engine fluctuations, and random accelerations from such causes as gas leakage or random solar radiation pressure effects. A block diagram of the radial-axis control system with noise inputs is shown in Figure 5.1. The measurement noise is denoted by $n_{\dot{x}}$, n_x; the engine noise is n_{ex}; and the random accelerations are n_{px}, n_{py}. A simple lag filter has been added to reduce the effect of the measurement noise. An optimum design can be achieved by choosing the control parameters (k_1, k_2, τ) to minimize the mean square value of the control acceleration F_{cx} (a description of this minimization procedure can be found in Reference 67). Because the uncontrolled system is unstable, this minimization is meaningful even when $n_{px} = n_{py} = 0$.

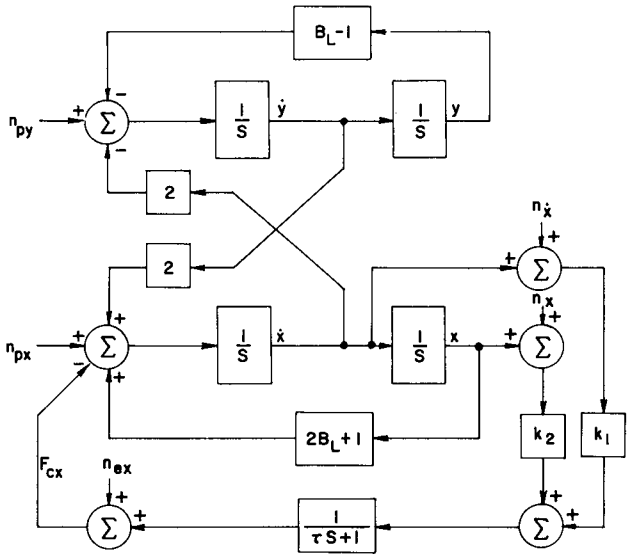

Figure 5.1–Radial-axis control system with noise inputs.

Optimization

From Figure 5.1, it can be seen that the control acceleration is

$$F_{cx}(s) = \frac{1}{\tau s + 1}\Big[(k_1 s + k_2)x(s) + (k_1 n_{\dot{x}} + k_2 n_x)\Big] + n_{ex}, \tag{5.1}$$

which can be written as

$$F_{cx}(s) = \frac{(k_1 n_{\dot{x}} + k_2 n_x)}{h(s)}\Big[s^4 - (B_L - 2)s^2 - (2B_L + 1)(B_L - 1)\Big] + \frac{(k_1 s + k_2)}{h(s)}\Big\{\Big[s^2 + (B_L - 1)\Big](n_{px} - n_{ex}) + 2sn_{py}\Big\} + n_{ex}, \tag{5.2}$$

where

$$h(s) = \tau s^5 + s^4 + \Big[k_1 - \tau(B_L - 2)\Big]s^3 + \Big[k_2 - (B_L - 2)\Big]s^2 + \Big[k_1 - \tau(2B_L + 1)\Big](B_L - 1)s + \Big[k_2 - (2B_L + 1)\Big](B_L - 1). \tag{5.3}$$

For the characteristic equation, $h(s) = 0$, the Routh stability conditions are

$$\tau \geq 0,$$

$$k_2 > (2B_L + 1), \tag{5.4}$$

and

$$\left(\frac{k_1}{k_2}\right) > \tau.$$

Writing the characteristic equation in the form

$$\frac{k_1\left(s + \frac{k_2}{k_1}\right)\Big[s^2 + (B_L - 1)\Big]}{(\tau s + 1)\Big[s^4 - (B_L - 2)s^2 - (2B_L + 1)(B_L - 1)\Big]} = -1, \tag{5.5}$$

the root-locus plot of Figure 5.2 is obtained.

The engine noise and random accelerations can usually be neglected in a first approximation, and the control acceleration then becomes

$$F_{cx}(s) = \frac{(k_1 n_{\dot{x}} + k_2 n_x)}{h(s)}\left[s^4 - (B_L - 2)s^2 - (2B_L + 1)(B_L - 1)\right]. \tag{5.6}$$

Assuming that $n_{\dot{x}}$ and n_x are independent, white, Gaussian processes, the mean square value of Equation 5.6 is

$$\overline{(F_{cx})^2} = N_{\dot{x}}\left[k_1^2 + k_2^2 R_N\right]\frac{1}{2\pi j}\int_{-j\infty}^{+j\infty}\frac{g(s)}{h(s)h(-s)}\,ds \equiv N_{\dot{x}} P_5, \tag{5.7}$$

where

$$g(s) = s^8 - 2(B_L - 2)s^6 + \left[(B_L - 2)^2 - 2(2B_L + 1)(B_L - 1)\right]s^4$$
$$+ 2(B_L - 2)(2B_L + 1)(B_L - 1)s^2 + (2B_L + 1)^2(B_L - 1)^2. \tag{5.8}$$

$N_{\dot{x}}$ and N_x are the noise levels, and $R_N \equiv (N_x/N_{\dot{x}})$. The integral of Equation 5.7 can be written as an algebraic function of the control parameters (k_1, k_2, τ) by using a special table of integrals (Reference 67). Because the resulting expressions are rather cumbersome, a numerical search procedure (Reference 68) is used to find a minimum value of the cost parameter P_5, while the stability conditions of Equation 5.4 are satisfied. It is found that the optimum values are

$$P_5 = \frac{k_1}{k_2}Q, \qquad k_2 = \frac{4}{3}(2B_L + 1), \qquad \tau = \frac{1}{3}\left(\frac{k_1}{k_2}\right), \qquad \frac{k_1}{k_2} = \sqrt{R_N}, \tag{5.9}$$

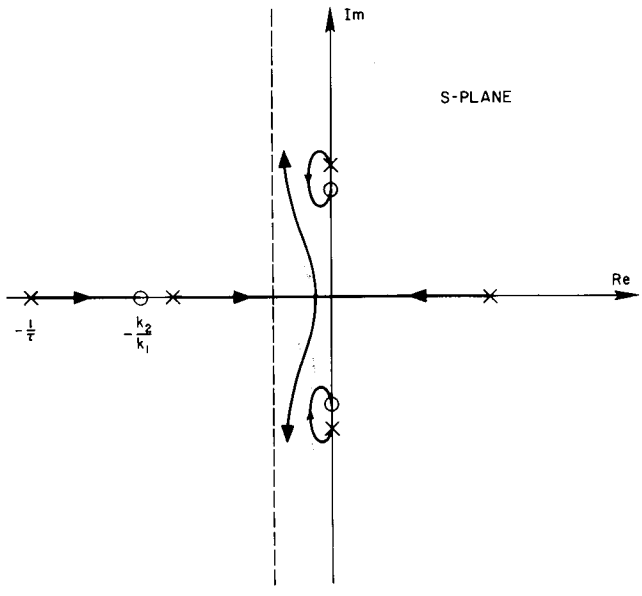

Figure 5.2–Root-locus plot for Equation 5.5. Gain is k_1. Not to scale.

where Q is a function of B_L and is plotted in Figure 5.3. Therefore, the minimum average control acceleration is given by*

$$\overline{|F_{cx}|} \cong 0.8\sqrt{\frac{k_1}{k_2}QN_{\dot{x}}}. \tag{5.10}$$

The effects of periodic coefficients (see Chapter IV) have not been considered in the foregoing optimization. This omission is probably not too serious as long as the unstable regions of the parameter space are avoided, but some method of assessing the influence of these coefficients would be useful. Equation 4.26 implies that an effective value of B_L,

$$B'_L \equiv B_L + e(2 + 3B_L), \tag{5.11}$$

*For a Gaussian process, $\overline{|F_{cx}|} = \frac{2}{\sqrt{2\pi}}(F_{cx})_{rms} \cong 0.8(F_{cx})_{rms}$.

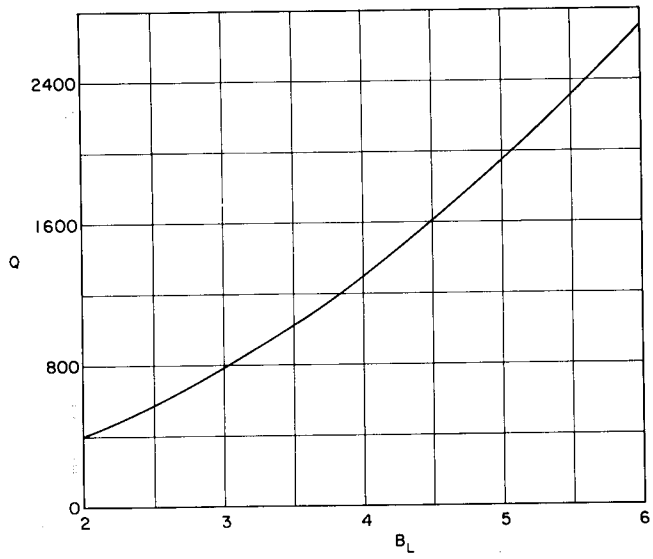

Figure 5.3–Cost parameter Q versus B_L.

may be more appropriate for the general case. Although this conjecture seems to be reasonable, verification is required.

Estimation of noise level

The noise level $N_{\dot{x}}$ can be estimated by using

$$N_{\dot{x}} = \left(\frac{\sigma_{\dot{x}}^2}{W_s T_1}\right) T_M, \tag{5.12}$$

where $\sigma_{\dot{x}}^2$ is the range-rate variance, W_s is the sample rate, T_1 is the time interval for a single set of measurements, and T_M is the time interval between sets of measurements. For deep space instrumentation facility (DSIF) measurements, $\sigma_{\dot{x}} \cong 0.02$ m/sec with $W_s = (\text{minute})^{-1}$ (Reference 69). Estimates of $\sigma_{\dot{x}}$ for onboard sensors can be found in References 70 and 71.

Costs at the Earth-Moon collinear points

The general results of Equation 5.9 can be used to find typical values for the station-keeping costs at the Earth-Moon collinear points. For the examples given here, periodic-coefficient stability results are taken into account while choosing the ratio k_1/k_2, but Equation 5.11 is not employed.

With DSIF measurements* and $T_M = 1$ day and $T_1 = 5$ minutes, Equation 5.12 gives $N_{\dot{x}} = 1.757 \cdot 10^{-11} = 6.912$ m^2/sec. The ratio k_1/k_2 is chosen to be 0.1, which means that $R_N = 0.01$. Taking $N_x = \left(\sigma_x^2/W_s T_1\right) T_M$ and solving for σ_x yields $\sigma_x = 0.751$ km. (This accuracy is easily attained with DSIF measurements.) Equations 5.9 and 5.10, along with Figure 5.3, give for L_1

$$k_1 = 1.505, \quad k_2 = 15.05,$$

$$\tau = 0.033, \quad P_5 \cong 204,$$

and

$$|\overline{F_{cx}}| = 4.790 \times 10^{-5} = 1.330 \times 10^{-8} g,$$

and for L_2

$$k_1 = 0.9841, \quad k_2 = 9.841,$$

$$\tau = 0.033, \quad P_5 \cong 86,$$

and

$$|\overline{F_{cx}}| = 3.110 \times 10^{-5} = 8.858 \times 10^{-9} g.$$

*It is assumed here that the satellite in the vicinity of L_2 is following a quasi-periodic orbit around the point and is visible from the Earth tracking station.

The values of $|\overline{F_{cx}}|$ for these examples are roughly equal to the average control accelerations that are needed for east-west station keeping of synchronous satellites.

2. Cost for Sinusoidal Control Acceleration with Noise

In some instances (see Chapter VIII), the station-keeping cost is given by $|\overline{F^*_{cx}}|$ where

$$F^*_{cx} = p(t) + F_{cx}, \tag{5.13}$$

$$p(t) = K_c \cos \omega t, \tag{5.14}$$

and F_{cx} is a random variable with a Gaussian distribution. Therefore, F^*_{cx} has a Gaussian density function

$$\Phi_{F^*}(x, t) = \frac{1}{\sigma_F \sqrt{2\pi}} \exp \left\{ -\frac{[x - p(t)]^2}{2\sigma_F^2} \right\} \tag{5.15}$$

with $\sigma_F \equiv \left(F_{cx}\right)_{\text{rms}}$ (for the radial-axis control of Figure 5.1, $\sigma_F = \sqrt{N_{\dot{x}} P_5}$). For this case, the average control acceleration is given by

$$|\overline{F^*_{cx}}| = E\left\{ \frac{\omega}{2\pi} \int_0^{2\pi/\omega} |F^*_{cx}(t)| dt \right\} = \frac{\omega}{2\pi} \int_0^{2\pi/\omega} E\left\{ |F^*_{cx}(t)| \right\} dt, \tag{5.16}$$

where

$$E\left\{ |F^*_{cx}(t)| \right\} = \int_{-\infty}^{+\infty} |x| \Phi_{F^*}(x, t) dx \tag{5.17}$$

and $E\{y\}$ is the "expected value" of a random variable y. After some rather lengthy manipulations (see Appendix A), Equation 5.16 becomes

$$|\overline{F^*_{cx}}| = \frac{e^{-u}}{\sqrt{2\pi}} \left\{ 2\sigma_F I_0(u) + \frac{K_c^2}{\sigma_F} \left[I_0(u) + I_1(u) \right] \right\}, \tag{5.18}$$

where $I_0(u)$ and $I_1(u)$ are modified Bessel functions and $u \equiv K_c^2/4\sigma_F^2$. Using well-known series expansions (Reference 72) for $I_0(u)$ and $I_1(u)$, two limiting cases of Equation 5.18 can be deduced:

Case 1, for small values of u,

$$|\overline{F^*_{cx}}| \cong \frac{2\sigma_F}{\sqrt{2\pi}} \left[1 + \frac{K_c^2}{4\sigma_F^2} \right] \tag{5.19}$$

and Case 2, for large values of u,

$$|\overline{F^*_{cx}}| \cong \frac{2K_c}{\pi} \left[1 + \frac{\sigma_F^2}{2K_c^2} \right]. \tag{5.20}$$

3. Cost for a Constant Displacement

A satellite is sometimes stationed at a constant distance δ from the libration point. This displacement may be intentional, or it may be the result of a bias error in the measurements. In either case, the station-keeping cost will be increased. If terms of $O(\delta^4)$ are neglected, this cost can be obtained from Equation 2.43. The special cases in which δ lies along a single coordinate axis are illustrative. If ρ and ν are neglected, these costs are approximately

for δ_x only,

$$F_{cx} = -(2B_L + 1)\delta_x \pm 3C_L\delta_x^2 - 4D_L\delta_x^3$$

and

$$F_{cy} = F_{cz} = 0; \tag{5.21}$$

for δ_y only,

$$F_{cx} = \mp\frac{3}{2}C_L\delta_y^2,$$

$$F_{cy} = (B_L - 1)\delta_y - \frac{3}{2}D_L\delta_y^3, \tag{5.22}$$

and

$$F_{cz} = 0;$$

and for δ_z only,

$$F_{cx} = \mp\frac{3}{2}C_L\delta_z^2,$$

$$F_{cy} = 0, \tag{5.23}$$

and

$$F_{cz} = B_L\delta_z - \frac{3}{2}D_L\delta_z^3.$$

The costs for a satellite in the vicinity of the L_2 point of the Earth-Moon system are given in Figure 5.4. Notice that the contribution of the nonlinear portion of Equations 5.21 to 5.23 is extremely small for this range of δ.

B. Solar Sail Control at the Earth-Moon Collinear Points

It has been shown that the magnitude of the control acceleration needed for station keeping in the vicinity of a collinear point of the Earth-Moon system may be extremely small. Therefore, it may be feasible to obtain this acceleration with a small solar sail. At first, the utilization of a solar sail to perform this task appears to be straightforward, until it is realized that the control-acceleration vector can never have a component directed toward the Sun. Furthermore, the direction of the incident solar radiation is varying continuously with respect to the xyz-coordinate system. Fortunately, these difficulties can be circumvented by using a method that was originally devised by Colombo (Reference 3), who demonstrated that the required accelerations could be obtained by forcing the libration-point satellite to follow a path that is synchronized with the Sun's motion.

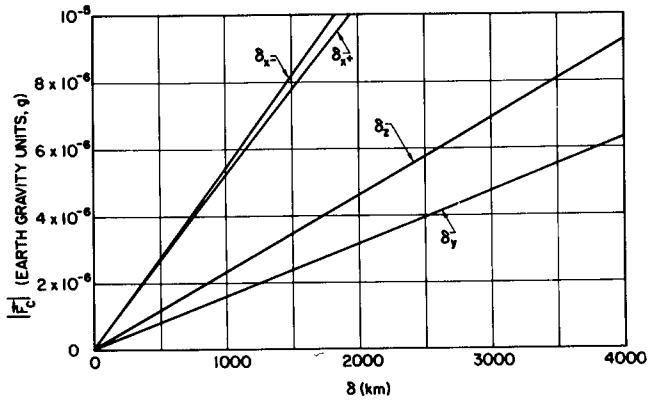

Figure 5.4--Station-keeping cost for a constant displacement from the L_2 point of the Earth-Moon system.

An analysis of a particular solar sail control technique is presented in this section. Colombo's strategy is employed, and explicit relations for the sail variations are derived. The analysis is limited to the xy-plane, and the effects of eccentricity and solar perturbations are neglected. Solar occultation periods are also neglected in this analysis. Although it is possible to use the solar sail for both attitude and position stabilization, only position control is considered here.

1. Basic Concepts

The geometry for a plane solar sail in the vicinity of a collinear libration point of the Earth-Moon system is depicted in Figure 5.5. For specular reflection of the incident solar rays, the equations of motion (cf. Equation 3.26) are

$$\ddot{x} - 2\dot{y} - (2B_L + 1)x = -K_p \cos^2 \psi \cos(\theta + \psi) = F_{cx}$$

and

$$\ddot{y} + 2\dot{x} + (B_L - 1)y = K_p \cos^2 \psi \sin(\theta + \psi) = F_{cy}, \tag{5.24}$$

where $\theta = \omega_s t$ ($\omega_s = 0.92519867$), K_p and ψ are bounded control variables ($K_p \geq 0$, $|\psi| \leq \pi/2$), and from Equation 3.1,

$$K_p = 2p_{\oplus}\left(\frac{A_s}{m}\right). \tag{5.25}$$

Following Colombo's suggestion, the libration-point satellite is required to follow a path $[x_0(t), y_0(t)]$, which is determined by finding the forced response of

$$\ddot{x}_0 - 2\dot{y}_0 - (2B_L + 1)x_0 = -K_0 \cos\theta$$

and

$$\ddot{y}_0 + 2\dot{x}_0 + (B_L - 1)y_0 = K_0 \sin\theta. \tag{5.26}$$

The connection between the control accelerations (see Figure 5.5) is given by

$$\mathbf{F}_c = \mathbf{F}_0 + \mathbf{F}'_c \tag{5.27}$$

with

$$\mathbf{F}_c = F_{cx}\mathbf{i} + F_{cy}\mathbf{j}, \tag{5.28}$$

$$\mathbf{F}_0 = K_0[-\cos\theta\,\mathbf{i} + \sin\theta\,\mathbf{j}], \tag{5.29}$$

and

$$\mathbf{F}'_c = F'_{c\xi}\mathbf{i} + F'_{c\eta}\mathbf{j}. \tag{5.30}$$

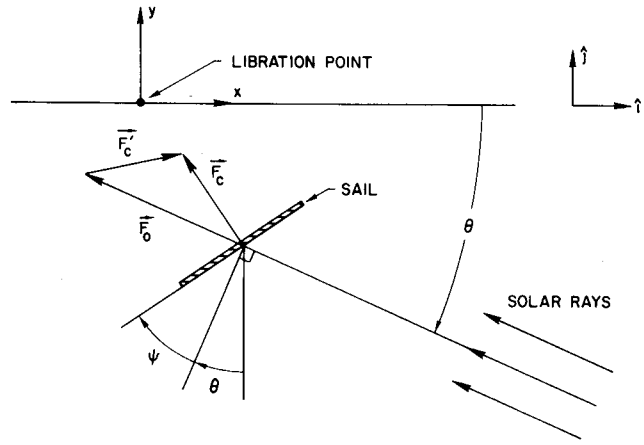

Figure 5.5–Plane solar sail in the vicinity of a collinear libration point of the Earth-Moon system.

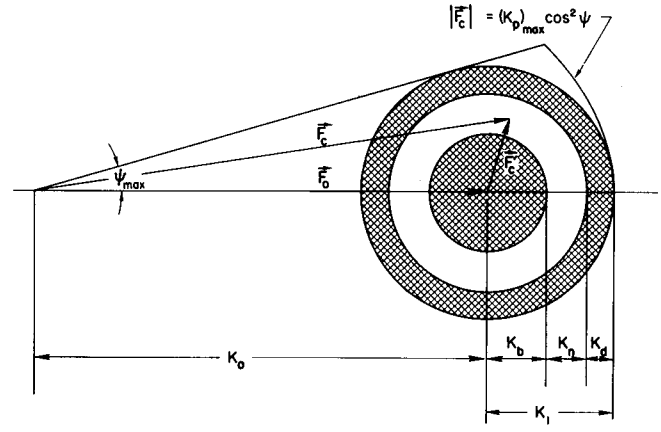

Figure 5.6–Solar sail acceleration diagram.

Using linear superposition, it is obvious that the equations of motion relative to the path $[x_0(t), y_0(t)]$ are

$$\ddot{\xi} - 2\dot{\eta} - (2B_L + 1)\xi = F'_{c\xi}$$

and (5.31)

$$\ddot{\eta} + 2\dot{\xi} + (B_L - 1)\eta = F'_{c\eta},$$

where $\xi = x - x_0$ and $\eta = y - y_0$.

A graphic exposition of the solar sail control technique can be obtained by inspecting the acceleration diagram of Figure 5.6. In this figure, the magnitudes of the control accelerations needed for station keeping are represented by K_b (measurement bias errors), K_n (measurement noise), and K_d (perturbations, etc., which are not eliminated by following a nominal path),

and

$$K_1 \equiv K_b + K_n + K_d. \tag{5.32}$$

It is easily seen that the required acceleration can be provided by suitably adjusting the control variables K_p and ψ. Figure 5.6 can also be used to determine $(K_p)_{max}$. From Equation 5.25, it can be seen that this specification is equivalent to finding the maximum size of the solar sail. The minimum required value of $(K_p)_{max}$ can be found by observing that, for this special case, the curve $|\mathbf{F}_c| = (K_p)_{max} \cos^2\psi$ has a common tangent with the circle of radius K_1. For $\psi_{max} \leq 30°$ ($\sin \psi_{max} = K_1/K_0$), the common tangent is at $\psi = 0°$, and it is obvious that

$$(K_p)_{max} = K_0 + K_1. \tag{5.33}$$

When $\psi_{max} \geq 30°$, the analysis is more involved, but it can be shown that

$$(K_p)_{max} = \frac{3\sqrt{3}}{4} K_0 \left[1 - \left(\frac{K_1}{K_0}\right)^2\right]^{-1/2}, \tag{5.34}$$

and the common point of tangency can be determined from

$$\cos \psi = \frac{2}{\sqrt{3}} \left[1 - \left(\frac{K_1}{K_0} \right)^2 \right]^{1/2} \tag{5.35}$$

2. Sail Variations with Radial-Axis Control

For a radial-axis control, $F'_{c\eta} = 0$, and Equations 5.24, 5.26, and 5.31 give

$$-K_p \cos^2 \psi \cos (\theta + \psi) + K_0 \cos \theta = F'_{c\xi}$$

and

$$K_p \cos^2 \psi \sin (\theta + \psi) - K_0 \sin \theta = 0. \tag{5.36}$$

It is convenient to use the definition

$$K_p \equiv K_0 + Q_p, \tag{5.37}$$

where Q_p represents the variable portion of K_p. The sail variations ψ and Q_p can be expressed as functions of the variables $F'_{c\xi}$ and θ. Equations 5.36 and 5.37 yield

$$\tan \psi = \frac{F'_{c\xi} \sin \theta}{K_0 - F'_{c\xi}} \tag{5.38}$$

and

$$Q_p = K_0 \left[\frac{(K_0 - F'_{c\xi})/\cos^3 \psi}{K_0 - F'_{c\xi}(1 - \cos \theta)} - 1 \right], \tag{5.39}$$

and if the radial-axis control of Equation 4.2 is used,

$$F'_{c\xi} = - k_1 \dot{\xi} - k_2 \xi. \tag{5.40}$$

When $F'_{c\xi} \ll K_0$, Equations 5.38 and 5.39 lead to the approximate relations

$$\psi \cong \frac{F'_{c\xi}}{K_0} \sin \theta$$

and

$$Q_p \cong - F'_{c\xi} \cos \theta. \tag{5.41}$$

3. Examples

The variation of the area of the solar sail is minimized by choosing $K_0 \gg K_1$. (The variation of ψ is also minimized.) It is quite possible that the mechanization of the solar sail control system will be less complicated if only small sail variations are required. Therefore, a value of $K_0 = 15\ K_1$ ($\psi_{max} = 3.82°$) is adopted for the examples given below.*

*Although sail variations are minimized when $K_0 \gg K_1$, the required sail area A_s is increased. This tradeoff is not considered here.

For both examples, it is assumed that $K_d \cong 0$, $\delta_\xi = 1$ km, and $m = 400$ kg. K_n is obtained from section A.1 of this chapter, and $p_\oplus = 4.50 \times \underline{10}^{-6}$ newtons/m^2. The forced response of Equation 5.26 is written as

$$x_0 = A_{x0} \cos \omega_s t$$

and (5.42)

$$y_0 = A_{y0} \sin \omega_s t.$$

With the values mentioned above, some of the important parameters for satellites in the vicinity of the Earth-Moon collinear points are found to be

for L_1

$$K_b = 2.938 \times 10^{-5} = 8.157 \times 10^{-9} g,$$

$$K_n = 4.790 \times 10^{-5} = 1.330 \times 10^{-8} g,$$

$$K_0 = 1.159 \times 10^{-3} = 3.218 \times 10^{-7} g,$$

$$A_{x0} = 14.8 \text{ km}, \qquad A_{y0} = 143.7 \text{ km},$$

$$A_s = 149.7 \text{ m}^2, \text{ and } (A_s/m) = 0.374 \text{ m}^2/\text{kg},$$

and for L_2

$$K_b = 1.920 \times 10^{-5} = 5.330 \times 10^{-9} g,$$

$$K_n = 3.110 \times 10^{-5} = 8.858 \times 10^{-9} g,$$

$$K_0 = 7.545 \times 10^{-4} = 2.128 \times 10^{-7} g,$$

$$A_{x0} = -10.4 \text{ km}, \qquad A_{y0} = 202.9 \text{ km},$$

$$A_s = 97.4 \text{ m}^2, \text{ and } (A_s/m) = 0.244 \text{ m}^2/\text{kg}.$$

Notice that the forced oscillation is counterclockwise for L_1 and clockwise for L_2. In both cases, $|A_{y0}| \gg |A_{x0}|$.

CHAPTER VI

ON-OFF CONTROL SYSTEM

It is quite possible that the station keeping of a libration-point satellite will be accomplished with an on-off control system. Accordingly, an analysis of the ensuing limit-cycle motion is in order. Two methods of analysis are presented in this chapter. The first is an exact method that makes use of Fourier expansions; the second is an approximate phase-plane technique.

Once again, a radial-axis control that requires only range and range-rate measurements is utilized. If eccentricity, perturbations, etc., are neglected, the equations of motion in the vicinity of a collinear libration point are

$$\ddot{x} - 2\dot{y} - (2B_L + 1)x = -F(\xi)$$

and

$$\ddot{y} + 2\dot{x} + (B_L - 1)y = 0, \tag{6.1}$$

where

$$\xi = \dot{x} + \lambda x, \tag{6.2}$$

and the assumed on-off control characteristic $F(\xi)$ has a deadzone ξ_d and a hysteresis loop of width 2δ (see Figure 6.1). An asymmetric characteristic was chosen because only "one-sided" limit cycles are considered here.* The constant λ in Equation 6.2 is just the slope of the "switching line" in the $\dot{x}$-x phase plane.

A. Limit Cycles: Exact Analysis

Conditions for the existence of limit cycles in Equation 6.1 can be found by using harmonic methods. Approximate methods (References 73 and 74) that neglect all harmonics higher than the first are very popular, but their validity is sometimes questionable. Therefore, the higher harmonics are retained in the analysis employed in this section. Although differing in some details, the exact harmonic method used here is essentially the same as a method of Tsypkin (References 75 and 76).

1. Application of Harmonic Method

A block diagram of the on-off control system is shown in Figure 6.2, and it is clear that

$$\xi(s) = G(s)F(s). \tag{6.3}$$

*One-sided limit cycles are possible because the uncontrolled system is unstable.

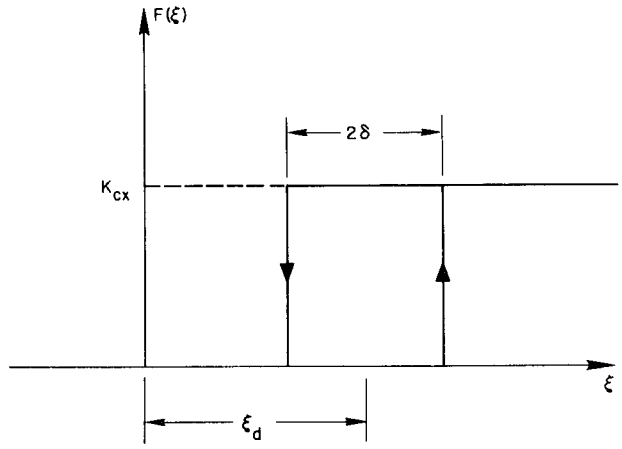

Figure 6.1–On-off control characteristic.

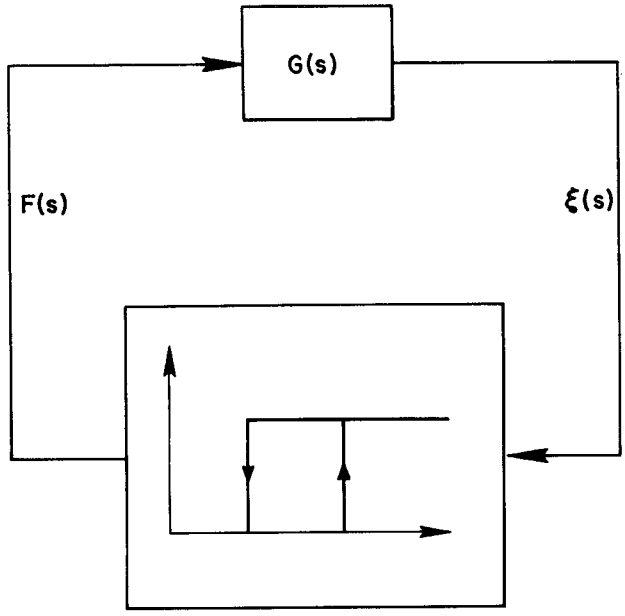

Figure 6.2–Block diagram of the on-off control system.

From Equations 6.1 and 6.2, it is found that the transfer function is

$$G(s) = \frac{(s+\lambda)\left[s^2 + (B_L - 1)\right]}{(2B_L + 1)(B_L - 1) + (B_L - 2)s^2 - s^4}. \quad (6.4)$$

For convenience, $g(s) \equiv 1/G(s)$, and Equation 6.3 becomes

$$g(s)\xi(s) = F(s). \quad (6.5)$$

Typical oscillation waveforms for a stable limit cycle are depicted in Figure 6.3.* In this figure

$$\theta = \omega t, \quad (6.6)$$

where ω is the limit-cycle frequency. The Fourier representations of ξ and F can be written

$$\xi(\theta) = a_0 + a_1 \sin\theta + \sum_{n=2}^{\infty} a_n \sin(n\theta + \psi_n) \quad (6.7)$$

and

$$F(\theta) = \frac{b_0}{2} + \sum_{n=1}^{\infty} (b_n \cos n\theta + c_n \sin n\theta). \quad (6.8)$$

Using the waveform for $F(\theta)$ in Figure 6.3, the Fourier coefficients of Equation 6.8 are found to be

$$b_0 = \frac{1}{\pi}\int_0^{2\pi} F(\theta)d\theta = \frac{K_{cx}(\theta_2 - \theta_1)}{\pi}, \quad (6.9)$$

$$b_n = \frac{1}{\pi}\int_0^{2\pi} F(\theta)\cos n\theta\, d\theta$$

$$= \frac{K_{cx}}{n\pi}(\sin n\theta_2 - \sin n\theta_1), \quad (6.10)$$

and

$$c_n = \frac{1}{\pi}\int_0^{2\pi} F(\theta)\sin n\theta\, d\theta = \frac{K_{cx}}{n\pi}(\cos n\theta_1 - \cos n\theta_2). \quad (6.11)$$

*Notice that there are discontinuities in $\dot{\xi}$ whenever the control is turned on or off. Tsypkin's graphical method as given in References 75 and 76 is not applicable to this special case. However, a modified method, which can be applied to problems with discontinuities of this type, has been given by Korolev (Reference 77).

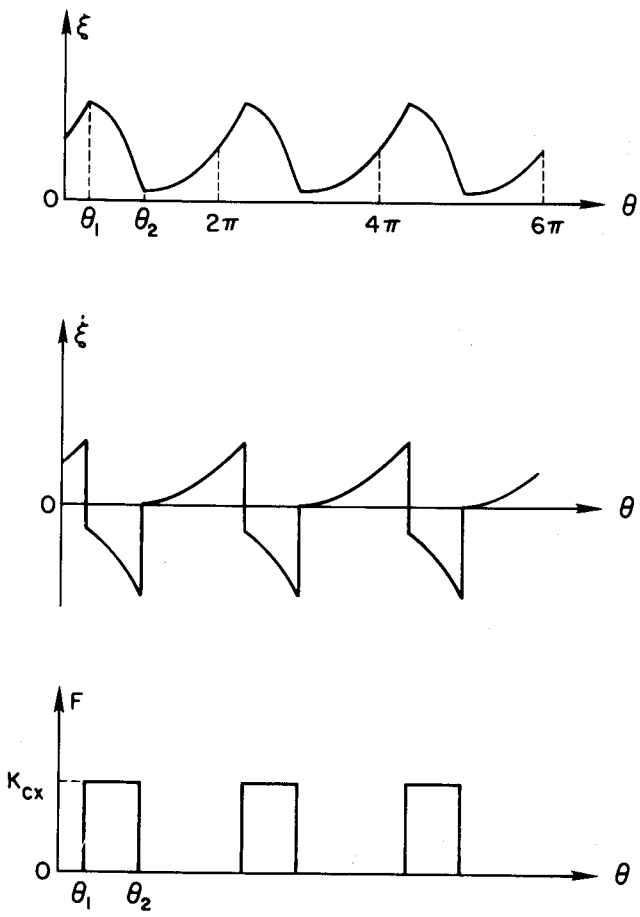

Figure 6.3–Oscillation waveforms ($\theta = \omega t$).

Writing

$$g(s) = g(j\omega) = R(\omega)e^{j\phi(\omega)} \tag{6.12}$$

and taking the inverse transform of Equation 6.5 gives

$$g(0)a_0 + R(\omega)a_1 \sin\left[\theta + \phi(\omega)\right] + \sum_{n=2}^{\infty} R(n\omega)a_n \sin\left[n\theta + \psi_n + \phi(n\omega)\right] = F(\theta). \tag{6.13}$$

Equation 6.13 leads to the relations

$$a_0 = \frac{K_{cx}(\theta_2 - \theta_1)}{2\pi g(0)}, \tag{6.14}$$

$$a_1 = \frac{2K_{cx}}{\pi R(\omega)} \sin\frac{\theta_2 - \theta_1}{2}, \tag{6.15}$$

$$a_n = \frac{2K_{cx}}{n\pi R(n\omega)} \sin\frac{n(\theta_2 - \theta_1)}{2}, \tag{6.16}$$

$$\phi(\omega) = \frac{1}{2}\left[\pi - (\theta_1 + \theta_2)\right], \tag{6.17}$$

and

$$\psi_n = \frac{1}{2}\left[\pi - n(\theta_1 + \theta_2)\right] - \phi(n\omega). \tag{6.18}$$

From Equations 6.4 and 6.12, it is found that

$$g(j\omega) = \frac{(2B_L + 1)(B_L - 1) - (B_L - 2)\omega^2 - \omega^4}{(\lambda + j\omega)\left[(B_L - 1) - \omega^2\right]}, \tag{6.19}$$

$$R(\omega) = \frac{\omega^4 + (B_L - 2)\omega^2 - (2B_L + 1)(B_L - 1)}{\left[\omega^2 - (B_L - 1)\right]\sqrt{\lambda^2 + \omega^2}} \equiv \frac{(\omega^2 - \alpha^2)(\omega^2 + \beta^2)}{(\omega^2 - \gamma^2)\sqrt{\lambda^2 + \omega^2}}, \tag{6.20}$$

and

$$\tan\phi(\omega) = -\frac{\omega}{\lambda}. \tag{6.21}$$

The constants α and β can be obtained from Table 2.3. $\alpha > \gamma$, and it is apparent that $R(\omega) < 0$ for the frequency range $\gamma < \omega < \alpha$. This frequency range is not examined in this study, and it will always be assumed that $R(\omega) > 0$.* Equations 6.14, 6.17, and 6.18 can now be written in the form

*In the frequency range $\gamma < \omega < \alpha$, the control is turned on when ξ is decreasing and is turned off when ξ is increasing. Therefore, the presence of a stable limit cycle in this frequency range is highly improbable.

$$a_0 = \frac{K_{cx}(\theta_2 - \theta_1)\lambda}{2\pi(2B_L + 1)}, \tag{6.22}$$

$$(\theta_1 + \theta_2) = \pi + 2\tan^{-1}\left(\frac{\omega}{\lambda}\right), \tag{6.23}$$

and

$$\psi_n = \frac{1}{2}\left[\pi - n(\theta_1 + \theta_2)\right] + \tan^{-1}\left(\frac{n\omega}{\lambda}\right). \tag{6.24}$$

From Figures 6.1 and 6.3, it is clear that the deadzone and hysteresis constants for the on-off control characteristic are given by

$$\xi_d = \frac{1}{2}\left[\xi(\theta_1) + \xi(\theta_2)\right] \tag{6.25}$$

and

$$\delta = \frac{1}{2}\left[\xi(\theta_1) - \xi(\theta_2)\right]. \tag{6.26}$$

Finally, with the aid of Equations 6.1 and 6.2, it can be shown that

$$x(\theta) = \frac{a_0}{\lambda} + \frac{a_1}{\sqrt{\lambda^2 + \omega^2}} \sin\left[\theta - \tan^{-1}\left(\frac{\omega}{\lambda}\right)\right] + \sum_{n=2}^{\infty} \frac{a_n}{\sqrt{\lambda^2 + (n\omega)^2}} \sin\left[n\theta + \psi_n - \tan^{-1}\left(\frac{n\omega}{\lambda}\right)\right] \tag{6.27}$$

and

$$y(\theta) = \frac{2a_1\omega}{\left[\omega^2 - (B_L - 1)\right]\sqrt{\lambda^2 + \omega^2}} \cos\left[\theta - \tan^{-1}\left(\frac{\omega}{\lambda}\right)\right] + \sum_{n=2}^{\infty} \frac{2na_n\omega}{\left[(n\omega)^2 - (B_L - 1)\right]\sqrt{\lambda^2 + (n\omega)^2}} \cos\left[n\theta + \psi_n - \tan^{-1}\left(\frac{n\omega}{\lambda}\right)\right]. \tag{6.28}$$

Notice that K_{cx} is just a scale factor, and the "normalized" limit cycle is completely determined by choosing the parameters

$(\theta_2 - \theta_1)$, where $(\theta_2 - \theta_1)/2\pi \equiv m$ is the fraction of the total time that the control is on,

λ, where λ is the slope of the switching line in the $\dot{x}$-x phase plane, and

ω, where ω is the limit-cycle frequency.

2. Closed-Form Solution

Although the results of the previous section are exact, they are in the form of infinite series. With results in this form, the synthesis of the control is sometimes inconvenient. Fortunately, some simplification is possible for the important special case where the control is on for half of the limit-cycle period and off during the other half. That is

$$\theta_2 - \theta_1 = \pi, \tag{6.29}$$

and with Equation 6.16, Equation 6.7 becomes

$$\xi(\theta) = a_0 + a_1 \sin\theta + \frac{2K_{cx}}{\pi}\sum_{n=1}^{\infty}\frac{(-1)^n \sin\left[(2n+1)\theta + \psi_{2n+1}\right]}{(2n+1)R\left[(2n+1)\omega\right]}. \tag{6.30}$$

From Equation 6.23

$$\theta_1 = \tan^{-1}\left(\frac{\omega}{\lambda}\right)$$

and

$$\theta_2 = \pi + \tan^{-1}\left(\frac{\omega}{\lambda}\right), \tag{6.31}$$

and

$$\sin\theta_1 = \frac{\omega}{\sqrt{\lambda^2+\omega^2}}$$

and

$$\sin\theta_2 = -\frac{\omega}{\sqrt{\lambda^2+\omega^2}}. \tag{6.32}$$

Similar expressions can be found for Equation 6.24, and it can be deduced that

$$\xi(\theta_1) = \frac{K_{cx}\lambda}{2(2B_L+1)} + \frac{2K_{cx}\omega}{\pi}\sum_{n=0}^{\infty}\frac{\left[(2n+1)^2\omega^2 - \gamma^2\right]}{\left[(2n+1)^2\omega^2 - \alpha^2\right]\left[(2n+1)^2\omega^2 + \beta^2\right]} \tag{6.33}$$

and

$$\xi(\theta_2) = \frac{K_{cx}\lambda}{2(2B_L+1)} - \frac{2K_{cx}\omega}{\pi}\sum_{n=0}^{\infty}\frac{\left[(2n+1)^2\omega^2 - \gamma^2\right]}{\left[(2n+1)^2\omega^2 - \alpha^2\right]\left[(2n+1)^2\omega^2 + \beta^2\right]}.$$

Substitution of Equation 6.33 into Equations 6.25 and 6.26 yields

$$\xi_d = \frac{K_{cx}\lambda}{2(2B_L+1)} \tag{6.34}$$

and

$$\delta = \frac{2K_{cx}\omega}{\pi}\left\{\frac{\alpha^2-\gamma^2}{\alpha^2+\beta^2}\sum_{n=0}^{\infty}\frac{1}{\left[(2n+1)^2 - (\alpha/\omega)^2\right]}\right.$$

$$\left. + \frac{\beta^2+\gamma^2}{\alpha^2+\beta^2}\sum_{n=0}^{\infty}\frac{1}{\left[(2n+1)^2 + (\beta/\omega)^2\right]}\right\}. \tag{6.35}$$

Closed-form expressions for the two infinite series are given in Reference 78, and Equation 6.35 becomes

$$\delta = \frac{K_{cx}}{2}\left[\frac{\alpha^2 - \gamma^2}{\alpha(\alpha^2 + \beta^2)}\tan\left(\frac{\pi\alpha}{2\omega}\right) + \frac{\beta^2 + \gamma^2}{\beta(\alpha^2 + \beta^2)}\tanh\left(\frac{\pi\beta}{2\omega}\right)\right] . \tag{6.36}$$

A graph of Equation 6.36 for $B_L = 4$ ($\alpha^2 = 4.2915$, $\beta^2 = 6.2915$, $\gamma^2 = 3$) is given in Figure 6.4.

It can be shown that the maximum and minimum values of $x(\theta)$ occur at $\theta = \theta_1 + (\pi/2)$ and $\theta = \theta_2 + (\pi/2)$, respectively. Substituting these values into Equation 6.27, it is found that

$$x_{max} = \frac{K_{cx}}{2(2B_L + 1)} + \Xi \tag{6.37}$$

and

$$x_{min} = \frac{K_{cx}}{2(2B_L + 1)} - \Xi , \tag{6.38}$$

where

$$\Xi = \frac{2K_{cx}}{\pi}\sum_{n=0}^{\infty}\frac{(-1)^n\left[(2n+1)^2\omega^2 - \gamma^2\right]}{(2n+1)\left[(2n+1)^2\omega^2 - \alpha^2\right]\left[(2n+1)^2\omega^2 + \beta^2\right]} \tag{6.39}$$

The summation formulae of Reference 78 can be used to write Equation 6.39 as

$$\Xi = \frac{2K_{cx}}{\pi\omega^2}\left\{\frac{\alpha^2 - \gamma^2}{\alpha^2 + \beta^2}\sum_{n=0}^{\infty}\frac{(-1)^n}{(2n+1)\left[(2n+1)^2 - (\alpha/\omega)^2\right]}\right.$$

$$\left. + \frac{\beta^2 + \gamma^2}{\alpha^2 + \beta^2}\sum_{n=0}^{\infty}\frac{(-1)^n}{(2n+1)\left[(2n+1)^2 + (\beta/\omega)^2\right]}\right\}$$

$$= \frac{K_{cx}}{2}\left\{\frac{\alpha^2 - \gamma^2}{\alpha^2(\alpha^2 + \beta^2)}\left[\sec\left(\frac{\pi\alpha}{2\omega}\right) - 1\right] + \frac{\beta^2 + \gamma^2}{\beta^2(\alpha^2 + \beta^2)}\left[1 - \operatorname{sech}\left(\frac{\pi\beta}{2\omega}\right)\right]\right\}$$

$$= \frac{K_{cx}}{2}\left[\left(\frac{\gamma}{\alpha\beta}\right)^2 + \frac{\alpha^2 - \gamma^2}{\alpha^2(\alpha^2 + \beta^2)}\sec\left(\frac{\pi\alpha}{2\omega}\right) - \frac{\beta^2 + \gamma^2}{\beta^2(\alpha^2 + \beta^2)}\operatorname{sech}\left(\frac{\pi\beta}{2\omega}\right)\right]. \tag{6.40}$$

A graph of Equation 6.40 for $B_L = 4$ is shown in Figure 6.5.

Equation 6.38 shows that $x_{min} < 0$ when $\Xi > K_{cx}/2(2B_L + 1)$. Intuitive reasoning suggests that limit cycles with $x_{min} < 0$ are unstable. This conjecture will be substantiated by the stability analysis given below.

B. Stability of Limit Cycles

The results of the previous section cannot be used with confidence until the stability of the predicted limit cycle is verified. Tsypkin (Reference 75) has devised a method that reduces this stability investigation

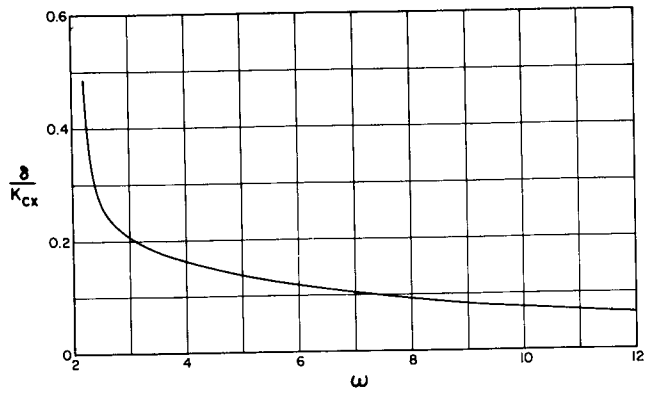

Figure 6.4–Hysteresis versus limit-cycle frequency ($B_L = 4$, $\theta_2 - \theta_1 = \pi$).

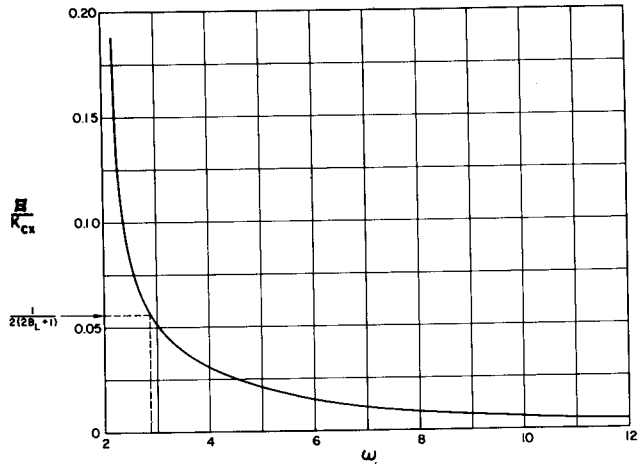

Figure 6.5–Ξ versus limit-cycle frequency ($B_L = 4$, $\theta_2 - \theta_1 = \pi$).

to that of an equivalent sampled-data system. A brief outline of this method is given below, and quantitative results are obtained for the special case where $\theta_2 - \theta_1 = \pi$.

1. Tsypkin's Method

Consider the perturbed limit-cycle motion of the system shown in Figure 6.2. The input to the on-off characteristic is

$$\xi(t) = \xi_{LC}(t) + \xi_\epsilon(t), \tag{6.41}$$

where $\xi_{LC}(t)$ corresponds to the assumed limit cycle, and $\xi_\epsilon(t)$ represents a small deviation. Similarly,

$$F(t) = F_{LC}(t) + F_\epsilon(t). \tag{6.42}$$

The deviation in the output $F_\epsilon(t)$ is just a sequence of pulses, of height K_{cx} and width Δt_n, which occur at the beginning or end of the switching instants t_n. Assuming that $\xi_\epsilon \ll \xi_{LC}$, this deviation can be represented by the impulse train

$$F_\epsilon(t) \cong K_{cx} \sum_{n=0}^{\infty} \Delta t_n \delta(t - t_n), \tag{6.43}$$

where $\delta(t)$ is the Dirac delta function, and following Korolev (Reference 77), Δt_n is expressed in terms of the conditions that immediately precede the switching instant

$$\Delta t_n \cong \frac{\xi_\epsilon(t_n^-)}{|\dot{\xi}_{LC}(t_n^-)|}. \tag{6.44}$$

For the special case where the on and off periods are equal (i.e., $\theta_2 - \theta_1 = \pi$), the switching intervals are $T = T_{LC}/2 = \pi/\omega$, and the deviation is given by

$$F_\epsilon(t) = \frac{K_{cx}}{|\dot{\xi}_{LC}(\theta_1^-)|} \sum_{n=0}^{\infty} \xi_\epsilon(t_n^-)\delta(t - t_n). \tag{6.45}$$

Consequently, for small deviations, the stability of the limit-cycle motion where $\theta_2 - \theta_1 = \pi$ can be determined by checking the stability of the sampled-data system shown in Figure 6.6.

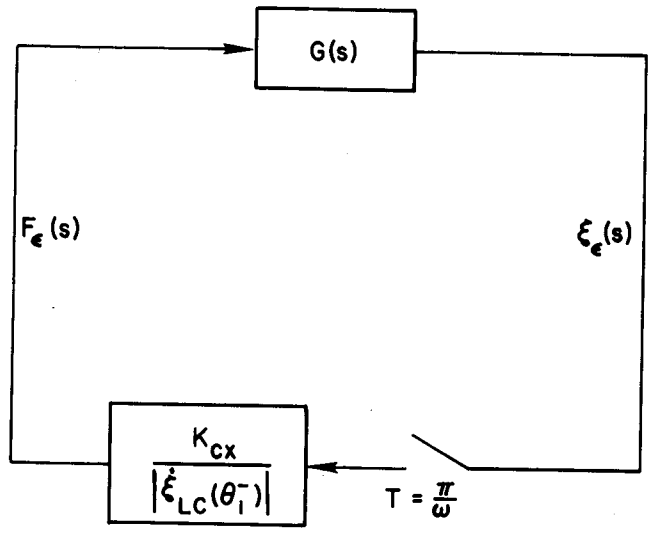

Figure 6.6–Sampled-data system for limit-cycle stability test ($\theta_2 - \theta_1 = \pi$).

2. Results for Special Case ($\theta_2 - \theta_1 = \pi$)

The characteristic equation for the sampled-data system of Figure 6.6 can be written in terms of the z-transform ($z \equiv e^{Ts}$) as

$$1 + kG_N(z) = 0, \tag{6.46}$$

where

$$k \equiv \frac{K_{cx}}{|\dot{\xi}_{LC}(\theta_1^-)|} \tag{6.47}$$

and

$$G_N(s) = -G(s) = \frac{P(s)}{Q(s)}. \tag{6.48}$$

Denoting the poles of $G_N(s)$ by p_n, the z-transform of $G_N(s)$ is (Reference 75)

$$G_N(z) = \sum_{n=1}^{4} \frac{P(p_n)}{Q'(p_n)}\left[\frac{e^{p_n T}}{z - e^{p_n T}}\right] = \left(\frac{\alpha^2 - \gamma^2}{\alpha^2 + \beta^2}\right)\frac{z\left[\cos \alpha T + (\lambda/\alpha)\sin \alpha T\right] - 1}{z^2 - 2z \cos \alpha T + 1}$$

$$+\left(\frac{\beta^2 + \gamma^2}{\alpha^2 + \beta^2}\right)\frac{z\left[\cosh \beta T + (\lambda/\beta) \sinh \beta T\right] - 1}{z^2 - 2z \cosh \beta T + 1}. \tag{6.49}$$

The denominator of Equation 6.47 is found by the following process. First, Equation 6.7 is differentiated with respect to time. This gives

$$\dot{\xi}_{LC}(\theta) = a_1 \omega \cos \theta + \sum_{n=2}^{\infty} a_n n\omega \cos (n\theta + \psi_n), \tag{6.50}$$

and at $\theta = \theta_1$

$$\cos \theta_1 = \frac{\lambda}{\sqrt{\lambda^2 + \omega^2}} \tag{6.51}$$

and

$$\dot{\xi}_{LC}(\theta_1) = \frac{2K_{cx}\omega\lambda}{\pi} \sum_{n=0}^{\infty} \frac{\left[(2n+1)^2\omega^2 - \gamma^2\right]}{\left[(2n+1)^2\omega^2 - \alpha^2\right]\left[(2n+1)^2\omega^2 + \beta^2\right]}$$

$$= \frac{K_{cx}\lambda}{2}\left[\frac{\alpha^2 - \gamma^2}{\alpha(\alpha^2 + \beta^2)} \tan\left(\frac{\pi\alpha}{2\omega}\right) + \frac{\beta^2 + \gamma^2}{\beta(\alpha^2 + \beta^2)} \tanh\left(\frac{\pi\beta}{2\omega}\right)\right]. \tag{6.52}$$

However, there is a discontinuity in $\dot{\xi}_{LC}(\theta)$ at $\theta = \theta_1$ (see Figure 6.3), and the Fourier series converges to the average value

$$\dot{\xi}_{LC}(\theta_1) = \frac{\dot{\xi}_{LC}(\theta_1^+) + \dot{\xi}_{LC}(\theta_1^-)}{2}. \tag{6.53}$$

It is obvious that

$$\dot{\xi}_{LC}(\theta_1^-) - \dot{\xi}_{LC}(\theta_1^+) = K_{cx}. \tag{6.54}$$

Therefore

$$\dot{\xi}_{LC}(\theta_1^-) = \dot{\xi}_{LC}(\theta_1) + \frac{K_{cx}}{2}, \tag{6.55}$$

and this expression is used in Equation 6.47. Notice that k is independent of K_{cx}.

Equation 6.46 is a fourth-degree polynomial in z. Because self-oscillations are examined here, one root of this characteristic equation is found at $z = -1$, and the stability of the assumed limit cycle depends on the locations of the three remaining roots. If these roots are located within the unit circle in the z-plane, the limit cycle is stable. Numerical calculations reveal that the limit cycles are stable for $\lambda > 0$ and $\omega > \omega_c$, where ω_c is a function of B_L only. For three important values of B_L, the critical frequencies are

$$B_L = 3.19042 \text{ (Earth-Moon } L_2 \text{ point)} \quad \omega_c = 3.102,$$

$$B_L = 5.14760 \text{ (Earth-Moon } L_1 \text{ point)} \quad \omega_c = 3.522,$$

and

$$B_L = 4.00000 \quad \omega_c = 3.287.$$

The variations of the roots for $B_L = 4$ are shown in Figures 6.7 and 6.8.

3. Procedure for General Case ($\theta_2 - \theta_1 \neq \pi$)

The characteristic equation for the general case where $\theta_2 - \theta_1 \neq \pi$ is more complicated than Equation 6.46. It is shown in Reference 75 that this characteristic equation is

$$1 + \left[\frac{K_{cx}}{|\dot{\xi}_{LC}(\theta_1^-)|} + \frac{K_{cx}}{|\dot{\xi}_{LC}(\theta_2^-)|}\right] G_N(z) + \frac{K_{cx}^2}{|\dot{\xi}_{LC}(\theta_1^-)||\dot{\xi}_{LC}(\theta_2^-)|}\left[G_N^2(z) - G_N(z, m)G_N(z, -m)\right] = 0, \tag{6.56}$$

where $G_N(z)$ is given by Equation 6.49 with $T = T_{LC} = 2\pi/\omega$, $m \equiv (\theta_2 - \theta_1)/2\pi$, and (References 75 and 79)

$$G_N(z, m) = \sum_{n=1}^{4} \frac{P(p_n)}{Q'(p_n)}\left[\frac{ze^{mp_nT}}{z - e^{p_nT}}\right] = z\left[\frac{N_1(z, m)}{D_1(z)} + \frac{N_2(z, m)}{D_2(z)}\right], \tag{6.57}$$

$$G_N(z, -m) = \sum_{n=1}^{4} \frac{P(p_n)}{Q'(p_n)}\left[\frac{e^{(1-m)p_nT}}{z - e^{p_nT}}\right] = \left[\frac{N_1(z, 1-m)}{D_1(z)} + \frac{N_2(z, 1-m)}{D_2(z)}\right], \tag{6.58}$$

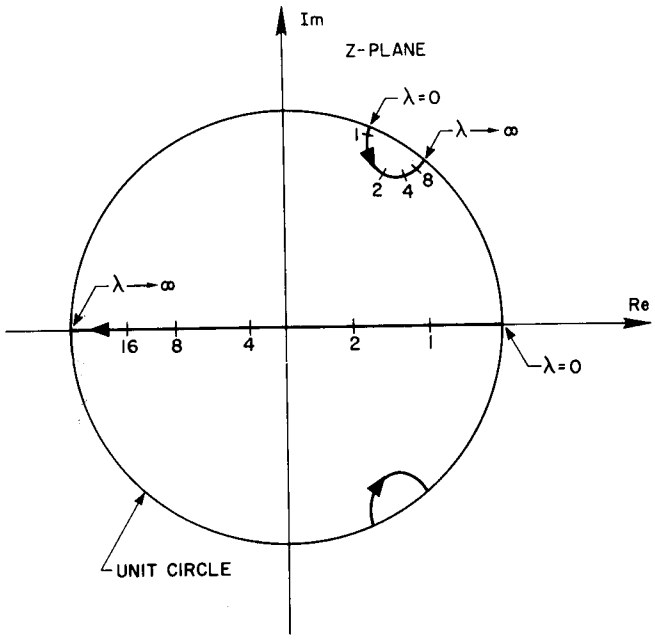

Figure 6.7–Root variations as a function of λ ($\theta_2 - \theta_1 = \pi$, $B_L = 4$, and $\omega = 4$).

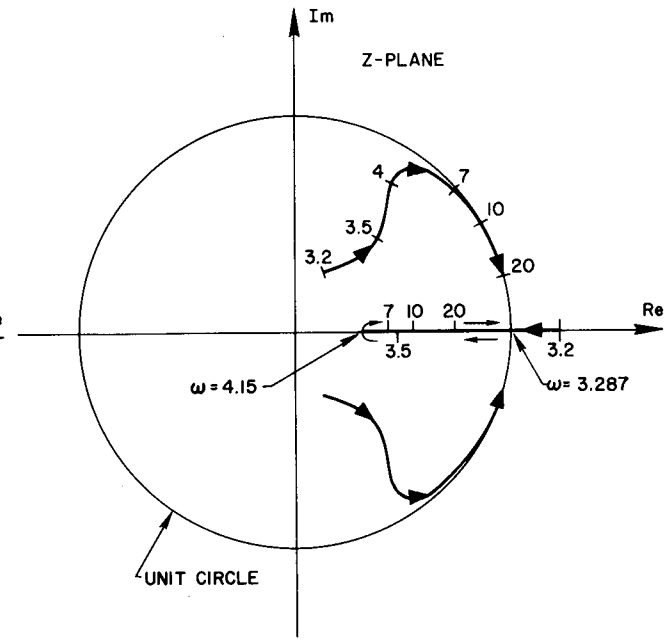

Figure 6.8–Root variations as a function of ω ($\theta_2 - \theta_1 = \pi$, $B_L = 4$, and $\lambda = 2$).

$$N_1(z, m) = \left(\frac{\alpha^2 - \gamma^2}{\alpha^2 + \beta^2}\right)\left\{z \cos \alpha mT - \cos (1 - m)\alpha T + \frac{\lambda}{\alpha}\left[z \sin \alpha mT + \sin (1 - m)\alpha T\right]\right\}, \tag{6.59}$$

$$N_2(z, m) = \left(\frac{\beta^2 + \gamma^2}{\alpha^2 + \beta^2}\right)\left\{z \cosh \beta mT - \cosh (1 - m)\beta T + \frac{\lambda}{\beta}\left[z \sinh \beta mT + \sinh (1 - m)\beta T\right]\right\}, \tag{6.60}$$

$$D_1(z) = z^2 - 2z \cos \alpha T + 1, \tag{6.61}$$

and

$$D_2(z) = z^2 - 2z \cosh \beta T + 1. \tag{6.62}$$

It can also be deduced that

$$\dot{\xi}_{LC}(\theta_1^-) = \dot{\xi}_{LC}(\theta_1) + \frac{K_{cx}}{2} \tag{6.63}$$

and

$$\dot{\xi}_{LC}(\theta_2^-) = \dot{\xi}_{LC}(\theta_2) - \frac{K_{cx}}{2}. \tag{6.64}$$

The roots of the characteristic equation can now be found. Although eight roots are obtained from Equation 6.56, four of them are extraneous and should be disregarded. These extraneous roots are just solutions of the quadratic equations, $D_1(z) = 0$ and $D_2(z) = 0$. Another root is found at $z = +1$, and the stability of the limit cycle is determined by the three remaining roots.

C. Solar Sail Control at the Sun-Earth L_1 Point

To illustrate the use of the preceding formulae, a solar sail control system for a satellite in the vicinity of the Sun-Earth L_1 point is considered here. By merely changing the area of the sail in the prescribed manner, the on-off control system shown in Figure 6.2 can be obtained. For the Sun-Earth L_1 point, the one-sided limit cycle is located between the Sun and the libration point.

Consider the case where $\theta_2 - \theta_1 = \pi$. To make use of graphical results, the constant B_{L1} is approximated by $B_{L1} \cong 4$. For $B_L = 4$, $\omega_c = 3.287$, and a good stability margin can be achieved by choosing a limit-cycle frequency of $\omega = 4$ ($T_{LC} = 2\pi/\omega = 91.31$ days). Figure 6.7 indicates that, for $\omega = 4$, small deviations from the nominal limit-cycle motion are adequately damped by choosing $\lambda = 2$. The choice of x_{min}, which specifies K_{cx}, is usually dictated by measurement accuracy limitations. For $x_{min} = 100$ km, the formulae of Section A.2 of this chapter give

$$K_{cx} = 1.613 \times 10^{-8} g, \quad x_{max} = 343.6 \text{ km},$$

$$\xi_d = 2.965 \times 10^{-6}, \quad \text{and} \quad \delta = 4.358 \times 10^{-6}.$$

Equation 3.1 shows that, for a satellite mass of 10 000 kg and $C_p = 2$, the area of the solar sail is only $A_s = 172.3$ m^2.

By using a conically shaped solar sail, it may be possible to stabilize the satellite's attitude as well as its position. Analyses of the attitude motion for a configuration of this type can be found in References 80 and 81.

D. Limit Cycles: Approximate Analysis

The results of Section A.1 of this chapter are not easy to apply when x_{max} and x_{min} are specified and the limit-cycle frequency ω is arbitrary. Therefore, an approximate technique that uses x_{max} and x_{min} as inputs is presented here.

By neglecting the gyroscopic coupling in Equation 6.1, a closed-form solution for all values of $\theta_2 - \theta_1$ can be obtained. Without this coupling, the y-axis motion is simple harmonic. The remaining portion of Equation 6.1 is just

$$\ddot{x} - (2B_L + 1)x = -F(\xi). \tag{6.65}$$

This equation is only second order and can be conveniently analyzed in the phase plane. However, before the phase-plane analysis is presented, the accuracy of this single-axis approximation is checked for the special case where $\theta_2 - \theta_1 = \pi$.

1. Accuracy of Single-Axis Approximation

Proceeding in the same manner as in Section A of this chapter, and denoting single-axis quantities with primes, it can be shown that

$$g'(s) = \frac{(2B_L + 1) - s^2}{s + \lambda}, \tag{6.66}$$

$$R'(\omega) = \frac{\omega^2 + (2B_L + 1)}{\sqrt{\lambda^2 + \omega^2}} \equiv \frac{\omega^2 + \epsilon^2}{\sqrt{\lambda^2 + \omega^2}}, \tag{6.67}$$

$$\tan \phi'(\omega) = -\frac{\omega}{\lambda}. \tag{6.68}$$

Equation 6.68 is identical to Equation 6.21, and many of the equations of Section A of this chapter are valid here. With these relations, it is easy to see that

$$\xi_d' = \frac{K_{cx}\lambda}{2(2B_L + 1)}, \tag{6.69}$$

$$\delta' = \frac{2K_{cx}}{\pi\omega} \sum_{n=0}^{\infty} \frac{1}{\left[(2n + 1)^2 + (\epsilon/\omega)^2\right]} = \frac{K_{cx}}{2\epsilon} \tanh\left(\frac{\pi\epsilon}{2\omega}\right), \tag{6.70}$$

$$x'_{max} = \frac{K_{cx}}{2(2B_L + 1)} + \Xi', \tag{6.71}$$

$$x'_{min} = \frac{K_{cx}}{2(2B_L + 1)} - \Xi', \tag{6.72}$$

and

$$\Xi' = \frac{2K_{cx}}{\pi\omega^2} \sum_{n=0}^{\infty} \frac{(-1)^n}{(2n + 1)\left[(2n + 1)^2 + (\epsilon/\omega)^2\right]} = \frac{K_{cx}}{2\epsilon^2}\left[1 - \operatorname{sech}\left(\frac{\pi\epsilon}{2\omega}\right)\right]. \tag{6.73}$$

With the exception of the quantities δ' and Ξ', the solutions for the single-axis and coupled systems are equivalent. Therefore, a measure of the accuracy of the single-axis approximation can be obtained by comparing these quantities. The percentage errors for the single-axis solutions are shown in Figure 6.9 for $B_L = 4$ ($\epsilon^2 = 9$). Although the discrepancy is quite large at the lower frequencies, it is less than 10% in both cases when $\omega > 6$.

2. Phase-Plane Method

The basic equations for the single-axis approximation are

$$\ddot{x} - (2B_L + 1)x = -F(\xi) \tag{6.74}$$

and

$$\xi = \dot{x} + \lambda x. \tag{6.75}$$

$F(\xi)$ is shown in Figure 6.1. The geometry for a typical limit cycle in the $\dot{x}$-x phase plane is illustrated in Figure 6.10. From the figure, it is obvious that

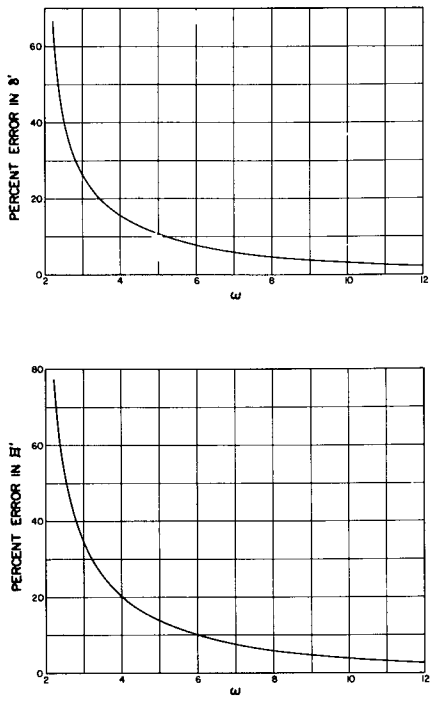

Figure 6.9–Errors for single-axis approximation versus limit-cycle frequency ($B_L = 4$, $\theta_2 - \theta_1 = \pi$).

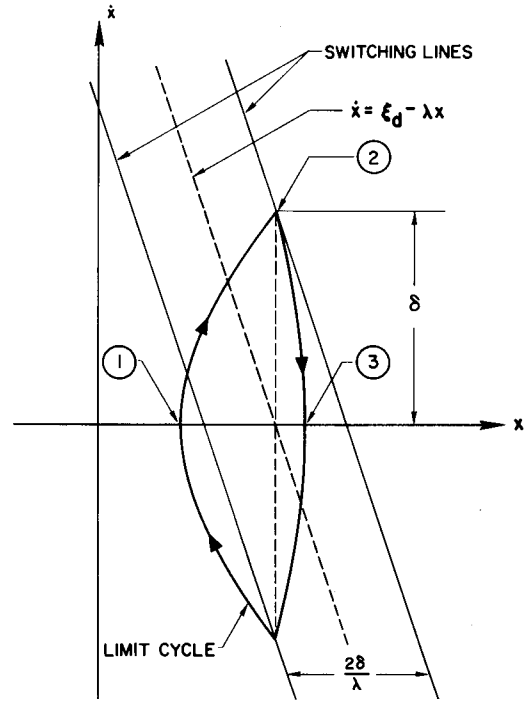

Figure 6.10–One-sided limit cycle in the $\dot{x}$-x phase plane.

$$\xi_d = \lambda x_2 \tag{6.76}$$

and

$$\delta = \dot{x}_2. \tag{6.77}$$

Between points 1 and 2, $F(\xi) = 0$, and integration of Equation 6.74 gives

$$\dot{x}^2 = \epsilon^2\left(x^2 - x_1^2\right), \tag{6.78}$$

$$\dot{x}_2 = \epsilon x_1\sqrt{q^2 - 1}, \tag{6.79}$$

and

$$t_{12} = \frac{1}{\epsilon}\log\left|q + \sqrt{q^2 - 1}\right|, \tag{6.80}$$

where

$$\epsilon^2 \equiv (2B_L + 1) \tag{6.81}$$

and

$$q \equiv \frac{x_2}{x_1} > 1. \tag{6.82}$$

Between points 2 and 3, $F(\xi) = K_{cx}$, and a single integration of Equation 6.74 in this region gives

$$\dot{x}^2 = \epsilon^2\left(x^2 - x_3^2\right) - 2K_{cx}(x - x_3) \tag{6.83}$$

and

$$\dot{x}_2^2 = \epsilon^2 q^2 x_1^2(1 - r^2) - 2K_{cx} q x_1(1 - r), \tag{6.84}$$

where

$$r \equiv \frac{x_3}{x_2} > 1. \tag{6.85}$$

From Equations 6.79 and 6.84,

$$K_{cx} = \frac{\epsilon^2(q^2r^2 - 1)}{2q(r - 1)} x_1. \tag{6.86}$$

With Equation 6.86, the necessary stability condition, $K_{cx} > \epsilon^2 x_3$, can be written in terms of q and r as

$$\frac{(q^2r^2 - 1)}{2q^2r(r - 1)} > 1. \tag{6.87}$$

Integration of Equation 6.83 yields

$$t_{23} = \frac{1}{\epsilon}\log\left|\frac{q^2r(2 - r) - 1}{(q^2r^2 - 1) - 2q(r - 1)\left[q + \sqrt{q^2 - 1}\right]}\right|. \tag{6.88}$$

Combining Equations 6.80 and 6.88 gives the limit-cycle period ($T_{LC} = 2\pi/\omega$)

$$T_{LC} = 2(t_{12} + t_{23}) = \frac{2}{\epsilon}\log\left|\frac{\left[q^2r(2 - r) - 1\right]\left[q + \sqrt{q^2 - 1}\right]}{(q^2r^2 - 1) - 2q(r - 1)\left[q + \sqrt{q^2 - 1}\right]}\right|. \tag{6.89}$$

3. Sample Calculation at the Earth-Moon L_2 Point

As an example of the usefulness of the approximate formulae given above, consider the on-off control of a satellite in the vicinity of the Earth-Moon L_2 point ($B_{L2} = 3.1904$, $\epsilon = 2.7168$). By specifying the amplitude ratios, $x_2/x_1 = 2 = q$, and $x_3/x_1 = 2.5 = qr$ (therefore $r = 1.25$), Equation 6.89 gives $T_{LC} = 1.407 = 6.12$ days. The fraction of the total time that the control is on can be determined from Equations 6.80 and 6.88:

$$m = \frac{t_{23}}{t_{12}} = 0.4512\ . \tag{6.90}$$

This means that the control is turned on continuously for a period of 2.76 days. For thrust periods of this duration, an electrical propulsion device would probably be utilized. Measurement accuracy considerations

influence the choice of x_1 (x_{min}). If x_1 = 10 km, then x_2 = 20 km, x_3 = 25 km, and Equation 6.86 gives $K_{cx} = 2.798 \times 10^{-7} g$. However, the average control acceleration is only $\overline{K_{cx}} = mK_{cx} = 1.262 \times 10^{-7} g$. Finally, the slope of the switching line is taken as $\lambda = 3$, and simple calculations yield $\xi_d = 1.561 \times 10^{-4}$ and $\delta = 1.224 \times 10^{-4}$.

The values listed above for K_{cx}, λ, ξ_d, and δ were used in an analog computer simulation of the coupled system (Equation 6.1). It was found that the error in T_{LC} was about 14.1% of the true value $(T_{LC})_{computer} = 1.233 = 5.36$ days. Additional results of this simulation are shown in Figure 6.11. Notice that x_3/x_1 is very close to the value used in the single-axis approximation ($qr = 2.5$).

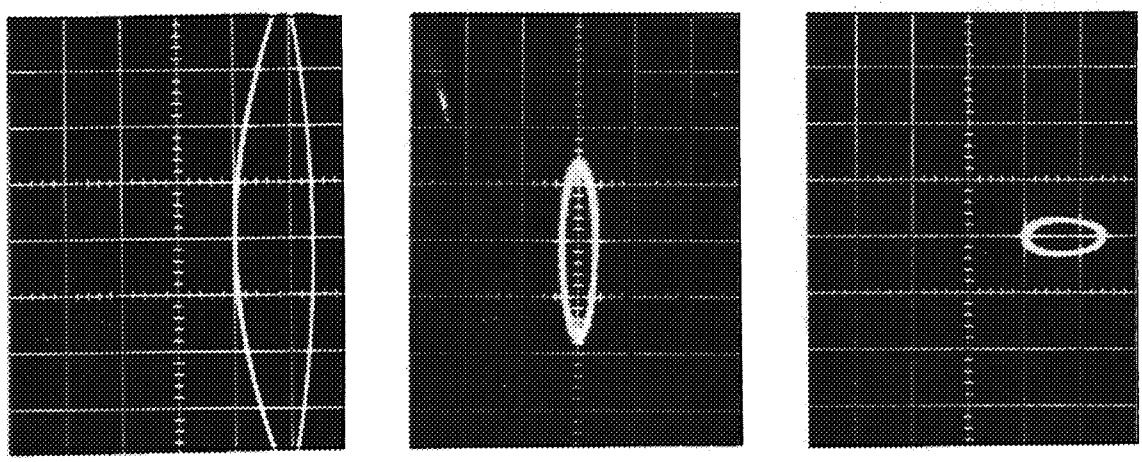

$\dot{x}$ versus x. Grid size is 0.027 m/sec × 10 km.

$\dot{y}$ versus y.

y versus x. Grid size is 10 km × 10 km

Figure 6.11–Analog computer simulation of Equation 6.1 for sample calculation at the Earth-Moon L_2 point. All trajectories are clockwise.

CHAPTER VII

STABLE CABLE

Consider two satellites of equal mass that are connected by a light cable of adjustable length. Is it possible to stabilize the position of the mass center of this configuration in the vicinity of a collinear libration point by simply changing the length of the cable with an internal mechanism? This intriguing possibility is examined below, and it is found that positional stability can be achieved by varying the length of the cable in a manner that takes advantage of the nonlinearities of the modified potential field in the vicinity of the libration point.

This problem was originally analyzed by Colombo (Reference 3), who also concluded that appropriate variations in the length of the connecting cable would produce positional stability. However, Colombo's analysis considered only linear variations of the modified potential field in the vicinity of the libration point, and it can be shown that his conclusion was based on a fallacious argument. (The adjustable length cable was treated as a workless constraint.)

A. Stabilization Procedure

In this section, the control logic for the cable variation is formulated, and the stability of the resulting system is examined. The geometry for the cable-connected satellite in the vicinity of a collinear libration point is shown in Figure 7.1. If the mass of the cable is neglected, the equations of motion for the cable-connected satellite are approximately (terms higher than second order are neglected in Equation 2.43, and it is assumed that $\rho = \nu = 0$)*

$$
\begin{aligned}
&\ddot{x}'_1 - 2\dot{y}'_1 - (2B_L + 1)x'_1 \pm \frac{3}{2}C_L\left[2x'^2_1 - \left(y'^2_1 + z'^2_1\right)\right] = F_x,\\
&\ddot{x}'_2 - 2\dot{y}'_2 - (2B_L + 1)x'_2 \pm \frac{3}{2}C_L\left[2x'^2_2 - \left(y'^2_2 + z'^2_2\right)\right] = -F_x,\\
&\ddot{y}'_1 + 2\dot{x}'_1 + (B_L - 1)y'_1 \mp 3C_L x'_1 y'_1 = F_y,\\
&\ddot{y}'_2 + 2\dot{x}'_2 + (B_L - 1)y'_2 \mp 3C_L x'_2 y'_2 = -F_y,\\
&\ddot{z}'_1 + B_L z'_1 \mp 3C_L x'_1 z'_1 = F_z,
\end{aligned}
\qquad (7.1)
$$

and

$$
\ddot{z}'_2 + B_L z'_2 \mp 3C_L x'_2 z'_2 = -F_z,
$$

*The upper signs hold at L_2, and the lower signs at L_1.

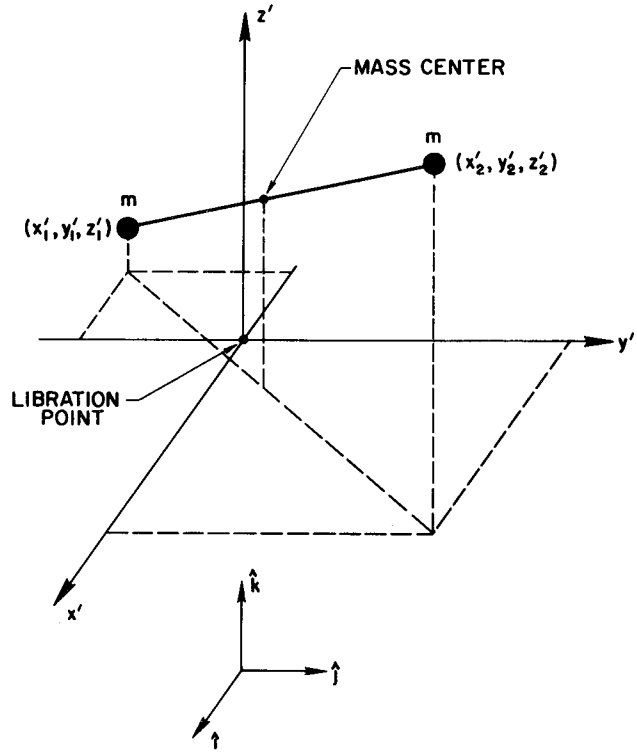

Figure 7.1—Cable-connected satellite in the vicinity of a collinear libration point.

where

$$\mathbf{F} = F_x\mathbf{i} + F_y\mathbf{j} + F_z\mathbf{k}, \tag{7.2}$$

and the tension in the cable is

$$\mathbf{T} = m\mathbf{F}. \tag{7.3}$$

Although fluctuations of the tension will occur whenever the cable is extended or retracted, it is assumed here that some tension will always be present; i.e., the cable does not become slack.

1. One-Dimensional Analysis

To gain some physical feeling for the stabilization procedure, an approximate, one-dimensional analysis is presented before considering the more complicated, three-dimensional system.

Shifting equilibrium point

Neglecting all coupling terms and assuming that the motion is limited to the x'-axis reduces Equation 7.1 to

$$\ddot{x}'_1 - (2B_L + 1)x'_1 \pm 3C_L x'^2_1 = F_x$$

and (7.4)

$$\ddot{x}'_2 - (2B_L + 1)x'_2 \pm 3C_L x'^2_2 = -F_x.$$

Elimination of F_x gives

$$\ddot{x}'_1 + \ddot{x}'_2 - (2B_L + 1)(x'_1 + x'_2) \pm 3C_L\left(x'^2_1 + x'^2_2\right) = 0. \tag{7.5}$$

Assume for the moment that the mass center of the satellite is at $x'_{cm} = \pm a$, and that the cable length ℓ is a constant ($\ell = a$). In this case

$$x'_1 = -\frac{a}{2} \pm \alpha$$

and (7.6)

$$x'_2 = \frac{a}{2} \pm \alpha.$$

For equilibrium $\ddot{x}'_1 = \ddot{x}'_2 = 0$, and using Equations 7.5 and 7.6, it is found that

$$\alpha = \frac{(2B_L + 1)}{6C_L} - \frac{1}{2}\left[\frac{(2B_L + 1)^2}{9C_L^2} - a^2\right]^{1/2} \cong \frac{3C_L}{4(2B_L + 1)}a^2. \tag{7.7}$$

Therefore, because of the nonlinear effect, the equilibrium point for the cable-connected satellite is dependent on the length of the cable.

To see how stabilization of the mass center might be attained by taking advantage of this consequence, consider a satellite near an L_2 point with an initial cable length of $\ell(0) = a_i$, and a corresponding equilibrium point at $x'_{eq}(0) = a_i$. Because of the natural instability of the instantaneous equilibrium point x'_{eq}, the mass center will always experience a repelling acceleration relative to this point. Now suppose that the mass center is initially located at $x'_{cm}(0) = a_i + \epsilon(0)$, and assume that $\dot{x}'_{cm}(0) = \dot{\epsilon}(0) = 0$. If $\epsilon(0) > 0$, the initial acceleration is $\ddot{x}'_{cm}(0) > 0$, and x'_{cm} will increase. However, by extending the cable, x'_{eq} can be increased, and it may be possible to shift the equilibrium point to the other side of the mass center; i.e., at some time t_f, $x'_{eq}(t_f) > a_i + \epsilon(t_f)$. This shift would decelerate the mass center, and if $\epsilon(0)$ is not too large, the motion of the mass center could be reversed. If $\epsilon(0) < 0$, the initial acceleration is $\ddot{x}'_{cm}(0) < 0$, and x'_{cm} will decrease. With this initial condition, the appropriate shift of the equilibrium point would be achieved by retracting the cable [notice that the equilibrium point cannot be shifted to the other side of the mass center when $\epsilon(0) < -a_i$].

Naturally, the magnitudes of the initial errors $[\epsilon(0), \dot{\epsilon}(0)]$ that can be tolerated with this stabilization method are bounded. This limitation will be discussed in Section B.1 of this chapter.

Cable control

For convenience, the coordinate translation

$$x' = x \pm a \tag{7.8}$$

is introduced. With this translation, Equation 7.5 becomes

$$\ddot{x}_1 + \ddot{x}_2 - (2B_L + 1)(x_1 + x_2 \pm 2a) \pm 3C_L\left[x_1^2 + x_2^2 \pm 2a(x_1 + x_2) + 2a^2\right] = 0, \tag{7.9}$$

and the equilibrium solution is

$$x_1 = -\frac{a}{2}$$

and (7.10)

$$x_2 = \frac{a}{2}.$$

This equilibrium solution is unstable if the cable length is constant, but the situation is quite different when the cable length is varied according to the control law

$$\ell \equiv x_2 - x_1 = \left[a \pm b(x_1 + x_2) \pm c(\dot{x}_1 + \dot{x}_2)\right]. \tag{7.11}$$

The form of this control law has been influenced by the qualitative arguments of the previous section.

Stability conditions for the constants a, b, and c can be determined by investigating small motions about the equilibrium solution of Equation 7.10. Substitution of

$$x_1 = -\frac{a}{2} + \xi_1$$

and (7.12)

$$x_2 = \frac{a}{2} + \xi_2$$

into Equations 7.9 and 7.11 [neglecting terms of $O(\xi^2)$] gives

$$\ddot{\xi}_1 + \ddot{\xi}_2 - (2B_L + 1)(\xi_1 + \xi_2) \pm 3C_L\left[a(\xi_2 - \xi_1) \pm 2\alpha(\xi_1 + \xi_2)\right] = 0 \tag{7.13}$$

and

$$(\xi_2 - \xi_1) = \pm\, b(\xi_1 + \xi_2) \pm c(\dot{\xi}_1 + \dot{\xi}_2). \tag{7.14}$$

The coordinate for the mass center is

$$x_{cm} = \frac{x_1 + x_2}{2} = \frac{\xi_1 + \xi_2}{2}. \tag{7.15}$$

From Equations 7.13, 7.14, and 7.15, it is clear that

$$\ddot{x}_{cm} + 3C_L ac\dot{x}_{cm} + \left[3C_L(ab + 2\alpha) - (2B_L + 1)\right]x_{cm} = 0. \tag{7.16}$$

Therefore, the mass center is asymptotically stable if

$$ac > 0 \tag{7.17}$$

and

$$(ab + 2\alpha) > \frac{2B_L + 1}{3C_L}. \tag{7.18}$$

The constant α can usually be neglected in Equation 7.18, and this stability condition can be approximated by

$$ab > \frac{2B_L + 1}{3C_L}. \tag{7.19}$$

For the Earth-Moon L_2 point ($B_{L2} = 3.1904$, $C_{L2} = 15.845$), Equation 7.19 gives $ab > 0.155$.

2. Three-Dimensional Analysis

Using the coordinate transformation (cf. Equation 7.8)

$$x' = x \pm \alpha, \quad y' = y, \quad z' = z \tag{7.20}$$

in Equation 7.1 gives

$$\ddot{x}_1 - 2\dot{y}_1 - (2B_L + 1)(x_1 \pm \alpha) \pm \frac{3}{2}C_L\left[2x_1^2 \pm 4\alpha x_1 + 2\alpha^2 - \left(y_1^2 + z_1^2\right)\right] = F_x,$$

$$\ddot{x}_2 - 2\dot{y}_2 - (2B_L + 1)(x_2 \pm a) \pm \frac{3}{2}C_L\left[2x_2^2 \pm 4ax_2 + 2a^2 - \left(y_2^2 + z_2^2\right)\right] = -F_x,$$

$$\ddot{y}_1 + 2\dot{x}_1 + (B_L - 1)y_1 \mp 3C_L(x_1 \pm a)y_1 = F_y,$$

$$\ddot{y}_2 + 2\dot{x}_2 + (B_L - 1)y_2 \mp 3C_L(x_2 \pm a)y_2 = -F_y, \tag{7.21}$$

$$\ddot{z}_1 + B_L z_1 \mp 3C_L(x_1 \pm a)z_1 = F_z,$$

and

$$\ddot{z}_2 + B_L z_2 \mp 3C_L(x_2 \pm a)z_2 = -F_z,$$

where a is given by Equation 7.7. For a cable length $\ell = a$, it is readily verified that an equilibrium solution of Equation 7.21 is

$$x_1 = -\frac{a}{2}, \quad x_2 = \frac{a}{2} \tag{7.22}$$

and

$$y_1 = y_2 = z_1 = z_2 = 0.$$

This equilibrium situation is depicted in Figure 7.2. Notice that stabilization about this equilibrium solution must control the relative orientation of the cable-connected satellite as well as the position of its mass center.

The cable control law for the three-dimensional case is not obvious, but after a few trials, a satisfactory control law was devised. This control law is given by

$$\begin{aligned}\ell^2 &= (x_2 - x_1)^2 + (y_2 - y_1)^2 + (z_2 - z_1)^2 \\ &= \left[a \pm b(x_1 + x_2) \pm c(\dot{x}_1 + \dot{x}_2) + \beta(y_1 - y_2)\right]^2,\end{aligned} \tag{7.23}$$

where a, b, c, and β are constants. It is hoped that the reasoning behind this particular formulation will be made clear by the stability investigation presented below.

Before proceeding to the stability analysis, some useful equations are obtained. Using Figure 7.1, it can be verified that (check Equation 7.2 and 7.20)

$$\frac{F_x}{F_y} = \frac{x_2 - x_1}{y_2 - y_1}, \tag{7.24}$$

$$\frac{F_x}{F_z} = \frac{x_2 - x_1}{z_2 - z_1}, \tag{7.25}$$

and

$$\frac{F_y}{F_z} = \frac{y_2 - y_1}{z_2 - z_1}. \tag{7.26}$$

Rearrangements of Equation 7.21 give

$$\ddot{x}_1 + \ddot{x}_2 - 2(\dot{y}_1 + \dot{y}_2) - (2B_L + 1)(x_1 + x_2 \pm 2a) \pm \frac{3}{2}C_L\left[2\left(x_1^2 + x_2^2\right) \pm 4a(x_1 + x_2)\right.$$

$$\left. + 4a^2 - \left(y_1^2 + y_2^2 + z_1^2 + z_2^2\right)\right] = 0, \tag{7.27}$$

$$\ddot{y}_1 + \ddot{y}_2 + 2(\dot{x}_1 + \dot{x}_2) + (B_L - 1)(y_1 + y_2) \mp 3C_L\left[(x_1 \pm a)y_1 + (x_2 \pm a)y_2\right] = 0, \tag{7.28}$$

$$\ddot{z}_1 + \ddot{z}_2 + B_L(z_1 + z_2) \mp 3C_L\left[(x_1 \pm a)z_1 + (x_2 \pm a)z_2\right] = 0, \tag{7.29}$$

$$2F_x = \ddot{x}_1 - \ddot{x}_2 - 2(\dot{y}_1 - \dot{y}_2) - (2B_L + 1)(x_1 - x_2) \pm \frac{3}{2}C_L\left\{2\left(x_1^2 - x_2^2\right)\right.$$

$$\left. \pm 4a(x_1 - x_2) - \left[\left(y_1^2 - y_2^2\right) + \left(z_1^2 - z_2^2\right)\right]\right\}, \tag{7.30}$$

$$2F_y = \ddot{y}_1 - \ddot{y}_2 + 2(\dot{x}_1 - \dot{x}_2) + (B_L - 1)(y_1 - y_2) \mp 3C_L\left[(x_1 \pm a)y_1 - (x_2 \pm a)y_2\right], \tag{7.31}$$

and

$$2F_z = \ddot{z}_1 - \ddot{z}_2 + B_L(z_1 - z_2) \mp 3C_L\left[(x_1 \pm a)z_1 - (x_2 \pm a)z_2\right]. \tag{7.32}$$

For small motions about the equilibrium solution of Equation 7.22

$$x_1 = -\frac{a}{2} + \xi_1, \qquad x_2 = \frac{a}{2} + \xi_2,$$

$$y_1 = \eta_1, \qquad y_2 = \eta_2, \tag{7.33}$$

$$z_1 = \zeta_1, \qquad z_2 = \zeta_2.$$

Substituting Equation 7.33 into Equations 7.23, 7.27, 7.28, and 7.29, and retaining only linear terms in (ξ, η, ζ) gives

$$(\xi_1 - \xi_2) \pm b(\xi_1 + \xi_2) \pm c(\dot{\xi}_1 + \dot{\xi}_2) + \beta(\eta_1 - \eta_2) = 0, \tag{7.34}$$

$$\ddot{\xi}_1 + \ddot{\xi}_2 - 2(\dot{\eta}_1 + \dot{\eta}_2) - (2B_L + 1)(\xi_1 + \xi_2 \pm 2a) \pm \frac{3}{2}C_L\left[a^2 + 2a(\xi_2 - \xi_1) \pm 4a(\xi_1 + \xi_2) + 4a^2\right] = 0, \tag{7.35}$$

$$\ddot{\eta}_1 + \ddot{\eta}_2 + 2(\dot{\xi}_1 + \dot{\xi}_2) + (B_L - 1)(\eta_1 + \eta_2) \mp 3C_L\left[\left(-\frac{a}{2} \pm a\right)\eta_1 + \left(\frac{a}{2} \pm a\right)\eta_2\right] = 0, \tag{7.36}$$

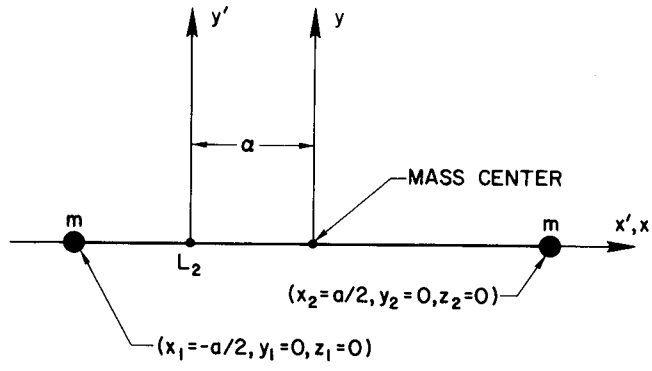

Figure 7.2–Equilibrium situation for the cable-connected satellite near an L_2 point.

and

$$\ddot{\zeta}_1 + \ddot{\zeta}_2 + B_L(\zeta_1 + \zeta_2) \mp 3C_L\left[\left(-\frac{a}{2} \pm \alpha\right)\zeta_1 + \left(\frac{a}{2} \pm \alpha\right)\zeta_2\right] = 0. \tag{7.37}$$

Two more equations are obtained by eliminating F_x, F_y, and F_z in Equations 7.24, 7.25, 7.30, 7.31, and 7.32. Again keeping only linear terms in (ξ, η, ζ), this yields

$$\ddot{\eta}_2 - \ddot{\eta}_1 + 2(\dot{\xi}_2 - \dot{\xi}_1) \mp \frac{3}{2}C_L a(\eta_1 + \eta_2) + 3(B_L - 3C_L\alpha)(\eta_2 - \eta_1) = 0 \tag{7.38}$$

and

$$\ddot{\zeta}_2 - \ddot{\zeta}_1 \mp \frac{3}{2}C_L a(\zeta_1 + \zeta_2) + \left[3(B_L - 3C_L\alpha) + 1\right](\zeta_2 - \zeta_1) = 0. \tag{7.39}$$

Equations 7.34 to 7.39 constitute six independent equations for the six unknowns (ξ_1, ξ_2, η_1, η_2, ζ_1, ζ_2). These equations will be used to test the stability of the controlled motion of the cable-connected satellite about the equilibrium solution of Equation 7.22.

The linearized motion out of the xy-plane is uncoupled, and the characteristic equation for this motion can be determined from Equations 7.37 and 7.39. A simple calculation gives

$$s^4 + a_1 s^2 + a_2 = 0, \tag{7.40}$$

where

$$a_1 = (4B_L + 1) - 12C_L\alpha \tag{7.41}$$

and

$$a_2 = \frac{1}{2}\left\{\left[B_L - \frac{3}{2}C_L(2\alpha \mp a)\right]\left[(3B_L + 1) - \frac{3}{2}C_L(6\alpha \pm a)\right] + \left[B_L - \frac{3}{2}C_L(2\alpha \pm a)\right]\left[(3B_L + 1) - \frac{3}{2}C_L(6\alpha \mp a)\right]\right\}. \tag{7.42}$$

Terms involving α and a^2 can usually be neglected, and the roots of Equation 7.40 are approximately $\pm j\sqrt{B_L}$, $\pm j\sqrt{3B_L + 1}$ ($j \equiv \sqrt{-1}$). Therefore, according to the linearized analysis, the out-of-plane motion of the cable-connected satellite is bounded. However, small oscillations, which could be caused by initial-condition errors, cannot be damped by the cable control.

The characteristic equation for the coupled motion in the xy-plane is obtained from Equations 7.34, 7.35, 7.36, and 7.38. After some tiresome manipulations, it is found that

$$s^6 + b_1 s^5 + b_2 s^4 + b_3 s^3 + b_4 s^2 + b_5 s + b_6 = 0, \tag{7.43}$$

where

$$b_1 = 3C_L ac - 2\beta, \tag{7.44}$$

$$b_2 = (k_2 + k_3 + 4 - k_1) + 3C_L ab, \tag{7.45}$$

$$b_3 = 3C_L(k_2 + k_3 + 2)ac + 2\left[k_1 - (k_2 + 4)\right]\beta, \tag{7.46}$$

$$b_4 = k_3(k_2 + 4) - k_1(k_2 + k_3) - \frac{9}{4}C_L^2 a^2 + 3C_L(k_2 + k_3 + 2)ab, \tag{7.47}$$

$$b_5 = 3C_L\left(k_2k_3 - \frac{9}{4}C_L^2 a^2\right)ac + 2\left(k_1k_2 + \frac{9}{2}C_L^2 a^2\right)\beta, \tag{7.48}$$

and

$$b_6 = \left(k_2k_3 - \frac{9}{4}C_L^2 a^2\right)(3C_L ab - k_1), \tag{7.49}$$

and

$$k_1 \equiv (2B_L + 1) - 6C_L\alpha, \tag{7.50}$$

$$k_2 \equiv (B_L - 1) - 3C_L\alpha, \tag{7.51}$$

and

$$k_3 \equiv 3B_L - 9C_L\alpha. \tag{7.52}$$

The determination of suitable values for the control parameters b, c, and β can be accomplished in an efficient manner by employing the root-locus technique. Taking $c = \beta = 0$, Equation 7.43 is written in the form

$$\frac{3C_L ab\left[s^4 + c_1s^2 + c_2\right]}{s^6 + d_1s^4 + d_2s^2 + d_3} = -1, \tag{7.53}$$

where

$$c_1 = k_2 + k_3 + 2, \tag{7.54}$$

$$c_2 = k_2k_3 - \frac{9}{4}C_L^2 a^2, \tag{7.55}$$

$$d_1 = k_2 + k_3 + 4 - k_1, \tag{7.56}$$

$$d_2 = -\left[k_1(k_2 + k_3) - k_3(k_2 + 4) - \frac{9}{4}C_L^2 a^2\right], \tag{7.57}$$

and

$$d_3 = -k_1\left(k_2k_3 - \frac{9}{4}C_L^2 a^2\right). \tag{7.58}$$

A root-locus plot of Equation 7.53 for the Earth-Moon L_2 point is given in Figure 7.3.* The root-locus plot shows that the system is neutrally stable when $ab > (ab)_3 = 0.600$. Notice that $(ab)_2$ corresponds to the critical gain for the one-dimensional case, i.e., $(ab)_2 \cong (2B_L + 1)/3C_L$ (cf. Equation 7.19). The critical gains $(ab)_2$ and $(ab)_3$ are listed in Table 7.1 for several libration points. In every case, $(ab)_3/(ab)_2 < 4$, and it can be concluded that neutral stability is insured at any libration point when

*It was found that the contributions of terms involving a^2 and α were negligible for the values of a that are used in the present study. With $a = 0$ in Equations 7.54 to 7.58, the critical gains are $(ab)_1 = 0.084$, $(ab)_2 = 0.155$, and $(ab)_3 = 0.600$. For $a = 10^{-2}$ in Equations 7.54 to 7.58, the critical gains are $(ab)_1 = 0.085$, $(ab)_2 = 0.155$, and $(ab)_3 = 0.599$.

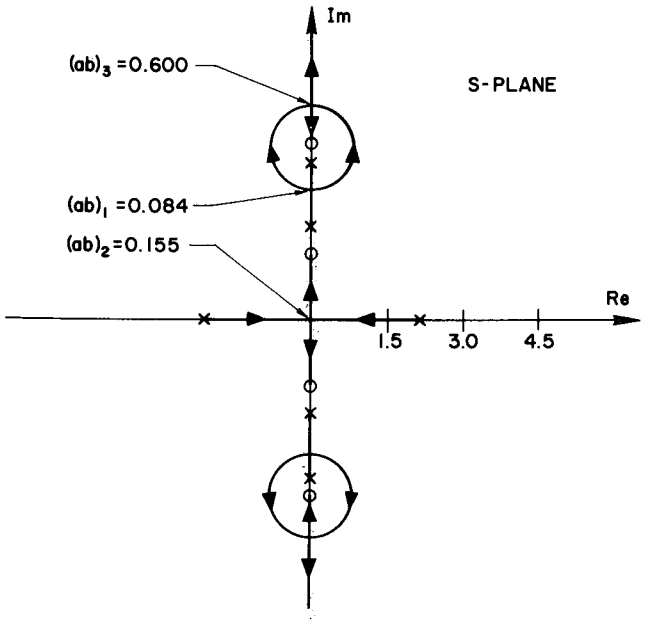

Figure 7.3–Root-locus plot for Equation 7.53 at the Earth-Moon L_2 point ($B_{L2} = 3.1904$, $C_{L2} = 15.845$). Gain is ab.

$$ab > \frac{4(2B_L + 1)}{3C_L}. \tag{7.59}$$

Damping is introduced by choosing appropriate values for the control parameters c and β. For this case, Equation 7.43 is written as

$$\frac{3C_L ac\left[b_1' s^4 + b_3' s^2 + b_5'\right]s}{s^6 + b_2 s^4 + b_4 s^2 + b_6} = -1, \tag{7.60}$$

where

$$b_1' = 1 - 2\beta', \tag{7.61}$$

$$b_3' = (k_2 + k_3 + 2) + 2\left[k_1 - (k_2 + 4)\right]\beta', \tag{7.62}$$

and

$$b_5' = \left(k_2 k_3 - \frac{9}{4} C_L^2 a^2\right) + 2\left(k_1 k_2 + \frac{9}{2} C_L^2 a^2\right)\beta', \tag{7.63}$$

and

$$\beta' \cong \frac{\beta}{3C_L ac}. \tag{7.64}$$

It should be emphasized that *both* c and β are needed in Equation 7.43 to obtain a damped system. The parameter β' (which determines β) must be chosen so that the zeros in Equation 7.60 are located *between* the poles on the imaginary axis. (This pole-zero configuration is not possible when $\beta' = 0$.) If this is not done, a segment of the root locus of Equation 7.60 will be in the right half of the s-plane.

Table 7.1–Critical gains for cable-connected satellite.

Libration point	$(ab)_3$	$(ab)_2$	$\frac{(ab)_3}{(ab)_2}$
Earth-Moon L_1	0.651	0.175	3.72
Earth-Moon L_2	.600	.155	3.87
Sun-Mercury L_2	.0144	.00378	3.81
Sun-Venus L_2	.0355	.00932	3.81
Sun-Earth L_2	.0380	.00999	3.80
Sun-Mars L_2	.0181	.00475	3.81
Jupiter-Io L_2	.0882	.0232	3.80
Jupiter-Ganymede L_2	.114	.0298	3.83
Jupiter-Enceladus L_2	.0140	.00369	3.79

By fixing the values of ab and β', a root-locus plot of Equation 7.60 for the gain ac can be constructed. The plot for the Earth-Moon L_2 point with $ab = 0.750$ and $\beta' = 0.200$ is shown in Figure 7.4. Although more damping would be desirable, the system is asymptotically stable for all values of the gain ac. When $ac = 0.100$, the roots are located at $-0.0475 \pm j1.2249$, $-0.7595 \pm j3.8841$, and $-0.4764 \pm j4.9958$, and from Equation 7.64, $\beta = 0.951$.

B. Other Considerations

Although the stability of *small* motions about the equilibrium solution of Equation 7.22 has been established, several questions concerning the theoretical feasibility of the cable control system are still unanswered. Some of these questions are considered in this section.

1. Cable Extension Limitation

The extension of the cable is made possible by the gravitational gradient in the vicinity of the libration point. Therefore, the acceleration of the cable's length $\ddot{\ell}$ is bounded $[\ddot{\ell}_{max} \cong (2B_L + 1)\ell]$.* This restriction has the effect of placing upper bounds on the initial errors that can be tolerated with the cable stabilization technique. In this section, *approximate* analytical estimates of these error bounds are obtained by using the one-dimensional model of Section A.1 of this chapter.

Denoting initial values with a subscript i, the coordinate translation of Equation 7.8 is specialized to†

$$x' = x + \alpha_i. \tag{7.65}$$

The coordinates of the two masses are

$$x_1 = -q + \epsilon$$

and

$$x_2 = q + \epsilon. \tag{7.66}$$

Initially, it is assumed that $q(0) = a_i/2$, $\dot{q}(0) = 0$, and $\epsilon(0) \sim O(a_i^2)$. Substitution of Equation 7.66 into Equation 7.4 gives (using Equation 7.65)

$$-\ddot{q} + \ddot{\epsilon} - (2B_{L2} + 1)(\epsilon - q + \alpha_i) + 3C_{L2}\left[q^2 - 2q\epsilon + \epsilon^2 + 2\alpha_i(\epsilon - q) + \alpha_i^2\right] = F_x \tag{7.67}$$

and

$$\ddot{q} + \ddot{\epsilon} - (2B_{L2} + 1)(q + \epsilon + \alpha_i) + 3C_{L2}\left[q^2 + 2q\epsilon + \epsilon^2 + 2\alpha_i(q + \epsilon) + \alpha_i^2\right] = -F_x. \tag{7.68}$$

If terms of $O(a_i^2)$ are neglected, Equation 7.67 or Equation 7.68 yields

$$\ddot{q} - (2B_{L2} + 1)q = -F_x. \tag{7.69}$$

*When the cable is retracted, $\ddot{\ell}_{max}$ is determined by the tensile strength of the cable.
†For clarity, double signs are deleted, and the analysis is limited to an L_2 point.

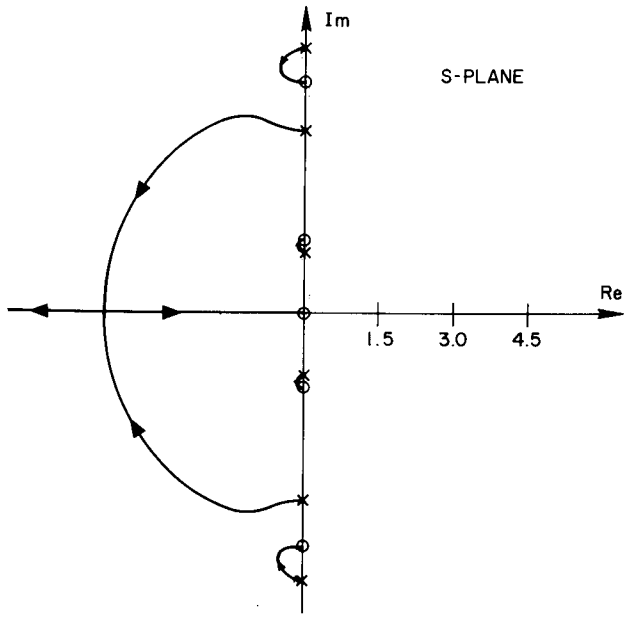

Figure 7.4--Root-locus plot for Equation 7.60 at the Earth-Moon L_2 point ($B_{L2} = 3.1904$, $C_{L2} = 15.845$). Gain is ac, $ab = 0.750$, and $\beta' = 0.200$.

During the cable extension period ($0 \leq t \leq t_1$) it is assumed that

$$F_x = (1 - \gamma)(2B_{L2} + 1)q = 0, \tag{7.70}$$

where $0 < \gamma < 1$. Equation 7.69 can now be written as

$$\ddot{q} - \gamma(2B_{L2} + 1)q = 0, \tag{7.71}$$

and with the initial conditions given above, the solution is

$$q(t) = \frac{a_i}{2}\cosh kt \tag{7.72}$$

and

$$\dot{q}(t) = \frac{ka_i}{2}\sinh kt, \tag{7.73}$$

where $k^2 \equiv \gamma(2B_{L2} + 1)$. When the cable is fully extended, $q(t_1) = a_m/2$, and the extension time t_1 can be obtained from

$$\cosh kt_1 = \frac{1}{\delta}, \tag{7.74}$$

where $\delta \equiv a_i/a_m$ $(0 < \delta < 1)$.

To find the motion of the mass center, add Equations 7.67 and 7.68 and neglect terms of $O(a_i^3)$. This yields (using Equation 7.7)

$$\ddot{\epsilon} - (2B_{L2} + 1)\epsilon + 3C_{L2}\left[q^2 - \frac{a_i^2}{4}\right] = 0. \tag{7.75}$$

For the cable extension period ($0 \leq t \leq t_1$), Equation 7.75 is

$$\ddot{\epsilon} - (2B_{L2} + 1)\epsilon + \frac{3}{8}C_{L2}\delta^2 a_m^2(\cosh 2kt - 1) = 0. \tag{7.76}$$

The solution of Equation 7.76 is given by

$$\epsilon(t) = [\epsilon(0) + (A + B)]\cosh k't + \frac{\dot{\epsilon}(0)}{k'}\sinh k't - (A + B\cosh 2kt), \tag{7.77}$$

where

$$k'^2 \equiv (2B_{L2} + 1),$$

$$A = \frac{3C_{L2}\delta^2 a_m^2}{8(2B_{L2} + 1)},$$

and

$$B = \frac{3C_{L2}\delta^2 a_m^2}{8(2B_{L2} + 1)(4\gamma - 1)}.$$

After the cable has been fully extended ($t \geq t_1$), Equation 7.75 becomes

$$\ddot{\epsilon} - (2B_{L2} + 1)\epsilon + \frac{3}{4}C_{L2}a_m^2(1 - \delta^2) = 0. \tag{7.78}$$

The solution of Equation 7.78 is

$$\epsilon(t) = \left[\epsilon(t_1) - A'\right] \cosh k'(t - t_1) + \frac{\dot{\epsilon}(t_1)}{k'} \sinh k'(t - t_1) + A', \tag{7.79}$$

where

$$A' = \frac{3C_{L2}a_m^2(1 - \delta^2)}{4(2B_{L2} + 1)}.$$

The maximum allowable initial conditions $[\epsilon(0), \dot{\epsilon}(0)]$ are determined by assuming that, at some time t_2

$$\dot{\epsilon}(t_2) = 0$$

and

$$\epsilon(t_2) = a_m - a_i \cong \frac{3C_{L2}a_m^2(1 - \delta^2)}{4(2B_{L2} + 1)} = A'. \tag{7.80}$$

Using Equation 7.80 in Equation 7.79, it is readily deduced that

$$\tanh k'(t_2 - t_1) = \frac{\dot{\epsilon}(t_1)}{k'\left[A' - \epsilon(t_1)\right]} = 1. \tag{7.81}$$

Finally, with the aid of Equations 7.74, 7.77, and 7.81, it is found that

$$\epsilon(0) + \frac{\dot{\epsilon}(0)}{\sqrt{2B_{L2} + 1}} = \frac{3C_{L2}a_m^2}{8(2B_{L2} + 1)} G(\gamma, \delta), \tag{7.82}$$

where

$$G(\gamma, \delta) = e^{-k't_1}\left[(2 - \delta^2) + \frac{\delta^2}{(4\gamma - 1)}(\cosh 2kt_1 + 2\sqrt{\gamma} \sinh 2kt_1)\right] - \frac{4\gamma\delta^2}{(4\gamma - 1)}. \tag{7.83}$$

When $\dot{\epsilon}(0) = 0$, the ratio $\epsilon(0)/\epsilon(t_2)$ may also be of some interest. From Equations 7.80 and 7.82, this can be written as

$$\frac{\epsilon(0)}{\epsilon(t_2)} = \frac{G(\gamma, \delta)}{2(1 - \delta^2)}. \tag{7.84}$$

Graphs of $G(\gamma, \delta)$ and $\epsilon(0)/\epsilon(t_2)$ are given in Figures 7.5 and 7.6, respectively.

From Equation 7.82 and Figure 7.5, it can be seen that the allowable initial conditions are maximized by choosing $\gamma = 1$, $\delta \cong 0.55$, and letting a_m become very large. However, other factors call for small values of a_m and γ and larger values of δ.* These tradeoffs are not investigated here.

As an example, consider a cable-connected satellite at the Earth-Moon L_2 point. For $\gamma = 0.50$, $\delta = 0.8$, and $a_m = 10^{-2} = 3844.05$ km, it is found that $G(\gamma, \delta) \cong 0.375$, $a_i = 3075.24$ km, and $\alpha_i = 39.61$ km. If $\dot{\epsilon}(0) = 0$, $\epsilon(0) = 11.60$ km, and $\epsilon(t_2) = 22.28$ km. If $\epsilon(0) = 0$, $\dot{\epsilon}(0) = 0.0839$ m/sec. Although this cable is rather long, significant reductions of the cable's length will require high measurement accuracy; e.g., $\epsilon(0) = 0.725$ km for $a_m = 961.01$ km.

2. Structural Comments

The structural aspects of extremely long, cable-connected satellites have received some attention in the literature (References 82 and 83). In Reference 83, the mechanical design of a device that would vary the length of the cable has also been considered. These studies have indicated that similar design problems for the cable-connected satellite proposed in this chapter would not be insurmountable.

To provide some idea of the magnitudes of the structural parameters for a cable-connected

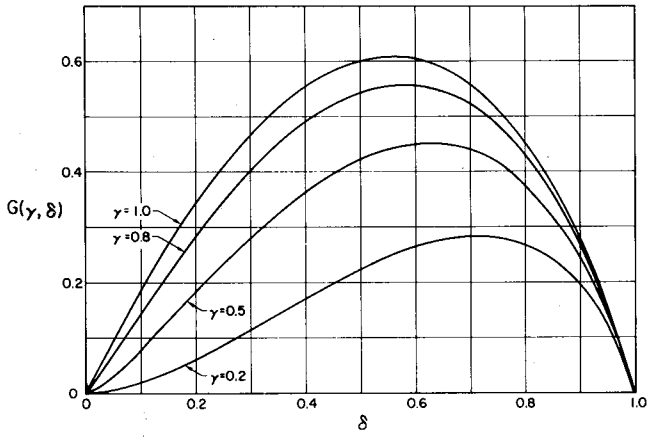

Figure 7.5–The function $G(\gamma, \delta)$.

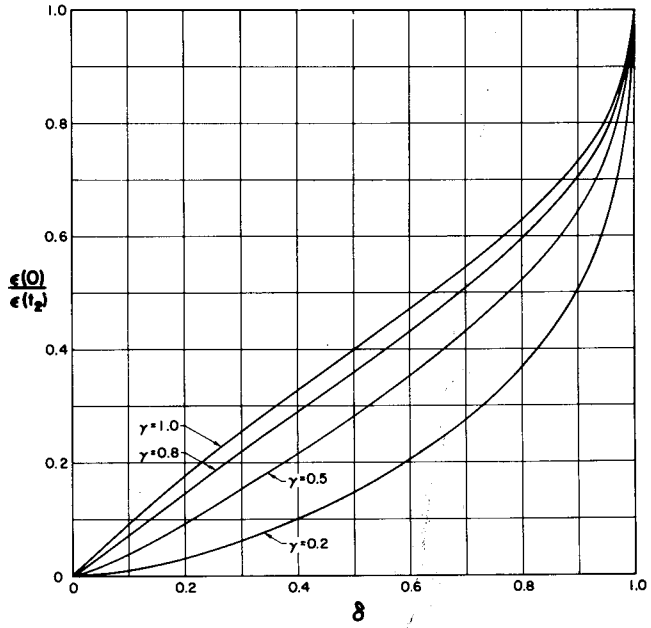

Figure 7.6–Mass center displacement ratio $\epsilon(0)/\epsilon(t_2)$ $[\dot{\epsilon}(0) = \dot{\epsilon}(t_2) = 0]$.

*One of these factors is the impulsive deceleration that takes place when the cable reaches its maximum length at $t = t_1$. From Equations 7.73 and 7.74, this impulsive deceleration is given by $\Delta\dot{x}_2(t_1) = \frac{1}{2}a_m[\gamma(2B_{L2}+1)(1 - \delta^2)]^{1/2}$. In actual practice, the deceleration will be distributed over a finite time interval that is determined by the maximum tensile strength of the cable. This deceleration period is neglected in the analysis presented in this section.

satellite at the Earth-Moon L_2 point, a few representative calculations are presented here. For the purposes of this calculation, it is assumed that

(1) $m = 10\,000$ kg.

(2) The cable is an aluminum wire (modulus of elasticity $\equiv E_{Al} = 1.03 \times 10^7$ psi, density $\equiv \rho_{Al} = 2.70$ gm/cm^3, and ultimate tensile strength $\equiv \sigma_{Al} = 30\,000$ psi).

(3) The nominal length of the cable is $\ell = 3844.05$ km.

(4) The cable tension is never greater than 10 times its nominal value.

With these assumptions, a few elementary calculations give*

$$T_{nom} \cong m(2B_{L2} + 1)\frac{\ell}{2} = 1.005 \times 10^5 \text{ dynes} \quad \text{(nominal cable tension)},$$

$$\sigma_{des} = \frac{\sigma_{Al}}{10} = 3000 \text{ psi} \quad \text{(design stress)},$$

$$d_c = 6.22 \times 10^{-3} \text{ cm} \quad \text{(cable diameter)},$$

and

$$m_c = 504.15 \text{ kg} \quad \text{(mass of cable)}.$$

*It has been suggested to the author that the time delay, due to the finite propagation speed of a longitudinal wave in the cable, could be troublesome. However, the propagation speed is just $\sqrt{E_{Al}/\rho_{Al}} = 5.12$ km/sec, which corresponds to a time delay of $t_d = 12.5$ minutes for a cable length of $\ell = 3844.05$ km. This time delay is clearly negligible.

CHAPTER VIII

APPLICATIONS

In this chapter, a number of possible applications for libration-point satellites are presented. Some of these proposals are original, while others are derived from previous suggestions. It is not the author's intention to present an all-inclusive list, but rather to give some indication of the usefulness of libration-point satellites.

A. Supporting Role for Lunar and Planetary Missions

1. Utilization of the Earth-Moon Collinear Points in Future Lunar Operations

Lunar communications

In the post-Apollo period, with the advent of semipermanent lunar bases and far-ranging surface vehicles, a capability for real-time communications between widely separated lunar terminals will be needed. For bases located on the far side of the Moon, an uninterrupted communications link with the Earth would also be desirable. In this section, it will be shown how these communications requirements can be satisfied by stationing relay satellites in the vicinity of the collinear libration points of the Earth-Moon system.

The possible use of libration-point satellites for communication between points on the lunar surface was first mentioned by Arthur C. Clarke (Reference 9) as early as 1950. However, it has been only recently that methods for using a *single* libration-point satellite to establish a communications link between the Earth and the far side of the Moon have been devised. Two of these methods, the "Lissajou orbit" and "halo orbit" concepts, were originally proposed by the present author in Reference 7. Another technique, the "hummingbird" concept, has been presented by Vonbun (Reference 18). A comparison of these methods is given below.

Lissajou orbit concept. Consider a satellite that is following a quasi-periodic orbit about the Earth-Moon L_2 point. Neglecting higher order corrections, the equations of the orbit are (see Chapter III)

$$x_n \cong A_{x1} \sin \omega_n t$$

and

$$y_n \cong A_{y1} \cos \omega_n t, \tag{8.1}$$

where $A_{x1} = kA_{y1}$, $k = 0.343336$, and $\omega_n = 1.86265$. The geometry for this orbit is given in Figure 8.1. If the satellite is simultaneously executing an out-of-plane oscillation, then (cf. Equation 3.29)

$$z_n = A_{z1} \cos(\omega_z t + \alpha_0), \tag{8.2}$$

where $\omega_z = 1.78618$ and α_0 is the initial phase angle. The trajectory of the satellite as seen from the Earth is just a Lissajou curve, and is depicted in Figure 8.2. Because the frequency difference between the periodic orbit and the z-axis oscillation is very small, the trajectory in Figure 8.2 can be viewed as a slowly changing elliptical path.

To set up an efficient communications link between the Earth and the far side of the Moon, the satellite should perform oscillations that are large enough to be visible from any point on the Earth facing the Moon (see Figure 8.3). Neglecting the small correction for A_{x1}, the radius of the occulted zone for Earth visibility is

$$A_{M\oplus} \cong \gamma_{L2}(R_\oplus + R_\leftmoon) + R_\leftmoon = 3099 \text{ km}, \tag{8.3}$$

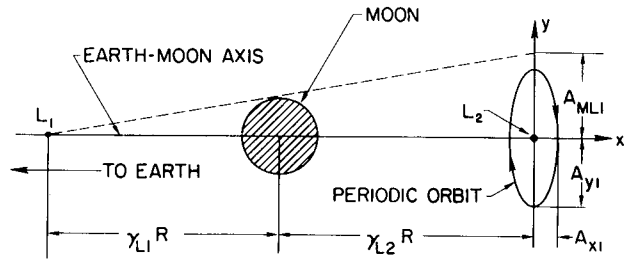

Figure 8.1–Geometry in the Moon's orbital plane. Not to scale.

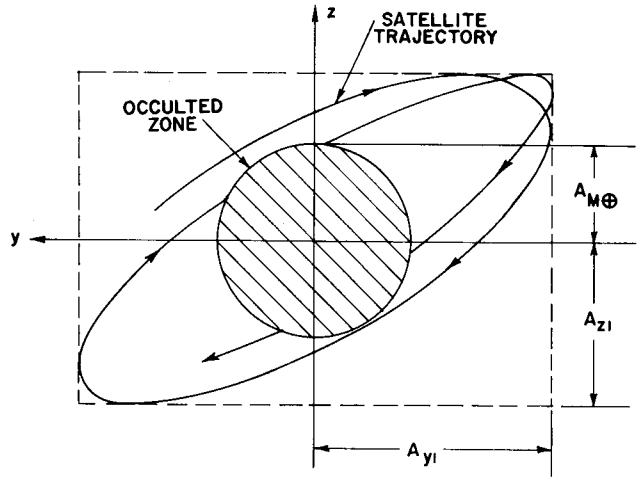

Figure 8.2–Satellite trajectory about the L_2 point as seen from the Earth. Not to scale.

where $R_\oplus = 6371$ km and $R_\leftmoon = 1738$ km (Reference 28). Slightly larger oscillations by the satellite near the L_2 point will enable it to obtain line-of-sight contact with the L_1 point as well as the Earth. By augmenting the oscillating satellite with a second satellite stationed at the L_1 point, a surface-to-surface communications link between the near and far sides of the Moon could be established. (This possibility was originally discussed by the present author in Reference 16.) Using Figure 8.1, it is easy to see that the radius of the occulted zone for this case is

$$A_{ML1} \cong \frac{\gamma_{L1} + \gamma_{L2}}{\gamma_{L1}} R_\leftmoon = 3671 \text{ km}. \tag{8.4}$$

Unfortunately, the oscillating satellite will still enter the occulted zone at periodic intervals. The fraction of the total time that the satellite will be hidden is approximately (using Equations 8.1 and 8.2 and Figure 8.2)

$$\tau_{yz} = \frac{4}{\pi^2} \sin^{-1}\left(\frac{A_M}{A_{y1}}\right) \sin^{-1}\left(\frac{A_M}{A_{z1}}\right). \tag{8.5}$$

For $A_{M\oplus} = 3099$ km and $A_{y1} = A_{z1} = 0.02 = 7688$ km, this fraction is only $\tau_{yz} \cong 0.070$, i.e., 7% of total time. However, occultation periods as long as

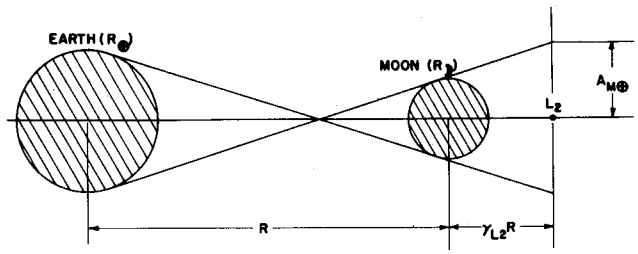

Figure 8.3–Geometry for Earth visibility. Not to scale.

$t_y = (2/\omega_n) \sin^{-1} (A_{M\oplus}/A_{y1}) \cong 1.94$ days will occur periodically. Because this time is rather long, some means for completely eliminating this occultation would be useful.

The satellite's motion relative to the quasi-periodic orbit can be controlled by any of the methods discussed in Chapters IV to VI. If the radial-axis control of Figure 5.1 is employed, the station-keeping cost could be as low as $|\overline{F_{cx}}| = 8.86 \times 10^{-9} g$ (see Section A.1 of Chapter V). Of course, this low cost can only be realized when higher order corrections are included in the nominal path calculation (see Chapter III).

Phase-jump control is one method to prevent occultation of the satellite oscillating about L_2. Whenever the satellite is about to enter the occulted zone, a control pulse is applied to alter the phase angle, but not the amplitude, of the z-axis oscillation so that the portion of the trajectory that passes through the occulted zone is bypassed. This change in phase angle is accomplished by impulsively reversing the direction of $\dot{z}$ without changing its magnitude (see Figure 8.4). From Equations 8.1 and 8.2, the parametric equations for the trajectory shown in Figure 8.2 can be written as

$$y_n = A_{y1} \cos \omega_n t$$

and (8.6)

$$z_n = A_{z1} \cos (\omega_n t + \alpha),$$

where $\alpha \equiv \alpha_0 - \epsilon t$ and $\epsilon \equiv \omega_n - \omega_z = 0.07647$. Since ϵ is small, the phase angle α will be approximated by an average value through one cycle. If α_c is the phase angle for the cycle that just misses the occulted zone, the magnitude of the control impulse is (see Figure 8.4)

$$|\Delta \dot{z}_n| = 2\omega_n A_{z1} \sin \alpha_c, \tag{8.7}$$

and since pulses must be imparted at intervals of

$$\Delta t = \frac{\pi - 2\alpha_c}{\epsilon}, \tag{8.8}$$

the average control acceleration is given by

$$|\overline{F_{cz}}| = \frac{2\epsilon\omega_n A_{z1} \sin \alpha_c}{\pi - 2\alpha_c}. \tag{8.9}$$

It follows from Equation 8.6 and the geometry of Figure 8.2 that

$$2r^2 = \left(A_{y1}^2 + A_{z1}^2\right) + \left(A_{y1}^2 + A_{z1}^2 \cos 2\alpha\right) \cos 2\omega_n t - \left(A_{z1}^2 \sin 2\alpha\right) \sin 2\omega_n t, \tag{8.10}$$

where r is the radial distance from the origin to the satellite. For a trajectory that just touches the occulted zone

$$2A_M^2 = \left(A_{y1}^2 + A_{z1}^2\right) - \left[\left(A_{y1}^2 + A_{z1}^2 \cos 2a_c\right)^2 + \left(A_{z1}^2 \sin 2a_c\right)^2\right]^{1/2} \tag{8.11}$$

$$\frac{A_{z1}}{A_M} = \left[\frac{\lambda^2 - 1}{\lambda^2 \sin^2 a_c - 1}\right]^{1/2}, \tag{8.12}$$

where $\lambda \equiv (A_{y1}/A_M)$. Substitution of Equation 8.12 into Equation 8.9 yields

$$|\overline{F_{cz}}| = 2\epsilon\omega_n A_M f(\lambda, a_c), \tag{8.13}$$

where

$$f(\lambda, a_c) \equiv \frac{\left(\lambda^2 - 1\right)^{1/2} \sin a_c}{\left(\pi - 2a_c\right)\left(\lambda^2 \sin^2 a_c - 1\right)^{1/2}}. \tag{8.14}$$

For a fixed value of λ, there exists a unique value of a_c, which minimizes the average control acceleration. An elementary analysis shows that this optimum value must satisfy the transcendental equation

$$2\left(\lambda^2 \sin^2 a_c - 1\right) \tan a_c = \pi - 2a_c . \tag{8.15}$$

The phase angle satisfying Equation 8.15 is given in Figure 8.5 as a function of λ.

Up to now, the higher order corrections to the trajectory of Equation 8.6 have been neglected. When these corrections are superimposed on the approximate trajectory, the occultation geometry will become more complicated. A simple way (possibly not the most efficient) to account for this complication is to define a new value of A_M (denoted by A'_M) in such a way that the true trajectory will not enter the original occulted zone so long as the approximate trajectory does not enter an occulted zone of radius A'_M.

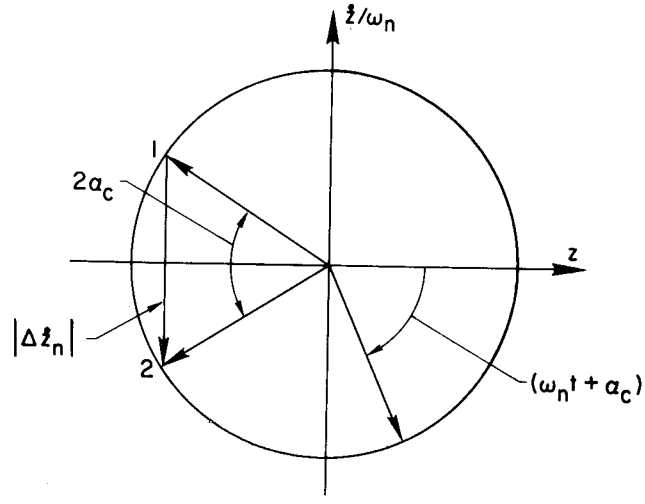

Figure 8.4–Phase plane representation of the control impulse.

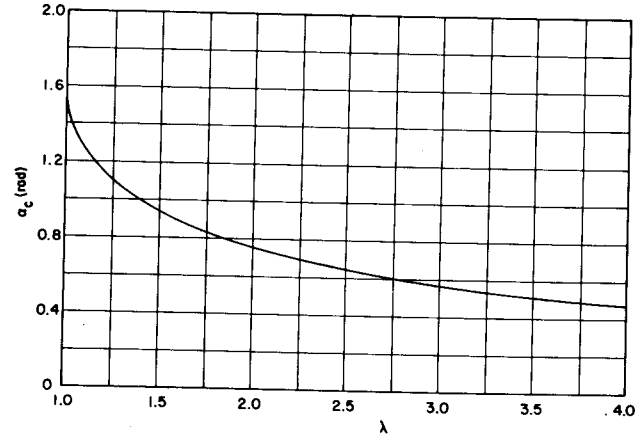

Figure 8.5–Optimum phase angle.

In Chapter III, it was found that the amplitude corrections caused by the lunar eccentricity were much larger than those from other effects. Therefore, amplitude corrections from effects other than the lunar eccentricity will be neglected here. Using the results of Chapter III, A'_M is taken as*

$$A'_M = A_M + \beta A_{y1} = \frac{A_M}{1 - \beta\lambda'}, \tag{8.16}$$

where $\lambda' \equiv (A_{y1}/A'_M)$ and $\beta \cong 0.17$. Replacing A_M in Equation 8.13 by A'_M from Equation 8.16 gives

$$|\overline{F_{cz}}| = 2\epsilon\omega_n A_M \frac{f(\lambda', \alpha_c)}{1 - \beta\lambda'} \equiv 2\epsilon\omega_n A_M g(\lambda', \alpha_c, \beta). \tag{8.17}$$

The function $g(\lambda', \alpha_c, \beta)$ for optimum values of α_c is plotted in Figure 8.6 as a function of λ'. For $\beta = 0.17$, a nearly optimum value of $g(\lambda', \alpha_c, \beta)$ is obtained by taking $\lambda' = 2$. With $A_{M\oplus} = 3099$ km, it is found that

$$A'_{M\oplus} = 4695 \text{ km}, \qquad \alpha_c = 43.17°,$$

$$A_{y1} = 9391 \text{ km}, \qquad A_{z1} = 8708 \text{ km},$$

$$\Delta t = 93.04 \text{ days}, \qquad |\Delta\dot{z}_n| = 59.08 \text{ m/sec},$$

and

$$|\overline{F_{cz}}| = 7.50 \times 10^{-7} g.$$

Halo orbit concept. Occultation of the satellite oscillating about L_2 can also be averted by using a frequency control technique. In this scheme, a single-axis control is used to synchronize the fundamental y-axis and z-axis oscillations. In other words, if higher order trajectory corrections are neglected, the control will produce a closed elliptical path in the yz-plane that always avoids the occulted zone. Although frequency control can be applied in any axis, the cost will be different for each case. Minimum costs for three important cases are given below. As in the previous section, the effect of the eccentricity correction is included by using A'_M for the radius of the occulted zone.

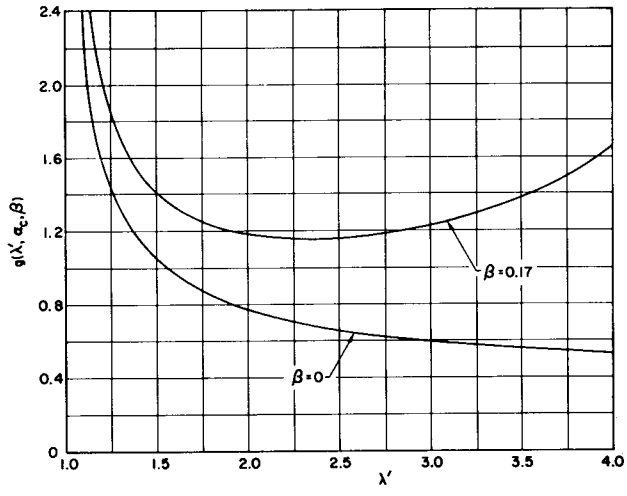

Figure 8.6–The function $g(\lambda', \alpha_c, \beta)$ for optimum values of α_c.

The frequency control method is most easily understood by examining the case where z-axis control is employed. In this case, it is assumed that the approximate satellite orbit in the xy-plane is given by Equation 8.1 with $A_{y1} \geq A'_M$. The z-axis control is used to force the satellite to follow the path

*The eccentricity correction for the z-axis oscillation is given in Appendix B. For this case, $A'_M = A_M + \beta A_{z1}$, where $\beta \cong 0.16$.

$$z_n = A'_M \cos \omega_n t, \tag{8.18}$$

(i.e., a feedback control is used to zero the coordinate ζ, where $\zeta = z - z_n$). The cost for the frequency change is given by $|\overline{F_{cz}}|$, where $F_{cz} = K_{cz} \cos \omega_n t$.* Because

$$\ddot{z}_n + B_{L2} z_n = F_{cz} = K_{cz} \cos \omega_n t, \tag{8.19}$$

it is easy to show that

$$K_{cz} = \left(\omega_n^2 - B_{L2}\right) A'_M = \left(\omega_n^2 - B_{L2}\right) \frac{A_M}{1 - \beta} \tag{8.20}$$

($\beta \cong 0.16$ for the z-axis). Therefore, the average control acceleration is

$$|\overline{F_{cz}}| = \left(\frac{2}{\pi}\right) K_{cz} = 0.2115\ A_M. \tag{8.21}$$

Similarly, for a y-axis control, $F_{cy} = K_{cy} \cos \omega_z t$, and it is found that (using Equations 3.10 to 3.12)

$$|\overline{F_{cy}}| = 0.1589\ A_M. \tag{8.22}$$

With y-axis frequency control, $|A_{x1}/A_{y1}| = 0.3379$ ($|A_{x1}/A_{y1}| = 0.3433$ for the natural oscillatory mode).

For an x-axis control, $F_{cx} = K_{cx} \cos \omega_z t$, and a simple calculation gives

$$|\overline{F_{cx}}| = 0.4703\ A_M, \tag{8.23}$$

with $|A_{x1}/A_{y1}| = 0.2799$.

Taking $A_{M\oplus} = 3099$ km, Equations 8.21 to 8.23 yield

$$|\overline{F_{cz}}| = 4.73 \times 10^{-7} g,$$

$$|\overline{F_{cy}}| = 3.56 \times 10^{-7} g,$$

and

$$|\overline{F_{cx}}| = 1.05 \times 10^{-6} g.$$

Hummingbird concept. In both of the concepts presented above, an "orbiting" satellite was used to set up a communications link between the Earth and the far side of the Moon. However, this communications link can also be obtained by using a satellite that is permanently displaced to one side of the Earth-Moon L_2 point. In this case, a continuous thrust control is needed to station the communications satellite at the nonequilibrium position. The control acceleration can be minimized by displacing the satellite along the y-axis, and is approximately (see Equation 5.22 and Figure 5.4)

*It is assumed here that noise inputs are negligible (see Section A.2 of Chapter V).

$$|\mathbf{F}_c| \cong |F_{cy}| \cong (B_{L2} - 1)\delta_y = 2.1904\ \delta_y. \tag{8.24}$$

When $\delta_y = A_{M\oplus} = 3099$ km, Equation 8.24 gives $|\mathbf{F}_c| = 4.90 \times 10^{-6} g$.

Although the displaced satellite would be stationary with respect to the libration point, its distance to the Moon would vary periodically because of lunar eccentricity. Of course, a constant distance between the satellite and the Moon could be maintained by simply canceling the eccentricity effect with additional thrust control. A rough calculation shows that the average control acceleration for this task would be about $|\overline{\mathbf{F}_c}| \cong 1.20 \times 10^{-5} g$.

Comparison of different techniques. It is clear that, of the three procedures considered above, the halo orbit concept with y-axis control is the most economical method for maintaining a *continuous* Earth-to-lunar far-side communications link. However, the cost for the halo orbit concept with z-axis control is only slightly higher, and other factors may influence the choice between the y-axis and z-axis controls. The cost for the halo orbit concept, with either y-axis or z-axis control, is lower than the cost for the hummingbird concept by an order of magnitude.

If occasional occultation periods can be tolerated, the Lissajou orbit concept should be considered. Uninterrupted communications would still be possible for intervals of about 3 months, and the station-keeping cost could be reduced by an order of magnitude. (This is two orders of magnitude below the cost for the hummingbird concept.) For emergency situations, when longer continuous communication intervals are required, the phase-jump control technique could be employed.

Concluding remarks. Methods for using a single libration-point satellite to obtain continuous communications between the Earth and the far side of the Moon have been presented. The possibility of using two libration-point satellites (one oscillating about the L_2 point while the other is stationed at L_1) to establish a point-to-point communication link covering most of the lunar surface has also been mentioned. The libration-point communication system would be useful during the early lunar exploration period, but its full potential will probably not be realized until more advanced lunar surface operations are carried out. For these more advanced missions, the libration-point network could also function as a navigation and control center for manned and unmanned surface vehicles.

Other proposals (References 84 to 86) for obtaining Earth-to-lunar far-side and long-range lunar surface-to-surface communication have recommended the use of relay satellites in lunar orbit. However, orbiting relay satellites have several obvious disadvantages. Some of these disadvantages are

(1) Many satellites are needed for adequate coverage.

(2) Tracking and acquisition problems are difficult. (These problems are considerably easier with libration-point satellites, because these satellites are almost stationary with respect to the lunar surface.)

(3) The contact time for any given satellite is relatively short, and frequent switchovers are necessary.

(4) The diverse antenna pointing requirements (satellite to Earth, satellite to lunar surface, and satellite to satellite) would complicate the attitude control problem.

Although orbiting satellites possess some advantages over libration-point satellites (e.g., communication distances are shorter and station keeping is usually not required), they do not appear to outweigh the disadvantages listed above. A recent investigation by Schmid (Reference 87) has also expressed a preference for the libration-point satellite technique. In Schmid's study, a quantitative comparison of lunar far-side communication requirements (power, beamwidth, antenna gain, bit rate, etc.) for a libration-point satellite and a 1000-km altitude satellite in a circular lunar orbit is presented.

Rendezvous technique

Present plans for the Apollo lunar landing mission call for the insertion of the combined spacecraft [command module (CM) and lunar landing vehicle (LLV)] into a low lunar orbit. The LLV will then descend to the lunar surface, stay there for 1 to 2 days, ascend to the lunar parking orbit, and rendezvous with the CM. The CM will then return to the Earth.

An alternate method uses the Earth-Moon L_1 point for a rendezvous instead of a lunar parking orbit. Although this rendezvous scheme has been examined by a number of people since 1960, the first published work was presented by Raithel (Reference 12) in 1966. Because the libration-point rendezvous method has several attractive advantages over the lunar orbit rendezvous method, a few comments are in order.

In Figure 8.7, two transfer trajectories between an Earth parking orbit and the L_1 point are illustrated. A direct transfer (trajectory #1) uses two impulses, while an indirect transfer (trajectory #2) employs a third impulse at the closest approach to the Moon. In both cases, the velocity increment (ΔV) at the Earth parking orbit is approximately equal to the ΔV that is required for escape velocity. A digital computer simulation is needed to obtain the remaining ΔV's because a patched-conic approximation is not very accurate for these calculations. Some computer results of Nicholson (Reference 88) are quoted here. For the direct transfer, $\Delta V_{L1} \cong 2350$ fps for a 4-day transit. For the indirect transfer, $\Sigma\Delta V \cong 1900$ fps (the ΔV near the Moon is about 1000 fps, and $\Delta V_{L1} \cong 900$ fps), but the trip time is 6 days. The same ΔV's are required for the reverse trajectories.

A transfer between the L_1 point and the Moon is also shown in Figure 8.7 (trajectory #3). In this transfer, $\Delta V_{L1} \cong 1700$ fps, and the impact velocity at the Moon is about 7790 fps for a 24-hour transit.

For landing sites near the lunar equator or for surface stay times of a few days, the total ΔV requirements for lunar orbit rendezvous are slightly lower than the ΔV requirements for libration-point rendezvous. However, for landings at higher lunar latitudes or longer stay times, rather large plane changes are often necessary, and the ΔV cost for these plane changes is significantly higher if lunar orbit rendezvous is employed (Reference 89). In some instances, this increased ΔV penalty is severe, and large portions of the lunar surface are not accessible with the present Apollo spacecraft. (An even greater restriction on lunar surface accessibility is imposed by requiring a continuous abort capability for the LLV.) On the other hand, the ΔV's for the libration-point rendezvous technique are virtually identical for any

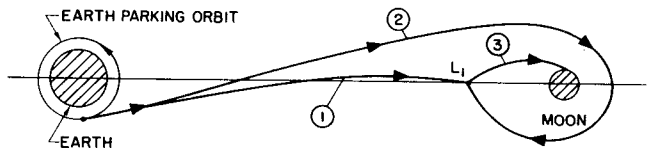

Figure 8.7–Transfer paths to and from the L_1 point in the Moon's orbital plane. Not to scale.

lunar landing site or stay time because the necessary plane changes can be accomplished quite cheaply at the L_1 point. This low-ΔV plane-change capability might very well favor a rendezvous at L_1 for lunar surface missions of long duration or high latitude.

Because the L_1 point is stationary with respect to the lunar surface, the libration-point rendezvous technique also has an important operational advantage, namely, an infinite launch window for the LLV to and from the lunar surface. This timing advantage, along with the low-ΔV plane-change capability, makes the L_1 point an ideal location for a lunar logistics staging depot (or a lunar-surface rescue facility). Supplies could be transported to and from the L_1 point with reusable shuttle vehicles. A low-thrust vehicle could be used between the Earth parking orbit and the L_1 point, but a high-thrust vehicle would be needed for the transfer between the L_1 point and the lunar surface.

From the preceding discussion, it is clear that a comprehensive investigation of the libration-point rendezvous concept is warranted. This investigation should consider several different transfer modes as well as various staging possibilities. The usefulness of the L_2 point for rendezvous should also be examined.

2. An Interplanetary Transportation System With Terminals at the Sun-Planet Collinear Points

A modified version of the libration-point rendezvous technique described above may be useful for planetary missions. Although a large variety of mission profiles with libration-point rendezvous could be contrived, only one possibility is presented here.

Consider a reusable shuttle vehicle that operates between the L_1 point of the Sun-Earth system and the L_2 point of a Sun-planet system. The outbound transfer path for the shuttle vehicle is shown in Figure 8.8; the inbound transfer path is just the mirror image of the outbound transfer path. Either a high- or low-thrust rocket could be used to perform the transfer, but it is quite possible that a hybrid system (high- and low-thrust) would be more efficient. The transfer of the interplanetary shuttle vehicle (ISV) is initiated by applying a small impulse at the Sun-Earth L_1 point and then starting the low-thrust engine. As the ISV passes close to the Earth (point A in Figure 8.8), a much larger impulse is administered. During the heliocentric portion of the transfer, only low thrust is employed. At the closest approach to the planet (point B in Figure 8.8), another large impulse is applied, and a planetary landing vehicle (PLV) is separated from the ISV and lands on the planet.* The ISV then proceeds to the Sun-planet L_2 point where capture is effected by another small impulse. A reverse procedure is used for the inbound transfer.

Additional shuttle vehicles can be used for the transfer of crew members, fuel, and other supplies between the Sun-Earth L_1 point and the Earth. This phase of the mission is similar to the elliptical orbit pickup procedure discussed in Reference 90.

From the ΔV standpoint, the libration-point rendezvous technique probably does not have any significant advantage over the elliptical orbit rendezvous method. However, the increased flexibility in the

*It may be more desirable to separate the PLV earlier or later, depending on the descent mode (atmospheric or propulsive braking), guidance requirements, staging ratios, and safety or other factors.

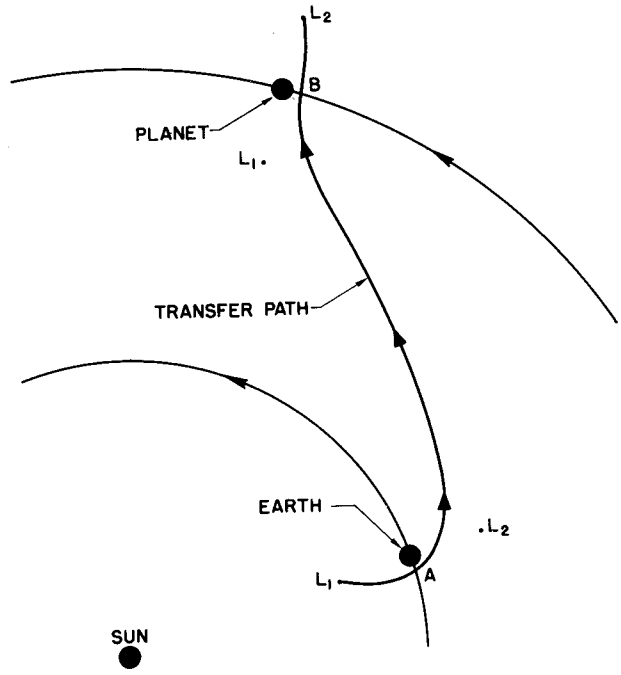

Figure 8.8–Transfer path between the Sun-Earth L_1 point and a Sun-planet L_2 point. Not to scale.

timing of various operations* (e.g., rendezvous, abort, and landing) may justify a quantitative investigation of the libration-point rendezvous concept.

3. Deep Space Communications Using a Relay Satellite at an Earth-Moon Equilateral-Triangle Point

Future deep space missions will require much higher rates of data transmission than have been attained to date. Laser communications systems show considerable promise for furnishing these high data rates (Reference 92). However, to avoid occultations caused by cloud cover and Earth rotation, a relay satellite between the deep space vehicle (DSV) and the Earth-based station will usually be required.† A microwave link is used between the Earth and the relay satellite, while an optical link (laser beam) is used between the relay satellite and the DSV.

The selection of the orbit for the relay satellite is very important, and the tradeoffs involved in this choice are discussed in Reference 93. Although a preference for a synchronous (24-hour) orbit was expressed in Reference 93, the possibility of stationing the relay satellite at an Earth-Moon equilateral-triangle libration point was not considered. It is hoped that the equilateral-triangle points will be considered in future tradeoff studies because these locations seem to possess certain advantages over a synchronous orbit. Some of these advantages are

(1) Less Earth occultation (almost none) of the optical communications link between the relay satellite and the DSV.

(2) The Earth can usually be excluded from the field of view of the communications receiver on the DSV. (The Earth is a strong noise source.)

(3) The maximum relative velocity normal to the line of sight between the relay satellite and the DSV is smaller. Therefore, the pointing requirements for the laser beam are less stringent.

(4) The ΔV cost for the initial placement of the relay satellite is reduced by about 0.5 km/sec (Reference 15).

Of course, the equilateral-triangle points also have some disadvantages when compared with a synchronous orbit (e.g., the path loss for the microwave link is greater), and a complete systems evaluation is needed before a final choice can be made.

*The timing problems associated with orbiting or landing missions to the satellites of Jupiter are particularly involved (Reference 91).

†Occultation could also be avoided by using a large number of Earth stations, but frequent switchovers would be necessary. Because the acquisition of a narrow laser beam is rather difficult, these switchovers would probably result in the loss of some data.

The libration-point communications system could also be used for another purpose. With two relay satellites, one at L_4 and the other at L_5, it would be possible to take advantage of the large separation distance (about 6.66×10^5 km) to establish an interferometric tracking and navigation system with a long baseline (Reference 94). However, because the baseline is rotating with respect to the DSV, it may be advisable to generate two more baselines by placing a third relay satellite at the Earth-Moon L_3 point. (The three baselines would form a triangle.)

B. Scientific Usefulness

1. A Multiple-Satellite System for Monitoring Solar-Induced Phenomena in and Beyond the Earth's Magnetosphere

Since 1957, scientific satellites have collected a large amount of data concerning particles and fields in the Earth's magnetosphere and in the interplanetary medium surrounding it (References 95 to 97). These measurements have led to many impressive discoveries of previously unknown phenomena, but future progress will be largely dependent on the ability to perform simultaneous observations at different locations. Only in this way will it be possible to separate temporal from spatial variations.

Good coverage of cislunar space has already been achieved by using several satellites in highly eccentric Earth orbits. However, beyond the Moon's orbit, the data are usually discrete. To improve this situation, Robinson (Reference 14) has suggested that a satellite should be placed in the Earth's orbit about 6×10^6 mi in front of the Earth (this corresponds to a Sun-Earth isosceles-triangle point at about $\theta \cong 4°$) where it would continuously monitor the interplanetary medium that will be occupied by the Earth 4 days later. Another possibility has been advanced by Meissinger and Greenstadt (Reference 17), who have examined the feasibility of obtaining long-term measurements in the Earth's geomagnetic tail by stationing a satellite in the vicinity of the Sun-Earth L_2 point. These stationary satellites would provide some of the data that are needed to discern the time variation of solar-induced phenomena in the Earth's neighborhood, but more spatial coverage would be desirable.

Symmetrical spatial coverage could be obtained with a network of four satellites, as shown in Figure 8.9. These satellites are stationed at the isosceles-triangle points I_1 and I_2 ($\theta = \pm 2°$)* and the collinear points L_1 and L_2.† When data collected at these points are compared with measurements taken in cislunar space, some interesting correlations may be apparent. It may also be possible to find some correlation with Earth weather data.

Notice that the satellite at the L_1 point could also function as an early warning station for solar flares. Although the warning time would only be about 8 to 25 minutes (average velocities of solar flares are between 1000 and 3000 km/sec), this may be sufficient for some purposes (e.g., a supersonic transport flying at a high altitude could descend to a safer altitude on short notice).

*The value of θ that is given here was chosen somewhat arbitrarily. The optimum choice can be determined only after considering various tradeoffs (station-keeping cost, communications requirements, scientific value, etc.).

†The placement of a second satellite at L_2 distance, but along the nominal direction of the geomagnetic tail, might also be profitable. By analyzing radio signals between this satellite and the satellite at L_2, it may be possible to monitor the electron density in a cross section of the geomagnetic tail. The station-keeping cost for the displaced satellite would be about $|\overline{F_{cy}}| \cong (B_{L2} - 1)\delta_y = 1.25 \times 10^{-6} g$, with $\delta_y = 1.05 \times 10^5$ km.

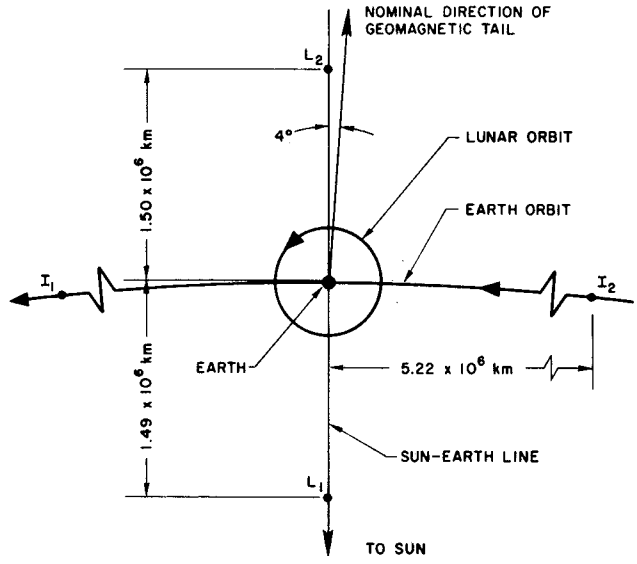

Figure 8.9–Multiple-satellite network. Satellites anchored at L_1, L_2, I_1, and I_2.

The station-keeping costs for the satellites at the isosceles triangle points can be obtained from Figure 2.8. For $\theta = \pm 2°$, the cost is $|\mathbf{F}_c| \cong 1.50 \times 10^{-6} g$. At the collinear points, the costs are negligibly small if DSIF tracking is utilized (see Chapter V).

2. Low-Frequency Radio Astronomy from the Earth-Moon L_2 Point

The low-frequency cutoff for Earth-based radio telescopes is about 10 MHz. This limit could be extended with an Earth-orbiting radio telescope, but it would be extremely difficult to observe frequencies below 1 MHz because the ionosphere of the Earth is a source of low-frequency radio noise. However, a radio telescope located at the Earth-Moon L_2 point would always be shielded from the Earth's ionosphere by the Moon.* Therefore, the Earth-Moon L_2 point may be an ideal location for low-frequency radio astronomy experiments. Of course, possible interference from the geomagnetic tail would not be completely eliminated, but the Earth-Moon L_2 point would remain outside of the tail region for periods of almost 3 weeks.

*The use of the Earth-Moon L_2 point as a site for radio astronomy was originally suggested by Hornby and Allen (Reference 15).

CONCLUSIONS AND RECOMMENDATIONS

The translation control of a satellite in the vicinity of a libration point can be accomplished in a rather simple manner. For instance, at an unstable collinear point, a single-axis control using only range and range-rate measurements is sufficient. Moreover, the station-keeping costs are very low (comparable to costs for synchronous satellite station keeping), and are well within the capability of present satellite translation control systems.

The control system can be mechanized in many ways, and some possibilities were presented in this study. (The author realizes that the engineering difficulties associated with the cable control technique are rather formidable, but the method is intriguing.) The author urges that specific designs of control systems for libration-point satellites be the focal point of future work; these studies should include detailed investigations of propulsion systems and measurement techniques.

The potential usefulness of a libration-point satellite is apparent (see Chapter VIII). Therefore, the early construction and flight testing of a libration-point satellite is strongly recommended. A costly development program may not be necessary because a satisfactory test vehicle could probably be obtained by modifying an Applications Technology Satellite. The Earth-Moon L_1 point might be a convenient location for station-keeping tests, but a lunar far-side communication capability could also be achieved if the tests were conducted in a quasi-periodic orbit around the Earth-Moon L_2 point.

ACKNOWLEDGMENTS

The author wishes to express his gratitude to his advisor, Prof. John V. Breakwell, for his inspirational guidance and continual availability throughout the course of this research. He also wishes to thank Ahmed Kamel for checking some of the mathematics.

Goddard Space Flight Center
National Aeronautics and Space Administration
Greenbelt, Maryland, January 6, 1970
311-07-21-01-51

REFERENCES

1. Szebehely, V., "Theory of Orbits: The Restricted Problem of Three Bodies," New York: Academic Press, Inc., 1967.
2. Steg, L., and De Vries, J. P., "Earth-Moon Libration Points: Theory, Existence and Applications," *Space Sci. Rev.* 5(2): 210–233, March 1966.
3. Colombo, G., "The Stabilization of an Artificial Satellite at the Inferior Conjunction Point of the Earth-Moon System," Smithsonian Astrophysical Observatory Special Report No. 80, November 1961.
4. Dusek, H. M., "Motion in the Vicinity of Libration Points of a Generalized Restricted Three-Body Model." *Progr. Astronaut. Aeronaut.: Methods in Astrodynamics and Celestial Mechanics* 17: 37–54, 1966.
5. Fleming, A. W., "Use of the Properties of Frequency Symmetry and Complex Symmetry in the Control of Linear Dynamical Systems," Stanford Univ. Dept. of Aeronautics and Astronautics SUDAAR-266, 36–44, May 1966.
6. Paul, E. W., and Shapiro, G., "Stabilization of the Lagrangian Solutions of the Three-Body Problem," *Astronaut. Acta* 11(6): 410–417, November–December 1965.
7. Farquhar, R. W., "Station-Keeping in the Vicinity of Collinear Libration Points with an Application to a Lunar Communications Problem," in "AAS Science and Technology Series: Space Flight Mechanics Specialist Symposium. Vol. 11," ed. M. L. Anthony, Tarzana, Calif.: AAS Publications, 1966, 519–535
8. Kononenko, A. F., "Libration Points Approach," Presented at XVIIIth International Astronautical Congress, International Astronautical Federation, September 1967.
9. Clarke, A. C., "Interplanetary Flight," London: Temple Press Books Ltd., 1950.
10. Cross, C. A., "Orbits for an Extra-Terrestrial Observatory," *J. Brit. Interplanet. Soc.* 13(4): 204–207, July 1954.
11. Michael, W. H., Jr., "Considerations of the Motion of a Small Body in the Vicinity of the Vicinity of the Stable Libration Points of the Earth-Moon System," NASA TR R-160, 1963.
12. Raithel, W., "The Role of the Cis-Lunar Libration Point in Lunar Operations" in "Proceedings of 3rd Space Congress," Canaveral Council of Technical Societies, March 1966.
13. Jamison, D., "Uses of the Trojan Libration Points of the Earth-Sun System," *J. Spacecraft Rockets* 3(4): 595–596, April 1966.
14. Robinson, A. I., "An Heliocentric Earth Orbit Precursor Planetoid," RAND Corporation P-3343, April 1966.
15. Hornby, H., and Allen, W. H., "Mission to the Libration Centers," *Astronaut. Aeron.* 4(7): 78–82, July 1966.
16. Farquhar, R. W., "Lunar Communications with Libration-Point Satellites," *J. Spacecraft Rockets* 4(10): 1383–1384, October 1967.

17. Meissinger, H. F., and Greenstadt, E. W., "Use of Electric Propulsion for Exploring the Distant Regions of the Geomagnetic Tail," AIAA Paper 68-120, January 1968.
18. Vonbun, F. O., "A Hummingbird for the L_2 Lunar Libration Point," NASA TN D-4468, April 1968.
19. Moulton, F. R., "An Introduction to Celestial Mechanics," New York: The Macmillan Co., 1914, p. 171.
20. Ovenden, M. W., and Roy, A. E., "On the Use of the Jacobi Integral of the Restricted Three-Body Problem," *Monthly Notices Roy. Astron. Soc.* 123(1): 1–14, 1961.
21. Kopal, Z., and Lyttleton, R. A., "On the Elliptic Case of the Restricted Problem of Three Bodies and the Remote History of the Earth-Moon System," *Icarus* 1: 455–458, 1963.
22. Szebehely, V., and Giacaglia, G. E. O., "On the Elliptic Restricted Problem of Three Bodies," *Astron. J.* 69(3): 230–235, April 1964.
23. De Prit, A., "A Note Concerning the Collinear Libration Centers," *Icarus* 4: 273–278, 1965.
24. Bennett, A., "Characteristic Exponents of the Five Equilibrium Solutions in the Elliptically Restricted Problem," *Icarus* 4: 177–187, 1965.
25. Bennett, A., "Analytical Determination of Characteristic Exponents. " *Progr. Astronaut. Aeronaut.: Methods in Astrodynamics and Celestial Mechanics* 17: 101–113, 1966.
26. Colombo, G., Lautman, D., and Munford, C., "On the Libration Orbits of a Particle Near the Triangular Point in the Semirestricted Three-Body Problem," *Astron. J.* 68(3): 159–162, April 1963.
27. Danby, J. M. A., "Stability of the Triangular Points in the Elliptic Restricted Problem of Three Bodies," *Astron. J.* 69(2): 165–172, March 1964.
28. Blanco, V. M., and McCuskey, S. W., "Basic Physics of the Solar System," Reading, Mass.: Addison-Wesley Publishing Co., Inc., 1961.
29. Makover, S. G., and Bokhan, N. A., "The Motion of Comet Encke-Backlund During 1898–1911 and a New Determination of the Mass of Mercury," *Soviet Phys. Doklady English Trans.* 5(5): 923–925, 1961.
30. Rabe, E., "Corrected Derivation of Astronomical Constants From the Observations of Eros 1926–1945," *Astron. J.* 72(7): 852–855, September 1967.
31. Rabe, E., "The Earth + Moon Mass and Other Astronomical Constants from the Eros Motion 1926–1965," *Astron. J.* 72(7): 856–864, September 1967.
32. Anderson, J. D., and Warner, M. R., "Determination of the Masses of the Moon and Venus, and the Astronomical Unit from the Radio Tracking of Mariner II," in "Trajectories of Artificial Celestial Bodies," ed. J. Kovalevsky, Berlin: Springer-Verlag, 1966, 216–246.
33. Clarke, V. C., Jr., "Constants and Related Data for Use in Trajectory Calculations as Adopted by the Ad Hoc NASA Standards Committee," Jet Propulsion Laboratory TR 32-604, March 6, 1964.
34. Michaux, C. M., "Handbook of the Physical Properties of the Planet Mars," NASA SP-3030, 1967, p. 12.
35. Camichel, H., Hugon, M., and Rösch, J., "Mesure du Diamètre de Mercure par la Méthode de Hertzsprung le 7 Novembre 1960," *Icarus* 3: 410–422, 1964.
36. De Vaucouleurs, G., "Geometric and Photometric Parameters of the Terrestrial Planets," *Icarus* 3: 187–235, 1964.
37. Bullen, K. E., "Implications of the Revised Mars Radius," *Nature* 211: 396, July 23, 1966.
38. Mohn, L., and Kevorkian, J., "Some Limiting Cases of the Restricted Four-Body Problem," *Astron. J.* 72(8): 959–963, October 1967.
39. Brown, E. W., and Shook, C. A., "Planetary Theory," New York: Dover Publications, Inc., 1964, Chapter 9.

40. Cesari, L., "Asymptotic Behavior and Stability Problems in Ordinary Differential Equations," 2nd Ed., Berlin: Springer-Verlag, 1963.
41. Plummer, H. C., "On Oscillating Satellites-1," *Monthly Notices Roy. Astron. Soc.* 63(8): 436–443, 1903.
42. Plummer, H. C., "On Oscillating Satellites-2," *Monthly Notices Roy. Astron. Soc.* 64(2): 98–105, 1903.
43. Acord, J. D., and Nicklas, J. C., "Theoretical and Practical Aspects of Solar Pressure Attitude Control for Interplanetary Spacecraft," *Progr. Astronaut. Aeronaut.: Guidance and Control-II*, 13: 73–101, 1964.
44. Colombo, G., "Sui Satelliti del Sistema Terra-luna," *Rendi. Accad. Naz. Lincei* [8] 28: 169–172, 1960.
45. Nicholson, F. T., "Effect of Solar Perturbation on Motion Near the Collinear Earth-Moon Libration Points," *AIAA J.* 5(12): 2237–2241, December 1967.
46. De Pontecoulant, G., "Theorie Analytique du Système du Monde," vol. 4, Paris: Bachelier, 1846.
47. Brown, E. W., "An Introductory Treatise on the Lunar Theory," New York: Dover Publications, Inc., 1960.
48. De Vries, J. P., "The Sun's Perturbing Effect on Motion Near a Triangular Lagrange Point," Proceedings of XIIIth International Astronautical Congress, 1962, New York: Springer-Verlag, 1964, pp. 432–450.
49. Tapley, B. D., and Lewallen, J. M., "Solar Influence on Satellite Motion Near the Stable Earth-Moon Libration Points," *AIAA J.* 2(4): 728–732, April 1964.
50. Schechter, H. B., and Hollis, W. C., "Stability of the Trojan Points in the Four-Body Problem," RAND Corporation RM-3992-PR, September 1964.
51. Breakwell, J. V., and Pringle, R., Jr., "Resonances Affecting Motion Near the Earth-Moon Equilateral Libration Points." *Progr. Astronaut. Aeronaut.: Methods in Astrodynamics and Celestial Mechanics* 17: 55–74, 1966.
52. Wolaver, L. E., "Effect of Initial Configurations on Libration Point Motion." *Progr. Astronaut. Aeronaut.: Methods in Astrodynamics and Celestial Mechanics* 17: 75–99, 1966.
53. Tapley, B. D., and Schutz, B. E., "Further Results on Solar Influenced Libration Point Motion," *AIAA J.* 3(10): 1954–1956, October 1965.
54. Schechter, H. B., "Three-Dimensional Nonlinear Stability Analysis of the Sun-Perturbed Earth-Moon Equilateral Points," AIAA Paper 67-566, August 1967.
55. Kolenkiewicz, R., and Carpenter, L., "Stable Periodic Orbits About the Sun-Perturbed Earth-Moon Triangular Points," NASA Goddard Space Flight Center X-643-67-484, October 1967.
56. Kaplan, W., "Operational Methods for Linear Systems," Reading, Mass.: Addison-Wesley Publishing Co., Inc., 1962, Chapter 7.
57. Elgerd, O. I., "Control Systems Theory," New York: McGraw-Hill Book Co., Inc., 1967.
58. Hale, J. K., "Oscillations in Nonlinear Systems," New York: McGraw-Hill Book Co., Inc., 1963.
59. Boucher, R. A., "Electrical Propulsion for Control of Stationary Satellites," *J. Spacecraft Rockets* 1(2): 164–169, March–April 1964.
60. Molitor, J. H., "Ion Propulsion System for Stationary-Satellite Control," *J. Spacecraft Rockets* 1(2): 170–175, March–April 1964.

61. Toms, R. S. H., and Kalensher, B. E., "Control of a Synchronous Satellite by Continuous Radial Thrust," *AIAA J.* 2(7): 1179-1188, July 1964.
62. Neufeld, M. J., "Orbit Correction," *Space/Aeronautics* 43(2): 48-55, February 1965.
63. Neufeld, M. J., and Anzel, B. M., "Synchronous Satellite Station-Keeping." *Progr. Astronaut. Aeronaut.: Communication Satellite Systems Technology* 19: 323-346, 1966.
64. Greene, R. H., "Early Bird Placement in a Stationary Orbit: Launch and Control System Maneuvers." *Progr. Astronaut. Aeronaut.: Communication Satellite Systems Technology* 19: 9-42, 1966.
65. Balsam, R. E., and Dunin, S. E., "Orbit Determination for Stationary Satellites," in "AAS Science and Technology Series: Space Flight Mechanics Specialist Symposium. Vol. 11," ed. M. L. Anthony, Tarzana, Calif.: AAS Publications, 1966, 123-136.
66. Balsam, R. E., and Anzel, B. M., "Determination of the Pacific Equilibrium Point for a Stationary Orbit," *J. Spacecraft Rockets* 4(10): 1289-1294, October 1967.
67. Newton, G. C., Jr., Gould, L. A., and Kaiser, J. F., "Analytical Design of Linear Feedback Controls," New York: John Wiley & Sons, Inc., 1957.
68. Rosenbrock, H. H., "An Automatic Method for Finding the Greatest or Least Value of a Function," *Computer Journal* 3: 175-184, 1960.
69. Sjogren, W. J., Trask, D. W., Vegos, C. J., and Wollenhaupt, W. R., "Physical Constants as Determined From Radio Tracking of the Ranger Lunar Probes," in "AAS Science and Technology Series: Space Flight Mechanics Specialist Symposium. Vol. 11," ed. M. L. Anthony, Tarzana, Calif.: AAS Publications, 1966, 137-154.
70. Bowers, E. J., Taylor, R. L., Thompson, E. H., and Knight, J. W., "Study of Basic Requirements for a Navigation, Guidance, and Control System for an Unmanned Lunar Landing Vehicle," NASA CR-61118, December 1965.
71. Lowry, J. H., "Electromagnetic Guidance Study," NASA CR-865, September 1967.
72. Abramowitz, M., and Stegun, I. A., eds., "Handbook of Mathematical Functions," Washington, D. C.: U. S. Government Printing Office, 1964.
73. Peschon, J., and Smets, H. B., "Nonlinear Control Systems: Selected Topics," in "Disciplines and Techniques of Systems Control," ed. J. Peschon, New York: Blaisdell Publishing Co.,1965, 187-266.
74. Siljak, D. D., "Analysis of Asymmetrical Nonlinear Oscillations in the Parameter Plane," *IEEE Trans. Auto. Control* 11(2): 239-247, April 1966.
75. Zypkin, Ja. S., (Ya. Z. Tsypkin), "Theorie der Relaissysteme der Automatischen Regelung," Munich: R. Oldenbourg-Verlag, 1958.
76. Gille, J. C., Pelegr[illegible] M. J., and Decaulne, P., "Feedback Control Systems," New York: McGraw-Hill Book Co., Inc., 1959. Chapter 26.
77. Korolev, N. A., "Periodic Modes in Relay Systems Containing Internal Feedback," *Automation and Remote Control* 17: 1083-1094, November 1956.
78. Mangulis, V., "Handbook of Series for Scientists and Engineers," New York: Academic Press, Inc., 1965, p. 80.
79. Kuo, B. C., "Analysis and Synthesis of Sampled-Data Control Systems," Englewood Cliffs, N. J.: Prentice-Hall, Inc., 1963.

80. Frye, W. E., and Stearns, E. V. B., "Stabilization and Attitude Control of Satellite Vehicles," *ARS J.* 29(12): 927–931, December 1959.
81. Gurko, O. V., and Slabkii, L. I., "The Use of Forces Derived From the Solar Gravitational and Radiation Fields for the Orientation of Cosmic Devices," *Artificial Earth Satellites* 16: 30–41, March 1964.
82. Sutton, G. W., and Diederich, F. W., "Synchronous Rotation of a Satellite at Less Than Synchronous Altitude," *AIAA J.* 5(4): 813–815, April 1967.
83. Taylor, G. E., and Hunter, J. R., "Structural Design and Operation of a Large Radio Astronomy Antenna," AIAA Paper 68-348, April 1968.
84. Nigam, R. C., and Kit, B. V., "Some Astrodynamical Aspects of Lunar Communications Using Satellites," Proceedings of XVIth International Astronautical Congress. Paris: Gauthier-Villars, 1966, 95–117.
85. Neuner, G. E., "Lunar Communication Satellites." *Progr. Astronaut. Aeronaut.: Communication Satellite Systems Technology* 19: 887–908, 1966.
86. Marinaccio, R. E., and Cavey, R. R., "Techniques for Lunar Surface Communications," *Microwave J.* 10(11): 51–57, October 1967.
87. Schmid, P. E., "Lunar Far-Side Communication Satellites," NASA TN D-4509, June 1968.
88. Nicholson, F. T., "Vehicle Motion Near the L_1 Earth-Moon Libration Point," General Electric Missile and Space Division PIR-4T43-006, June 1966.
89. Penzo, P. A., and Johnson, R. W., "The Extended Stay Lunar Exploration Mission," in "Advances in the Astronautical Sciences: Post Apollo Space Exploration. Vol. 20, part 2," ed. F. Narin, Tarzana, Calif.: AAS Publications, 1966, 1027–1060.
90. Luidens, R. W., Burley, R. R., Eisenberg, J. D., Kappraff, J. M., Miller, B. A., Shovlin, M. D., and Willis, E. A., Jr., "Manned Mars Landing Mission by Means of High-Thrust Rockets," NASA TN D-3181, January 1966.
91. Luidens, R. W., and Edgar, J., "Round-Trip Trajectories to Moons of Jupiter," NASA TN D-4167, October 1967.
92. Kalil, F., "Optical and Microwave Communications–A Comparison," NASA TN D-3984 (corrected copy), May 1968.
93. Gubin, S., Marsten, R. B., and Silverman, D., "Lasers vs Microwaves in Space Communications," *J. Spacecraft Rockets* 3(6): 818–827, June 1966.
94. Wheelon, A. D., "Midcourse and Terminal Guidance," in "Space Technology," ed. H. S. Seifert, New York: John Wiley & Sons, Inc., 1959, chap. 26, pp. 18–20.
95. Anon., "Significant Achievements in Particles and Fields 1958-1964," compiled by W. Hess, G. Mead, and M. P. Nakada, NASA SP-97, 1966.
96. Schardt, A. W., and Opp, A. G., "Significant Achievements in Space Science 1965–Particles and Fields," NASA SP-136, 1967, pp. 31–88.
97. Schardt, A. W., and Opp, A. G., "Significant Achievements in Space Science 1966–Particles and Fields," NASA SP-155, 1967, pp. 204–287.

APPENDIX A

DERIVATION OF EQUATION 5.18

Given the Gaussian density function

$$\Phi_{F^*}(x, t) = \frac{1}{\sigma_F \sqrt{2\pi}} \exp \left\{ - \frac{[x - p(t)]^2}{2\sigma_F^2} \right\} \tag{A1}$$

with

$$p(t) = K_c \cos \omega t, \tag{A2}$$

it is required to find the average control acceleration

$$\overline{|F^*_{cx}|} = \frac{\omega}{2\pi} \int_0^{2\pi/\omega} E\left\{ |F^*_{cx}(t)| \right\} dt \tag{A3}$$

where

$$E\left\{ |F^*_{cx}(t)| \right\} = \int_{-\infty}^{+\infty} |x| \Phi_{F^*}(x, t)\, dx = - \int_{-\infty}^{0} x \Phi_{F^*}(x, t)\, dx + \int_0^{+\infty} x \Phi_{F^*}(x, t)\, dx. \tag{A4}$$

With the change of variables

$$y \equiv \frac{x - p(t)}{\sigma_F}, \tag{A5}$$

Equation A4 becomes

$$\begin{aligned} E\left\{ |F^*_{cx}(t)| \right\} &= - \frac{1}{\sqrt{2\pi}} \int_{-\infty}^{-p/\sigma_F} [p + \sigma_F y] e^{-y^2/2}\, dy + \frac{1}{\sqrt{2\pi}} \int_{-p/\sigma_F}^{+\infty} [p + \sigma_F y] e^{-y^2/2}\, dy \\ &= \frac{p}{\sqrt{2\pi}} \left[\int_{-\infty}^{p/\sigma_F} e^{-y^2/2}\, dy - \int_{-\infty}^{-p/\sigma_F} e^{-y^2/2}\, dy \right] \\ &\quad + \frac{\sigma_F}{\sqrt{2\pi}} \left[\int_{-p/\sigma_F}^{+\infty} y e^{-y^2/2}\, dy - \int_{-\infty}^{-p/\sigma_F} y e^{-y^2/2}\, dy \right] \\ &\equiv G_1(t) + G_2(t). \end{aligned} \tag{A6}$$

In $G_2(t)$, let $v \equiv -y^2/2$, then

$$G_2(t) = \frac{2\sigma_F}{\sqrt{2\pi}} \int_{-\infty}^{-p^2/2\sigma_F^2} e^v \, dv = \frac{2\sigma_F}{\sqrt{2\pi}} e^{-p^2/2\sigma_F^2}. \tag{A7}$$

The time average of Equation A7 is

$$\begin{aligned} H_2 &\equiv \frac{\omega}{2\pi} \int_0^{2\pi/\omega} G_2(t)\, dt = \frac{1}{2\pi} \int_0^{2\pi} G_2\left(\frac{\tau}{\omega}\right) d\tau = \frac{2\sigma_F}{(2\pi)^{3/2}} \int_0^{2\pi} \exp\left[-\frac{K_c^2 \cos^2 \tau}{2\sigma_F^2}\right] d\tau \\ &= \frac{2\sigma_F}{(2\pi)^{3/2}} \exp\left[-\frac{K_c^2}{4\sigma_F^2}\right] \int_0^{2\pi} \exp\left[-\frac{K_c^2}{4\sigma_F^2} \cos 2\tau\right] d\tau \\ &= \frac{4\sigma_F}{(2\pi)^{3/2}} \exp\left[-\frac{K_c^2}{4\sigma_F^2}\right] \int_0^{\pi} \exp\left[-\frac{K_c^2}{4\sigma_F^2} \cos \tau\right] d\tau = \frac{2\sigma_F}{\sqrt{2\pi}} e^{-u} I_0(u), \end{aligned} \tag{A8}$$

where $I_0(u)$ is a modified Bessel function and $u \equiv K_c^2/4\sigma_F^2$. The time average of $G_1(t)$ can be written

$$\begin{aligned} H_1 &\equiv \frac{\omega}{2\pi} \int_0^{2\pi/\omega} G_1(t)\, dt = \frac{1}{2\pi} \int_0^{2\pi} G_1\left(\frac{\tau}{\omega}\right) d\tau \\ &= \frac{K_c}{(2\pi)^{3/2}} \int_0^{2\pi} \left[\int_{-\infty}^{p/\sigma_F} e^{-y^2/2}\, dy - \int_{-\infty}^{-p/\sigma_F} e^{-y^2/2}\, dy\right] \cos \tau \, d\tau \\ &\equiv \frac{K_c}{(2\pi)^{3/2}} \int_0^{2\pi} \left[\Phi\left(\frac{p}{\sigma_F}\right) - \Phi\left(-\frac{p}{\sigma_F}\right)\right] \cos \tau \, d\tau. \end{aligned} \tag{A9}$$

Integrating by parts, Equation A9 becomes

$$H_1 = \frac{K_c}{(2\pi)^{3/2}} \left\langle \left\{\left[\Phi\left(\frac{p}{\sigma_F}\right) - \Phi\left(-\frac{p}{\sigma_F}\right)\right] \sin \tau\right\}_0^{2\pi} - \int_0^{2\pi} \left[\dot{\Phi}\left(\frac{p}{\sigma_F}\right) - \dot{\Phi}\left(-\frac{p}{\sigma_F}\right)\right] \sin \tau \, d\tau \right\rangle . \tag{A10}$$

The first portion of Equation A10 vanishes. Making use of the relation

$$\dot{\Phi}\left(\pm \frac{p}{\sigma_F}\right) = \Phi'\left(\pm \frac{p}{\sigma_F}\right) \frac{d(\pm\, p/\sigma_F)}{d\tau} = \mp \frac{K_c}{\sigma_F} \sin \tau \exp\left[-\frac{p^2}{2\sigma_F^2}\right], \tag{A11}$$

the remaining portion of Equation A10 is converted to

$$H_1 = \frac{2K_c^2}{(2\pi)^{3/2}\sigma_F}\int_0^{2\pi} \sin^2\tau \exp\left[-\frac{K_c^2\cos^2\tau}{2\sigma_F^2}\right]d\tau$$

$$= \frac{2K_c^2}{(2\pi)^{3/2}\sigma_F}e^{-u}\left[\int_0^{\pi} e^{-u\cos\tau}d\tau - \int_0^{\pi}\cos\tau\, e^{-u\cos\tau}d\tau\right]$$

$$= \frac{K_c^2}{\sqrt{2\pi}\,\sigma_F}e^{-u}\left[I_0(u) + I_1(u)\right]. \tag{A12}$$

Therefore, the average control acceleration is given by

$$\overline{|F_{cx}^*|} = H_1 + H_2 = \frac{e^{-u}}{\sqrt{2\pi}}\left\{2\sigma_F I_0(u) + \frac{K_c^2}{\sigma_F}\left[I_0(u) + I_1(u)\right]\right\}. \tag{A13}$$

APPENDIX B

ECCENTRICITY CORRECTION FOR THE Z-AXIS OSCILLATION AT THE EARTH-MOON L_2 POINT

Following the procedures used in Chapter III, it is readily deduced that the differential equation for the eccentricity correction of the z-axis oscillation at a collinear libration point is (see Equation 2.43c)

$$\ddot{z}_{n2} + B_L z_{n2} = 3\rho B_L z_{n1}, \tag{B1}$$

where

$$\rho = - e \cos t \tag{B2}$$

and

$$z_{n1} = A_{z1} \cos \omega_z t. \tag{B3}$$

The solution of Equation B1 can be written in the form

$$z_{n2} = A_{z2} \cos (\omega_z + 1)t + A'_{z2} \cos (\omega_z - 1)t. \tag{B4}$$

At the Earth-Moon L_2 point, $B_{L2} = 3.19042$, $e = 0.05490$, and $\omega_z = 1.78618$. With these constants, it is found that

$$A_{z2} = 0.057460\ A_{z1}$$

and (B5)

$$A'_{z2} = - 0.10416\ A_{z1}.$$